CRUSTAL STUDIES AROUND THE WESTERN CANARY ISLANDS

A thesis submitted

for

the degree of Doctor of Philosophy

of the University of London

by

Eric Bosshard, Dipl.Sc.Nat.ETH

August, 1969

Geophysics Department
Imperial College
London, S.W.7.

ABSTRACT

Marine refraction seismic and gravity investigations were carried out during May/June 1967 and January/February 1968 in the area of the western Canary Islands. They were aimed at defining the crustal structure in this area and at answering the question of the origin of the Canaries.

The results show that the four western islands of Hierro, La Palma, Gomera and Tenerife are in an area where the crust is essentially oceanic, whereas Gran Canaria lies in the transitional zone between oceanic and continental crust. The islands do not form part of the African continent but are independent volcanic edifices which erupted along NE-SW striking fracture zones. The origin of the western Canaries is closely related to the formation of this fault pattern.

INDEX

	Page
CHAPTER 1: INTRODUCTION	5
Situation of the Canary Islands Hypotheses for the Origin of the Canary Islands Design of the Seismic and Gravity Surveys	
CHAPTER 2: SEISMIC INVESTIGATION	10
2.1 Seismic Refraction Profiles	10
2.1.1 Meteor Expedition	10
2.1.2 John Murray Expedition	15
2.2 Continuous Reflection Profiling	23
2.2.1 Meteor Expedition	23
2.2.2 John Murray Expedition	25
CHAPTER 3: PROCESSING AND INTERPRETATION OF THE SEISMIC DATA	27
3.1 Data Processing	27
3.1.1 Reduction of Data	27
3.1.2 Time-Distance Graph	30
3.1.3 Digital Processing	31
3.2 Interpretation of the Meteor Data	33
3.2.1 Unreversed Profiles A and D	35
3.2.2 Reversed Profile BC	38
3.3 Interpretation of the John Murray Work	43
3.3.1 Model A	46
3.3.2 Model B and Model C	50
3.3.3 Model D	59
3.3.4 Model E	62
3.4 Results of the John Murray Work	65
3.4.1 Line E	65
3.4.2 Line F recorded on Tenerife	67
3.4.3 Line F recorded on La Palma	71
3.4.4 Line G	71
3.4.5 Line H	74
3.4.6 Line I	74
3.5 Interpretation of Lines A and D with Model F	74
3.6 Continuous Reflection Records	78
3.6.1 Airgun Profile La Palma-Gomera-Hierro	78
3.6.2 Sparker Profile Tenerife-Gomera	78
3.6.3 Sparker Profile Tenerife-Gran Canaria	80
3.6.4 Sparker Profile parallel to the East Coast of Gran Canaria	80

	Page
3.7 Error Estimations	81
3.7.1 Least Squares and Confidence Regions for Line Parameters	81
3.7.2 Variance of the Computed Depths	83
3.7.2.1 Horizontal Layering	83
3.7.2.2 Dipping Layers	85
3.7.2.3 Least Squares Fitting of Models	86
CHAPTER 4: MARINE GRAVITY INVESTIGATION	89
4.1 Data Collection	89
4.2 Data Reduction	90
4.3 Bouguer Anomalies	91
4.3.1 Terrain Correction	93
4.3.2 Densities involved in the Bouguer Correction	97
4.4 Calculation of the Depth of the MOHO	102
4.4.1 Computing Technique	104
4.4.2 Sphericity Correction	107
4.4.3 Successive Approximation	108
4.4.4 Advantages and Disadvantages of the Method	110
4.4.5 Results	113
4.5 Structural Model for Tenerife	115
4.6 Structural Model for Gran Canaria	117
4.7 Error Consideration	119
CHAPTER 5: DISCUSSION OF THE RESULTS	120
5.1 Seismic Velocities	120
5.1.1 Group 1: 2.85-3.56 km/sec	123
5.1.2 Group 2: 3.90-4.75 km/sec	123
5.1.3 Group 3: 5.35-6.00 km/sec	125
5.1.4 Group 4: 6.60-7.50 km/sec	126
5.1.5 Group 5: 7.65-8.12 km/sec	129
5.2 Estimation of the Refractors' Thicknesses	129
5.3 Bouguer Anomalies	132
5.4 Free-air Anomalies	136
5.5 Geology of the Canary Islands	141
5.5.1 Gran Canaria	141
5.5.2 Tenerife	143
5.5.3 Gomera	145
5.5.4 La Palma	146
5.5.5 Hierro	147
5.5.6 Summary	148
5.6 Causes for the Origin of the Canary Islands	150
5.6.1 Origin on the Mid-Atlantic Ridge	151
5.6.2 Connections with the African Continent	152
5.6.3 Hypothesis for the Origin of the Western Canaries	155
CHAPTER 6: CONCLUSIONS	157
ACKNOWLEDGEMENTS	160
BIBLIOGRAPHY	161

CHAPTER 1

INTRODUCTION

The Canary archipelago consists of an island group situated between 27°37' and 29°24' north latitude and 18°10' and 13°37' west longitude. The islands are separated from the African mainland by a minimum distance of about 100 km. The width of the group from east to west is 460 km and their total area is about 7950 km^2. The archipelago is formed by seven main islands, viz. Lanzarote, Fuerteventura, Gran Canaria, Tenerife, Gomera, La Palma and Hierro, and a number of small islets (Fig. 1). The relief of the islands is remarkable, as the highest summit of all the Atlantic islands is found on Tenerife. Mt. Pico Teide has an altitude of 3718 metres above sea level. Since most of the Canaries rise from about 3500 metres depth, their maximum elevations are between 4200-7200 metres.

The Canaries are strung out into the Atlantic Ocean and the submerged parts of the islands form a continuous sub-surface ridge, rising some 1500 metres above the surrounding ocean floor (Fig. 1). This ridge is referred to as the "Canaries Ridge" in the following chapters, in analogy to the Hawaiian Ridge. Accepting the 2000 metres isobath as the edge of the continents (HEEZEN et al., 1959), the eastern part of this topographic feature lies on the continental slope and its western extremity on the continental rise.

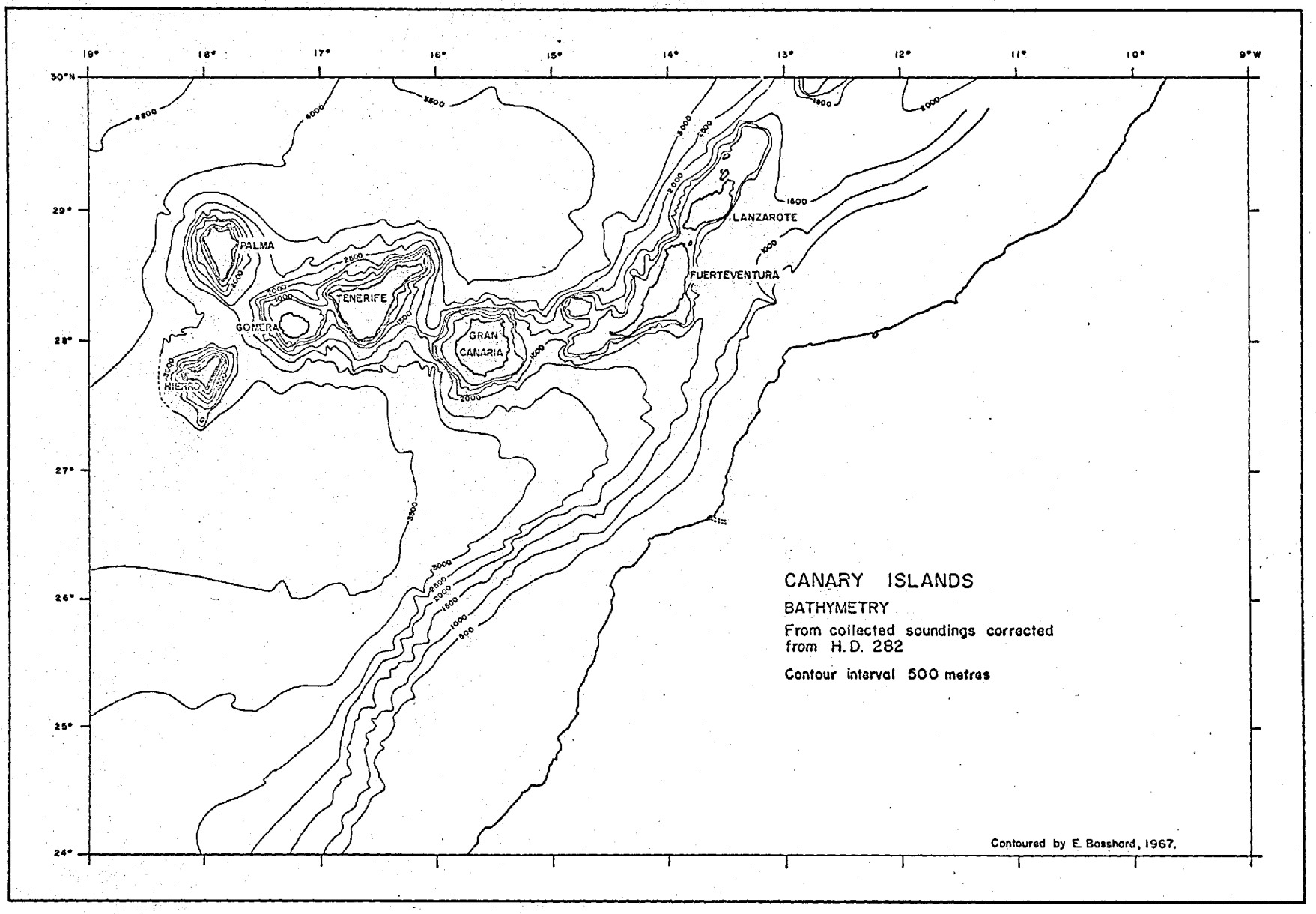
19°
18°
17°
16°
15°
14°
13°
12°
11°
10°
9°W
30°N
29°
28°
27°
26°
25°
24°
PALMA
TENERIFE
GOMERA
HIERRO
GRAN CANARIA
LANZAROTE
FUERTEVENTURA
CANARY ISLANDS
BATHYMETRY
From collected soundings corrected from H.D. 282
Contour interval 500 metres
Contoured by E. Bosshard, 1967.

Fig.1

This particular situation of the Canaries led many geologists to postulate widely differing views concerning their origin.

In the search for the mythological continent Atlantis which had sunk, the Macaronesian Insular Region was at one time regarded as the remains of this ancient continent. This Macaronesian Insular Region is comprised of the east Atlantic volcanic archipelagos of the Azores, Madeira, the Salvagens, the Canary Islands and the Cabo Verde Group.

However, VON BUCH (1825) suggested that the Canaries were formed by vigorous uplifting of marine strata. Both the calderas on La Palma and Tenerife supposedly proved his hypothesis.

In contradiction to this view, LYELL (1855) argued that the Canaries were the result of a long-lasting volcanic activity with lava and tuff accumulations, beginning at the ocean floor.

HERNANDEZ-PACHECO (1910) was among the geologists who proposed a relationship between the Canary archipelago and the African continent. He considered that the Canaries emerged along four major fractures and pointed out the similarity between these lineaments and the tectonic trends on the neighbouring continent.

HAUSEN (1958) went even further by suggesting that there was a connection between the Hercynian tectonic lineaments in Africa and the dykes on Fuerteventura's basal complex. Later he even suggested the existence of a pre-Canarian subcontinent

which had disintegrated (HAUSEN, 1962), the fragments of this foreland supposedly forming the nuclei of the Canary Islands.

In a comparative study of vertical movements in the Macaronesian Insular Region, KREJCI-GRAF (1961) argued that the oldest formations on the Canaries are similar to the Atlas Mountains of Northwest Africa. He suggested that the islands probably owe their origin to the same tectonic processes which formed the Atlas. Between Cretaceous and Paleogene times, the strata on the ocean floor was compressed, forming steep warps. At the same time magma intruded and subsequent vulcanism created the islands. After their initiation, repeated uplift and subsidence took place and the sediments thus exposed are no older than Tertiary age.

Since earlier investigations on the Canary Islands failed to give an adequate answer to the question of their origin, it was decided to conduct a combined marine gravity and refraction seismic survey in this area.

It is well known that the depth of the Mohorovičic Discontinuity is a criterion for defining whether the crust is of oceanic or continental type. Therefore, it was essential to determine this depth around the Canaries in order to find a suitable solution to the question of their origin. To achieve this, a seismic refraction investigation was carried out around the islands. The regional features of the crustal structure were obtained from marine gravity investigations.

Since the problem under investigation was complicated, the period of the survey was spread over two seasons' work in order to obtain as much data as possible. In the

first year, particular attention was given to collecting seismic and gravity data around the islands. To avoid possibly doubtful interpretation, no risks were taken in shooting too close to the complex structure of the islands. The four refraction lines shot were up to 100 km long, ensuring that P-wave arrivals from the Upper Mantle could be obtained as first arrivals.

Once the structural trend around the islands was established, seismic investigations were extended in the second stage to the area close to the islands. The combined data were used to interpret the complicated P-wave velocity configuration in this region.

During both stages, continuous seismic reflection profiling was also carried out in various parts of the island group in order to provide a picture of the low-velocity sediment distribution. Accurate echo-sounding provided the data necessary to improve the existing bathymetric map which was essential for an accurate interpretation of the marine gravity data.

Finally, the information gained during this investigation was correlated with earlier gravity work on the islands (MACFARLANE, 1968) and all the relevant geological data, to obtain the answer to the problem of the origin of this island group.

CHAPTER 2

SEISMIC INVESTIGATION

The crustal studies investigation around the Western Canary Islands was spread over two years. It was initiated in the year 1967 when this department collaborated with the scientists of the Bundesanstalt für Bodenforschung, Hannover, on a cruise to the continental slopes of Spanish Sahara and the Canaries with the German Research Ship F.S. Meteor (Fig. 2). The area under investigation by this department is shown in Fig. 6 and marked zone B. The following year, in January-February 1968, this investigation was further extended with the R.R.S. John Murray (Fig. 4).

The details of this refraction and continuous seismic profiling work are outlined below.

2.1 Seismic Refraction Profiles

2.1.1 Meteor Expedition

Four long refraction lines were shot using the two-ship method: Line A to the north of the Canaries ridge; Lines B and C, a reversed profile, to the west of La Palma-Hierro; and line D to the south of Gomera-Tenerife (Fig. 6). F.S. Meteor acted as the stationary recording vessel and the Spanish Hydrographic Ship Tofinio (Fig. 5) as the shooting boat. Where the weather was favourable a second recording station was set up some 10 km away on an auxiliary motor boat.

A conventional recording technique was used. The hydrophones used were Electro-Technical Labs EVP 5,7 and 10 with pressure compensation and resonant frequencies of 8-9 Hz,

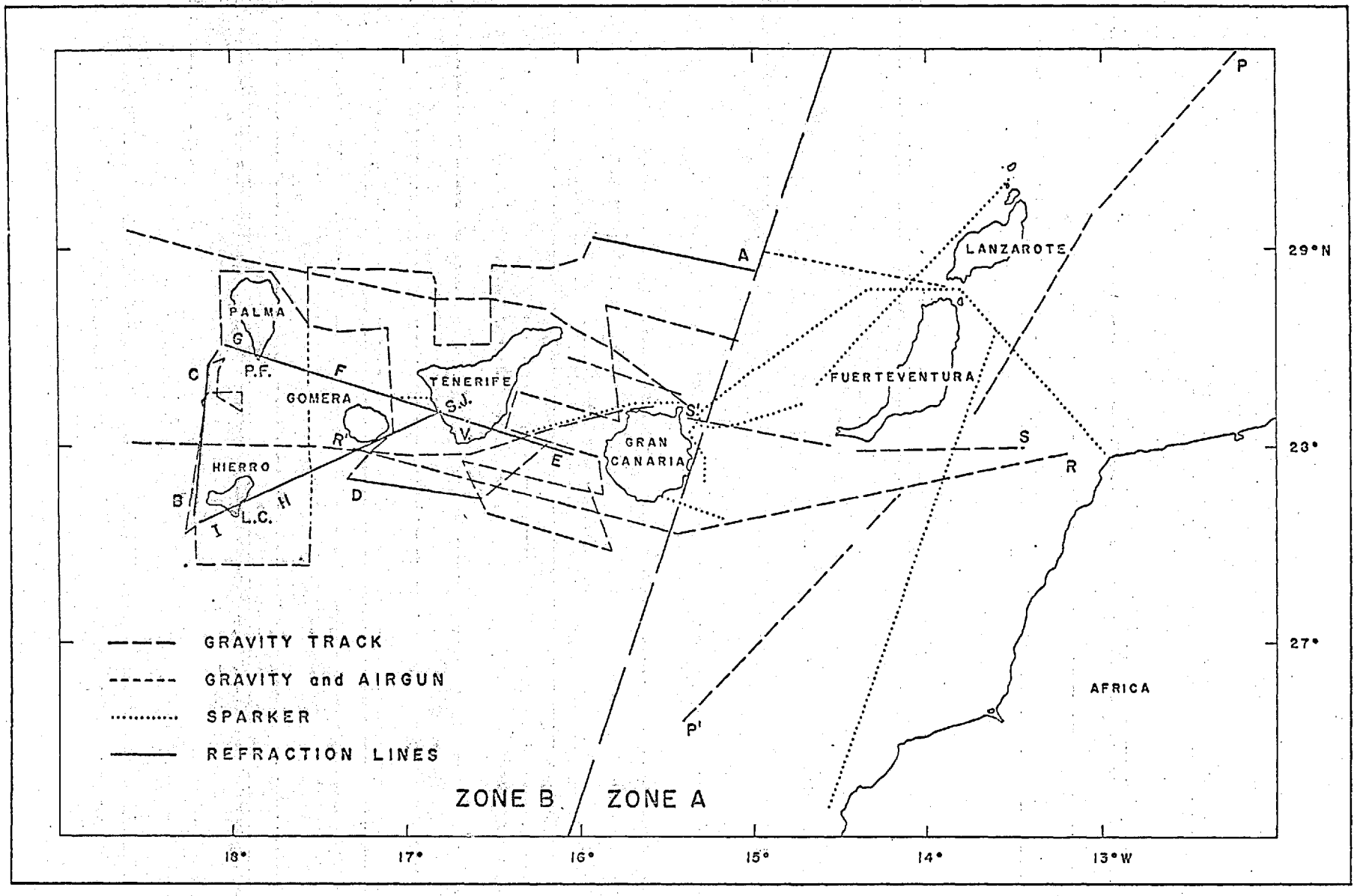
P
A
LANZAROTE
29°N
PALMA
G
C
P.F.
F
GOMERA
TENERIFE
S.J.
S'
FUERTEVENTURA
V.
R'
GRAN
CANARIA
S
23°
HIERRO
E
R
B
H
D
L.C.
I
GRAVITY TRACK
GRAVITY and AIRGUN
SPARKER
REFRACTION LINES
P'
AFRICA
27°
ZONE B
ZONE A
18°
17°
16°
15°
14°
13°W

Fig.6

Fig.2: F.S.Meteor in the harbour of Santa Cruz de Tenerife

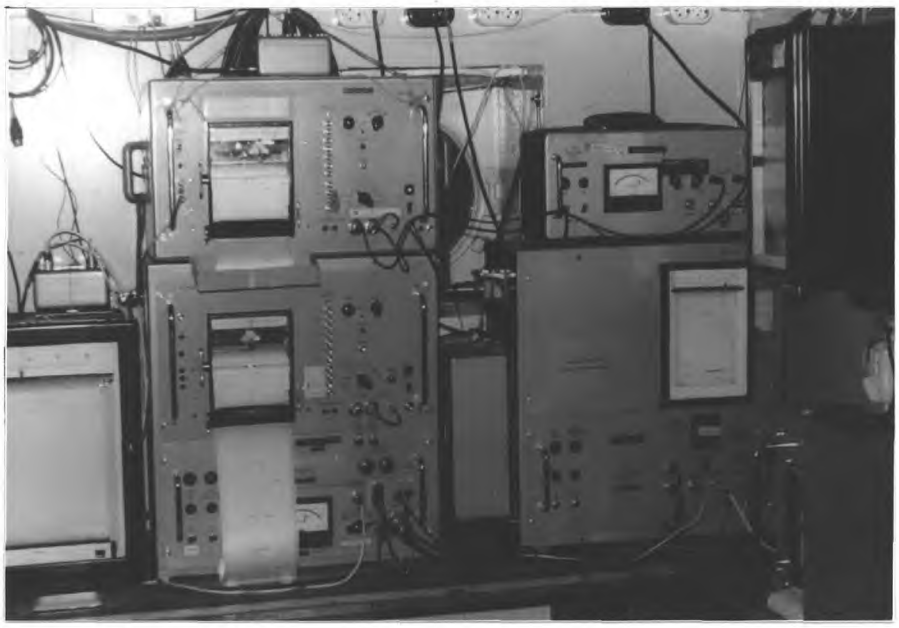

Fig.3: Analog recorders of the Graf-Askania Sea Gravimeter on board F.S.Meteor

suspended at 70 metres depth below the surface of the sea. The electronics on board consisted of a Geospace III A-amplifier with standard filter banks and a seismic SIE-recording oscillograph. The shot instant was transmitted by radio-telephone from the shooting vessel and directly recorded on to the seismogram.

The shots were fired electrically with a condenser-exploder type ZEB/A 80K/C of WASAG-Chemie AG, Essen, Germany. The charges were detonated at a depth of approximately 20 metres below the surface.

The Loran navigational system was used to determine the positions of F.S. Meteor during the shooting days. They were checked with astronomical fixes and Radar sights every two hours or so. A very accurate Radar on F.S. Meteor was used to guide the shooting boat, to determine the distances from the shots to the detector and to locate the position of the auxiliary motor boat. After each shooting day the ship retracted the profile to record the sea bottom profile by a precision depth recorder.

2.1.1.1 Line A

Line A was recorded at 28°53'N, 15°00'W and extended westwards to 29°03'N, 15°55'W. Thirty-five shots were fired at intervals ranging from 1 km to 6 km. The charge size varied from 20 kg to 100 kg. The weather was generally moderate with wind forces up to 6 and waves up to 2 m high.

2.1.1.2 Lines B and C

These two lines were located between 27°39'N, 18°13'W and 28°25'N, 18°08'W and constituted a reversed profile. Twenty shots were fired on line B at intervals from 2 km to 5 km

Fig.4: R.R.S.John Murray in the harbour of Bilbao

Fig.5:Spanish Hydrographic Ship Tofiño

which were recorded at 27°39'N, 18°13'W. The charge sizes varied from 20 kg to 100 kg. Since the weather conditions were bad the shooting was disrupted between Hierro and La Palma and could only be resumed at the end of the profile.

Thirty-eight shots were detonated on line C at intervals from 1 to 5 km. F.S. Meteor was kept on the leeward side of La Palma because of poor weather. When cruising southwards with the wind from aft, Tofinio had no trouble firing the charges which ranged between 20 kg and 100 kg.

2.1.1.3 Line D

This line was recorded at 27°50'N, 17°20'W and extended eastwards to 27°44'N, 16°34'W. Forty shots were fired at an interval of 1-5 km. Again, during this exercise, the weather was rough and F.S. Meteor had to be kept close to the shore of Gomera where the sea was comparatively calm.

2.1.2 John Murray Expedition

The second stage was undertaken with R.R.S. John Murray in 1968 (Fig. 4) during the months of January/February.

The general plan was to shoot two long lines: one from east to west across Gran Canaria, Tenerife and La Palma; and a second one running northeast-southwest across Tenerife, Gomera and Hierro (Fig. 6). R.R.S. John Murray had to act as the shooting boat and the seismic energy was recorded on various islands simultaneously. It was designed to have a few days' break in between these two lines to enable the land parties to change the recording sites and at the same time carry out a rough interpretation of the data.

Unfortunately, an engine breakdown forced the R.R.S. John Murray into the harbour of Bilbao engendering much loss of time. This necessitated a shortening of the original programme. The East-West line started between Gran Canaria and Tenerife and the Northeast-Southwest line between Tenerife and Gomera, and both had to be completed in four working days.

2.1.2.1 The East-West Line

This line was split into three profiles, viz. profile E between Gran Canaria and Tenerife; profile F between Tenerife and La Palma; and profile G west of La Palma. The recording sites for all three profiles were on Tenerife at Vilaflor (28°07'30"N, 16°38'45"W, altitude 1210 m above sea level) and on La Palma at Punta Fuencaliente (28°27'N, 17°50'30"W, altitude 10 m above sea level) as shown in Fig. 6.

An electric shot firing technique was used to detonate the charges in the sea. The shot instant was transmitted by radio-telephone to the shore stations where it was recorded on the seismograms. It consisted of a steady tone of 1600 Hz which was simultaneously interrupted with the firing of the charge. This signal generator was built at the Geophysics Department, where the condenser-exploder was also modified.

One major drawback was the slow winding winch on John Murray used for reeling the firing cable in and out. This caused unnecessary waste of time between shots. In addition, it meant that the cruising speed had to be considerably reduced if narrow spacing of the shots was desired, e.g. close to the recording stations. Therefore, the length of a profile which could be shot in one day was seriously limited.

Fig.7:Shooting on R.R.S.John Murray

Preparing a 125 lb - charge

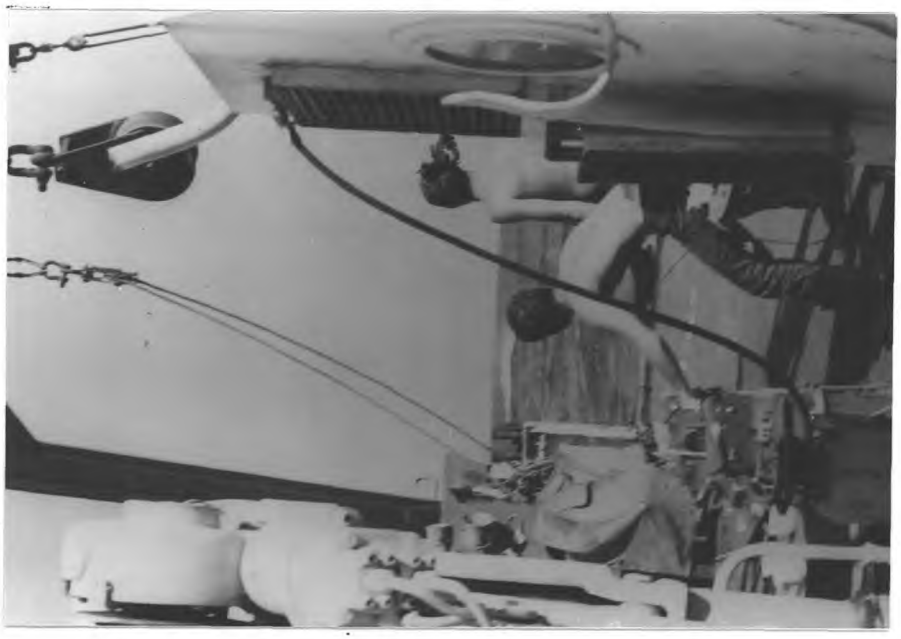

Fire!

The charges were allowed to sink freely between 60 sec and 120 sec, according to their size, to give John Murray enough time to sail away. Charges heavier than 150 lb could not be shot without affecting the ship's instruments, so only charges up to 100 lb were used (Fig. 7). The navigation was done by Radar since no Loran receiver was installed on board. The location of every shot point was determined by taking the bearings of at least three landmarks and plotting their reciprocal bearings and ranges with the Decca Radar and Plotter on board. This procedure enabled an accurate determination of the shot positions.

The recording station on Tenerife consisted of a seismic telemetring device (GURNEY, 1964). This system was originally designed by Dr. M.N. Hill of Cambridge University and enabled a ship to lay radio-equipped buoys with hydrophones and record seismic arrivals at considerable distances. Figure 8 shows the block diagram of this system.

In the buoy, hydrophone signals are amplified and frequency-modulate a sub-carrier of 3375 Hz. The transmitter of 27 MHz is in turn amplitude-modulated with the sub-carrier and establishes the radio link with the recording ship. The radio receiver on board produces an amplitude-limited output at sub-carrier frequency which can be recorded on magnetic tape. Variations in the carrier's frequency are proportional to the hydrophone signals. These are reconstituted in a final demodulator stage and can be directly recorded with a seismic camera.

Two buoys were laid out some 1.5 km apart in the general direction of the profile. They had been adapted to use on land and tested at Imperial College Field Station,

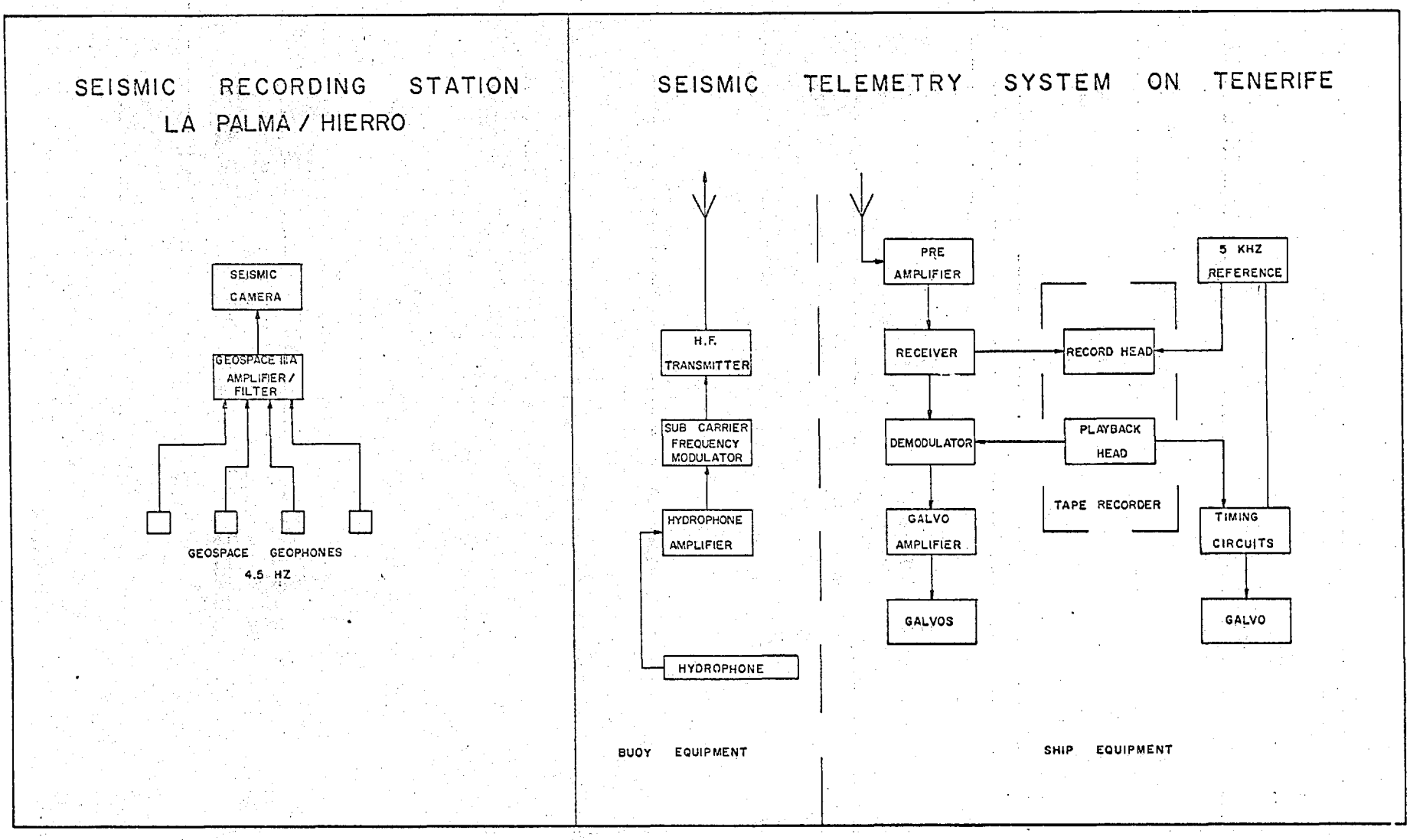
SEISMIC RECORDING STATION
LA PALMA / HIERRO
SEISMIC CAMERA
GEOSPACE III A AMPLIFIER / FILTER
GEOSPACE
GEOPHONES
4.5 HZ
SEISMIC TELEMETRY SYSTEM ON TENERIFE
H.F. TRANSMITTER
SUB CARRIER FREQUENCY MODULATOR
HYDROPHONE AMPLIFIER
HYDROPHONE
BUOY EQUIPMENT
PRE AMPLIFIER
RECEIVER
DEMODULATOR
GALVO AMPLIFIER
GALVOS
5 KHZ REFERENCE
RECORD HEAD
PLAYBACK HEAD
TAPE RECORDER
TIMING CIRCUITS
GALVO
SHIP EQUIPMENT

Fig.8

Silwood Park, prior to the expedition. Instead of hydrophones, Geospace-geophones with a resonance frequency of 4.5 Hz were used. The recording was done with the same receiver, demodulator and tape recorder system as those used for the radio-sonobuoys. Additionally the output of the demodulators was recorded with a seismic camera. Communication with the working parties was effected with a transmitter/receiver type Curlew of Coastal Radio.

The recording station on La Palma consisted of four Geospace 4.5 Hz geophones laid out in a 500 m long east-west spread. A Geospace III A amplifier with standard filters and an SIE recording oscillograph were used (Fig. 8). A Marconi Kestral III transmitter/receiver linked this station with Vilafior and John Murray.

2.1.2.1.1 Profile E

700 lb of Geophex explosive were detonated in 13 shots between 27°57'30"N, 16°02'30"W and 28°04'N, 16°21'30"W. The charge sizes varied from 25 lb to 150 lb. These shots were only recorded on Tenerife.

2.1.2.1.2 Profile F

Twenty-seven shots amounting to 1125 lb of explosives were fired between 28°13'N, 16°57'W and 28°28'N, 17°48'30"W. Owing to size of the charges, the shots fired close by Tenerife could only be recorded on this island and, similarly, the shots close to La Palma were too weak to be recorded on Tenerife. The shots were fired at intervals from 1.6 km to 4 km. The shooting was interrupted in the middle of the profile for

several hours due to the loss of a major section of the shooting cable.

2.1.2.1.3 Profile G

Nine charges amounting to 225 lb of explosives were detonated between 28°29'30"N, 17°54'W and 28°31'N, 18°02'W and were only received on La Palma. Owing to the limited time available, this line could not be extended as far to the west as originally planned, despite the fact that it was shot late at night. Therefore, no direct link to the recording station of the Meteor profile C could be established (see Fig. 6).

2.1.2.2 The Northeast-Southwest Line

This line was divided into profile H between Tenerife and Hierro and profile I west of Hierro. The seismic energy was recorded on Tenerife at San Juan (28°10'30"N, 16°48'W, altitude 15 m above sea level) and on Hierro at Los Cariles (27°39'30"N, 17°59'W, altitude 230 m above sea level). The instrumentation of the San Juan site was identical with the one at Vilaflor. Similarly, Hierro's instrumentation was the same as that used in La Palma (Fig. 9). The shooting technique was also the same as in the earlier exercise.

2.1.2.2.1 Profile H

2200 lb of explosives were fired in 21 shots between 28°08'30"N, 16°54'W and 27°43'N, 17°55'W. Large shots of 150 lb, suspended 50 m below the surface, were fired between Gomera and Tenerife in an attempt to obtain first arrivals from the Upper Mantle on Hierro. Unfortunately, the recording site on Hierro, was rather poor and no deep arrivals could be observed. On the same day commercial blasting on Tenerife completely masked the

Recording station on Hierro

Fig.9: Geospace IIIA amplifier and filter unit and SIE-camera as used on La Palma and Hierro

arrivals from the John Murray, rendering interpretation of the San Juan seismograms impossible.

2.1.2.2.2 Profile I

Only 5 shots, using 200 lb of explosive, were fired between 27°39'15"N, 18°05'30"W and 27°37'N, 18°11'30"W. Owing to the extremely short time available for the northeast-southwest line, profile I was completed late at night. The shooting ended at the last possible minute after a shooting day of 17 working hours.

2.2 Continuous Reflection Profiling

During the two expeditions the refraction profiles were supplemented by continuous reflection profiling by an air-gun and a sparker system respectively.

2.2.1 Meteor Expedition

An air-gun system (Fig. 10) was installed on board F.S. Meteor, consisting of two guns of 150cc capacity each. Two diesel driven compressors supplied the compressed air required. The electromagnetic valves in the guns were triggered every six seconds by a low-frequency oscillator, releasing the stored energy.

Both guns were towed some 20 feet behind the stern at a depth of some 3-4 feet whereas the hydrophone was kept at about 150 metres behind the ship and 2-3 feet below the surface. The reflected energies were received by a hydrophone array consisting of 10 hydrophones connected in parallel and were recorded on magnetic tape. The arrivals were also monitored on electrosensitive paper by two ELAC depth recorders so that

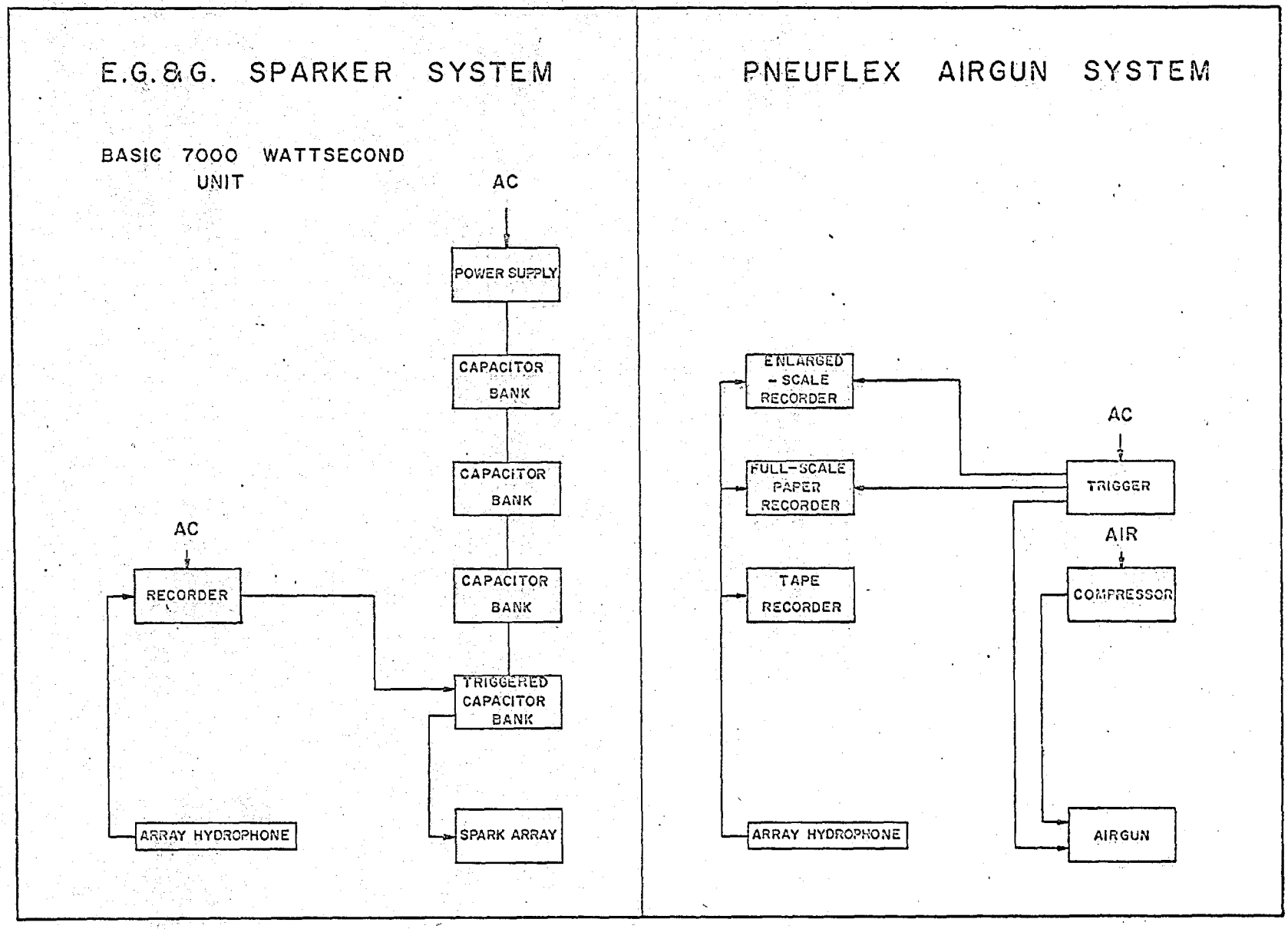
E.G.&G. SPARKER SYSTEM
BASIC 7000 WATTSECOND UNIT
AC
POWER SUPPLY
CAPACITOR BANK
CAPACITOR BANK
CAPACITOR BANK
AC
RECORDER
TRIGGERED CAPACITOR BANK
ARRAY HYDROPHONE
SPARK ARRAY
PNEUFLEX AIRGUN SYSTEM
ENLARGED - SCALE RECORDER
FULL-SCALE PAPER RECORDER
TAPE RECORDER
ARRAY HYDROPHONE
AC
TRIGGER
AIR
COMPRESSOR
AIRGUN

Fig.10

one of them covered the whole time scale whereas the second one enlarged the section containing the bottom and sub-bottom reflections.

2.2.2 John Murray Expedition

A 32000 joule E.G.&G. sparker equipment installed on board R.R.S. John Murray (Fig. 10) was used to carry out the reflection profiling. Unfortunately, the ship's power supply was inadequate and at the most 8000 joules out of the possible 32000 joules could be generated. The sparks were fired at intervals of 1 to 5 seconds and the reflected energy, picked up by a hydrophone array, was recorded on electrosensitive paper (Fig. 11). Although the recommended cruising speed for sparker operation is about 6-7 knots, this speed could not be maintained due to lack of time. Despite the fact that the hydrophone array and the sparkarray were towed some 3 feet and 5 feet respectively below the sea-surface, the noise level on the records was so high that not many reflections could be observed.

Fig.11: E.G.&G.Sparker System on board R.R.S.John Murray

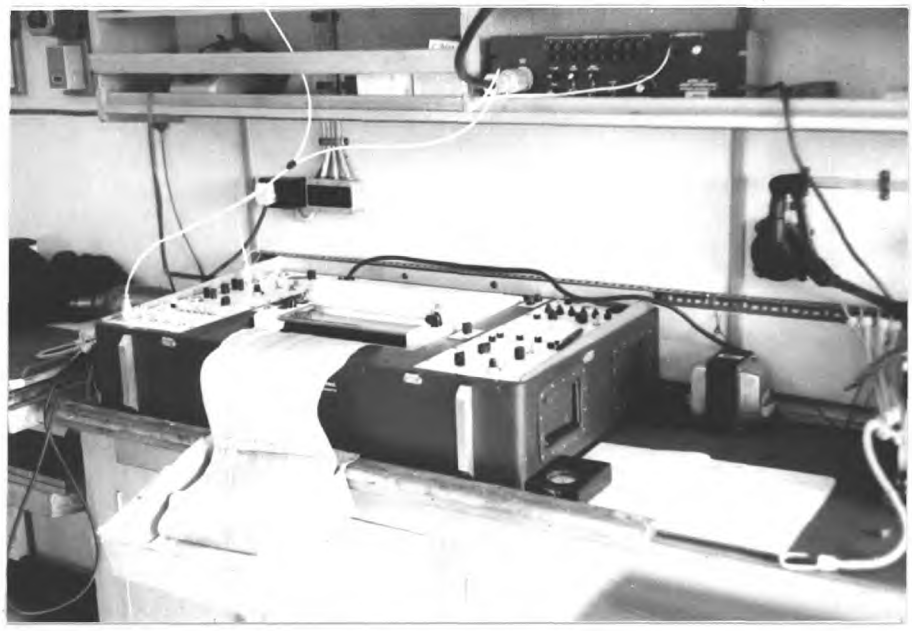

Sparker recorder

Hydrophone and spark arrays

CHAPTER 3

PROCESSING AND INTERPRETATION OF THE SEISMIC DATA

3.1 Data Processing

For suitable interpretation, the field refraction data were subjected to corrections, the details of which are outlined in the following paragraphs.

3.1.1 Reduction of Data

The broad outline for correction of marine refraction data is as described by OFFICER et al.(1959). The two corrections applied are one for the surface of reference at sea level and the other for the varying bottom topography. These can be written in the form

$$T = T_{SR} + T_{BT} \qquad (1)$$

where T_{SR} = surface reference correction

T_{BT} = bottom topography correction

T = Total correction

The datum plane was chosen to be at sea level. Then the correction for the depth of the shot and the depth of the hydrophone, i.e. the surface reference correction, can be written as follows (see Fig. 12):

$$T_{SR} = \frac{d_s}{C_o} \cdot \cos\left(\sin^{-1} \frac{C_1}{C_{na}}\right) + \frac{d_H}{C_o} \cdot \cos\left(\sin^{-1} \frac{C_1}{C_{nb}}\right) \qquad (2)$$

where d_s = depth of shot

d_H = depth of hydrophone

C_o = velocity of sound in the surface layer of the ocean

C_1 = average velocity of sound in the ocean

C_{na}, C_{nb} = apparent velocities of a refractor.

The topographic correction for the variations in the bottom relief can be written for the A-portion of a reversed profile in the form:

$$T_{BTA} = \frac{d_T}{C_1} \cdot \cos(\sin^{-1} \frac{C_1}{C_{na}}) - \frac{d_T}{C_x} \cdot \cos(\sin^{-1} \frac{C_x}{C_{na}}) \qquad (3)$$

where T_{BTA} = topographic correction for A-portion of a reversed profile

d_T = change of bottom topography with reference to an arbitrary bottom baseline

C_1 = average acoustic velocity in the ocean

C_{na} = apparent velocity of a refractor

C_X = seismic velocity of the sub-bottom layer, i.e. the layer responsible for changes in bottom topography.

The quantity d_T is measured above or below a mean bottom baseline at an offset distance of

$$D = H \cdot \tan(\sin^{-1} \frac{C_1}{C_{na}})$$

where H = depth of water under the shot

C_1, C_{na} as in equation (3).

A similar formula to equation (3) is used to allow for the changes in bottom topography under the recording stations. According to OFFICER et al. (1959) a measurable difference is caused only in the most exceptional case, by using C_{na} in the second term of equation (2).

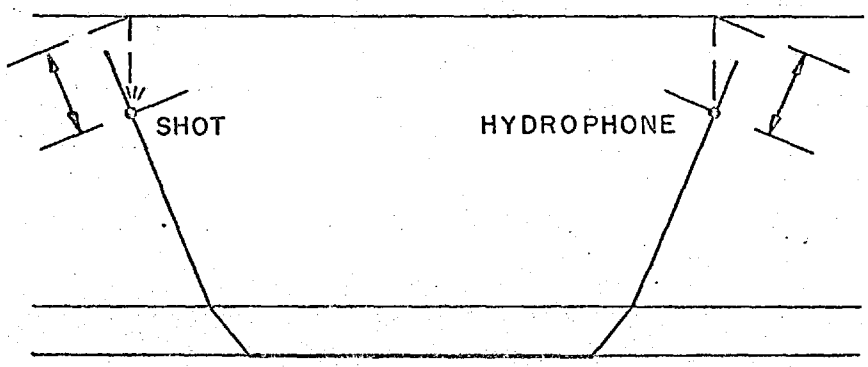

RAYPATH FOR SURFACE OF REFERENCE CORRECTION

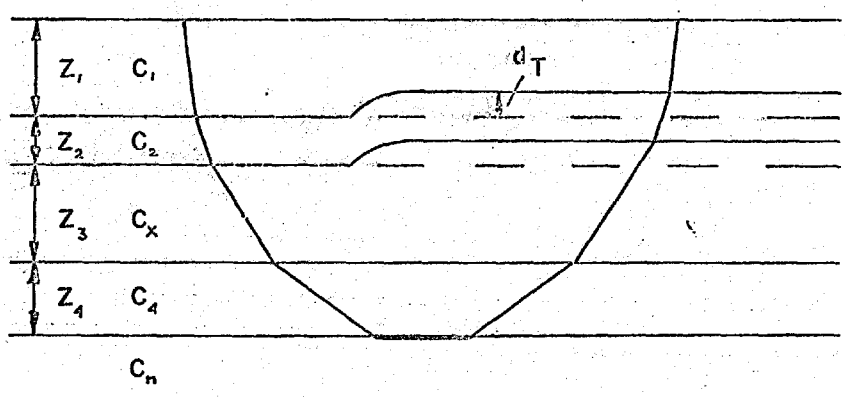

RAYPATH FOR TOPOGRAPHIC CORRECTION

Fig.12

At all the refraction stations the velocities C_o and C_1 were determined with an ultrasonic probe (WEIGEL, 1967). The velocities C_{na} were taken from a first plot of the refraction data. For the profiles A, B, C and D the depths of the hydrophones were known to be 70 m. The depths of the shots were also known since the charges were suspended below the surface. When shooting with R.R.S. John Murray the charges were allowed to sink freely. The depths of the shots were calculated from the time between dropping and firing the charges and their sinking rates. The latter were determined experimentally on board.

When effecting the topographic correction, the bottom baseline was chosen according to the bottom topography under each profile. The velocity C_x, taken as the velocity of the first high speed layer beneath the bottom, was 3.2 km/sec assuming that the bottom relief was caused by this layer.

3.1.2 Time-Distance Graphs

The recorded travel times were used to produce the conventional time-distance graphs. The distances between the recording station and the shooting boat were corrected for the distances shot-shooting vessel. They were based on the ship's and shooting operator's logs.

The plot of the travel times versus distance was matched with the appropriate refraction lines. Fitting a small number of well-defined straight lines is in most cases the best procedure according to OFFICER et al.(1959). This was especially true here where the shots were spaced between 1 km and 5 km yielding no information as to the behaviour of the refractors in between.

3.1.3 Digital Processing

On visual examination of the seismograms from Vilaflor it was apparent that a systematic high frequency noise was superimposed. In order to clarify first arrivals the noise frequencies had to be eliminated. Since no recordings on magnetic tape were available to play back improved records through analog filters, the existing seismograms had to be digitized to smooth the traces. This was done with a mechanical digitizer (Type Oscar Model J.). The amplitude values were taken at intervals of 10 milliseconds and were punched on IBM cards. The smoothing of the traces was done by digital computer and the theory of this smoothing operation is outlined below.

When the smoothing function is $y(x)$ with the parameters $a_o \ldots\ldots a_n$ and the amplitude values at the points X_ς ($\varsigma = 1, \ldots r$) are Y_ς, the smoothing is done so that

$$Q(a_o, a_1, \ldots, a_n) = \sum_{\varsigma=1}^{r} (Y_\varsigma - y(X_\varsigma))^2 = \text{minimum} \qquad (1)$$

The condition for Q being a minimum is

$$\frac{\partial Q}{\partial Q_i} = 0 \ (i=o, \ldots n) = 2 \sum_{\varsigma=1}^{r} (Y_\varsigma - y(X_\varsigma)) \frac{\partial y(X_\varsigma)}{\partial Q_i} \qquad (2)$$

In the case of a smoothing parabola, the function $y(x)$ is

$$y(x) = a_o + a_1 x + a_2 . x^2 + \ldots. + a_n x^n \qquad (3)$$

and substituted in equation (2) we obtain

$$\sum_{\varsigma=1}^{r} (Y_\varsigma - \sum_{v=o}^{n} a_v . X_\varsigma^v) . X_\varsigma^i = 0 \qquad (4)$$

where $i=o, \ldots n$

Equation (4) can be transformed to

$$\sum_{v=o}^{n} (a_v \sum_{\varsigma=1}^{r} . X_\varsigma^{v+i}) = \sum_{\varsigma=1}^{r} Y_\varsigma . X_\varsigma^i \qquad (5)$$

where $i=o, \ldots n$.

Terming $\sum_{\rho=1}^{r} a_\rho b_\rho = [ab]$ and $\sum_{v=o}^{n} [x^{v+i}] \cdot a_v = [x^i \cdot Y]$

and $\sum_{\rho=1}^{r} x_\rho^n = [x^n]$ and $[x^o] = r$

for i=o, ... n, we obtain a system of normal equations for a_i:

$$\begin{aligned}
i=o\quad & r.a_o + [x] \cdot a_1 + [x^2] \cdot a_2 + \ldots + [x^n] \cdot a_n = [Y] \\
i=1\quad & [x] \cdot a_o + [x^2] \cdot a_1 + [x^3] \cdot a_2 + \ldots + [x^{n+1}] a_n = [xY] \\
i=n\quad & [x^n] \cdot a_o + [x^{n+1}] \cdot a_1 + [x^{n+2}] \cdot a_2 + \ldots + [x^{2n}] \cdot a_n = [x^n Y]
\end{aligned} \qquad (6)$$

In the present case a second order parabola was fitted by least squares to five successive points of the original trace. The amplitude value of the centre point of the parabola was assigned as a new amplitude value to the third of the five points. By shifting the parabola in steps of 1 along the trace, every point of the trace obtained a new, weighted amplitude value. Hence equation (6) was of the form

$$\begin{aligned}
[x^o] \cdot a_o + [x] \cdot a_1 + [x^2] \cdot a_2 &= [Y] \\
[x] \cdot a_o + [x^2] \cdot a_1 + [x^3] \cdot a_2 &= [xY] \\
[x^2] \cdot a_o + [x^3] \cdot a_1 + [x^4] \cdot a_2 &= [x^2 Y]
\end{aligned} \qquad (7)$$

Having five values for x (i.e. -2, -1, 0, +1, +2) with corresponding amplitude values Y_{v-2}, Y_{v-1}, Y_v, Y_{v+1}, Y_{v+2} it followed that

$$\begin{aligned}
[x] = [x^3] &= 0 \text{ and } [x^o] = 5 \\
[x^2] &= 10 \quad \text{and} \quad [x^4] = 34 \\
[Y] &= Y_{v-2} + Y_{v-1} + Y_v + Y_{v+1} + Y_{v+2} \\
[xY] &= -2Y_{v-2} - Y_{v-1} + Y_{v+1} + 2Y_{v+2} \\
[x^2 Y] &= 4Y_{v-2} + Y_{v-1} + Y_{v+1} + 4Y_{v+2}
\end{aligned} \qquad (8)$$

Substituting (8) in (7) resulted in

$$5 \cdot a_o + o \cdot a_1 + 10 \cdot a_2 = [Y]$$
$$r \cdot a_o + 10 \cdot a_1 + 0 \cdot a_2 = [xY]$$
$$10 \cdot a_o + 0 \cdot a_1 + 34 \cdot a_2 = [x^2Y] \qquad (9)$$

and the coefficients became

$$a_o = \frac{-3Y_{v-2} + 12Y_{v-1} + 17Y_v + 12Y_{v+1} - 3Y_{v+2}}{35}$$

$$a_1 = \frac{-2Y_{v-2} - Y_{v-1} + Y_{v+1} + 2Y_{v+2}}{10}$$

$$a_2 = \frac{10Y_{v-2} - 5Y_{v-1} - 10Y_v + 5Y_{v+1} + 10Y_{v+2}}{70} \qquad (10)$$

The smoothed value Y_v was equal to $y(0) = a_o$ and hence could be calculated from

$$Y_v = \frac{-3Y_{v-2} + 12Y_{v-1} + 17Y_v + 12Y_{v+1} - 3Y_{v+2}}{35} \qquad (11)$$

for $3 \leq v \leq n-2$

A programme for the IBM 7094 computer was written to calculate the smoothed values of a trace. Since the first and last two points did not yield properly smoothed values they were omitted when plotting the smoothed trace by digital computer. The whole procedure was repeated by using the smoothed values as new input values until the trace was reasonably free from noise and high frequency. Figure 13 illustrates the digitized seismic trace of shot 189 and three subsequently smoothed traces.

3.2 Interpretation of the Meteor Data

Interpretation of the time-distance curves was based on the following assumptions:

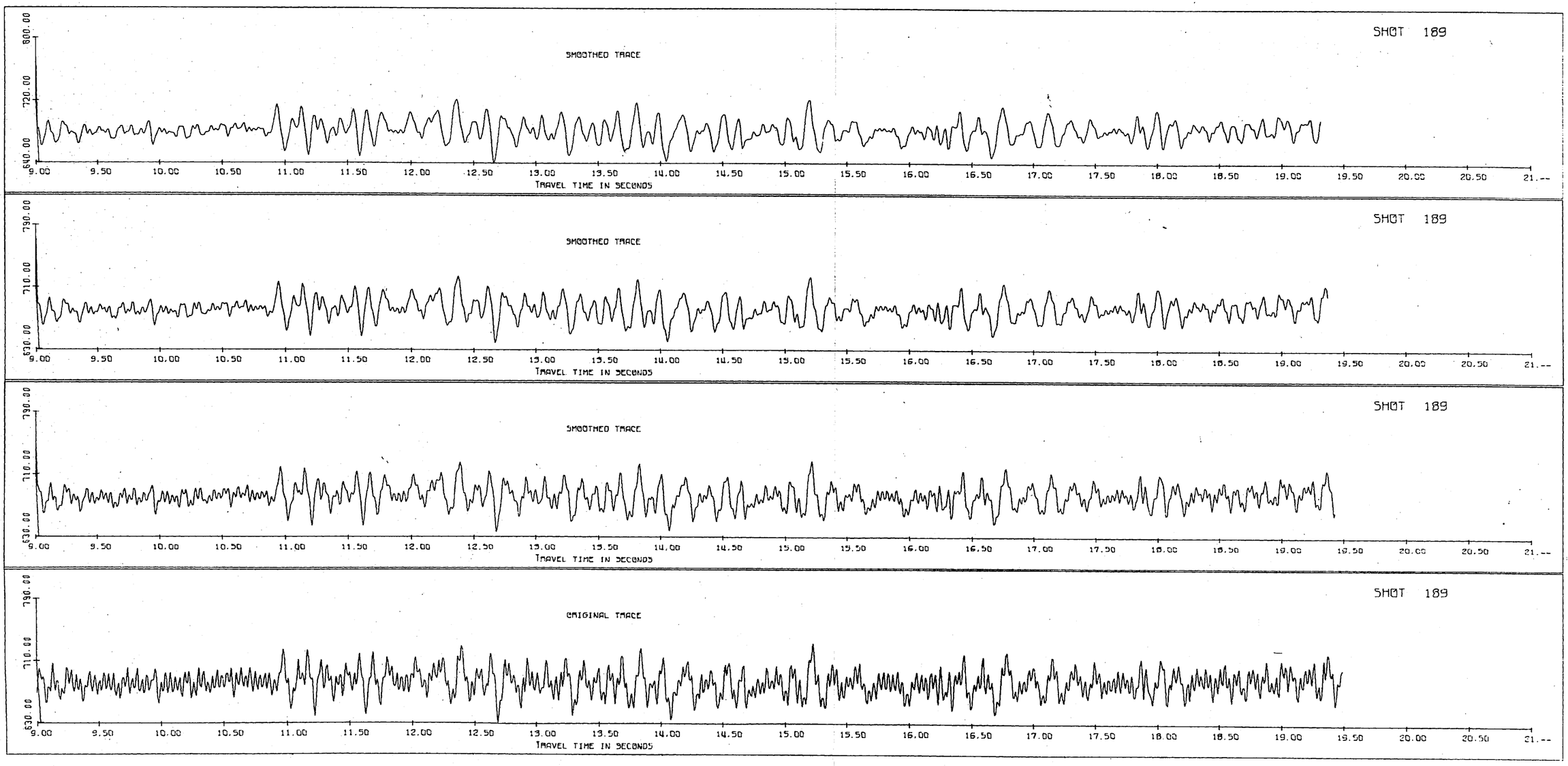

Fig.13

B0360310029001

i) the crustal structure consists of homogeneous, isotropic layers with constant velocities which change abruptly at the boundaries.

ii) The vertical plane through the geophone and the shot intersects the plane interfaces perpendicularly.

iii) The velocities of the headwaves increase with depth so that $v_i < v_k$ when $i < k$.

iv) The shot is a point source.

Two entirely different techniques were used for interpretation. Whereas all of the profiles from the Meteor work could be treated according to the well known multilayer case, various models were calculated to fit the travel times of the John Murray profiles.

3.2.1 Unreversed Profiles A and D

These two lines were shot in opposite directions as split-profiles. They were treated separately when calculating the refractors' thicknesses.

Assuming a horizontal two-dimensional multilayer case, the thicknesses could be calculated from the formula

$$T_n = 2 \sum_{k=1}^{n-1} \frac{Z_k \cdot \cos i_{kn}}{V_k}$$

where Z_k = thickness of the k^{th} refractor

V_k = its velocity of P-waves

T_n = intercept time for the n^{th} refractor

$\sin i_{kn} = V_k/V_n$ = critical angle of incidence.

3.2.1.1 Profile A

The time-distance graph is shown in Fig. 14. Five refractors with apparent velocities of 3.35, 4.42, 6.00, 7.05

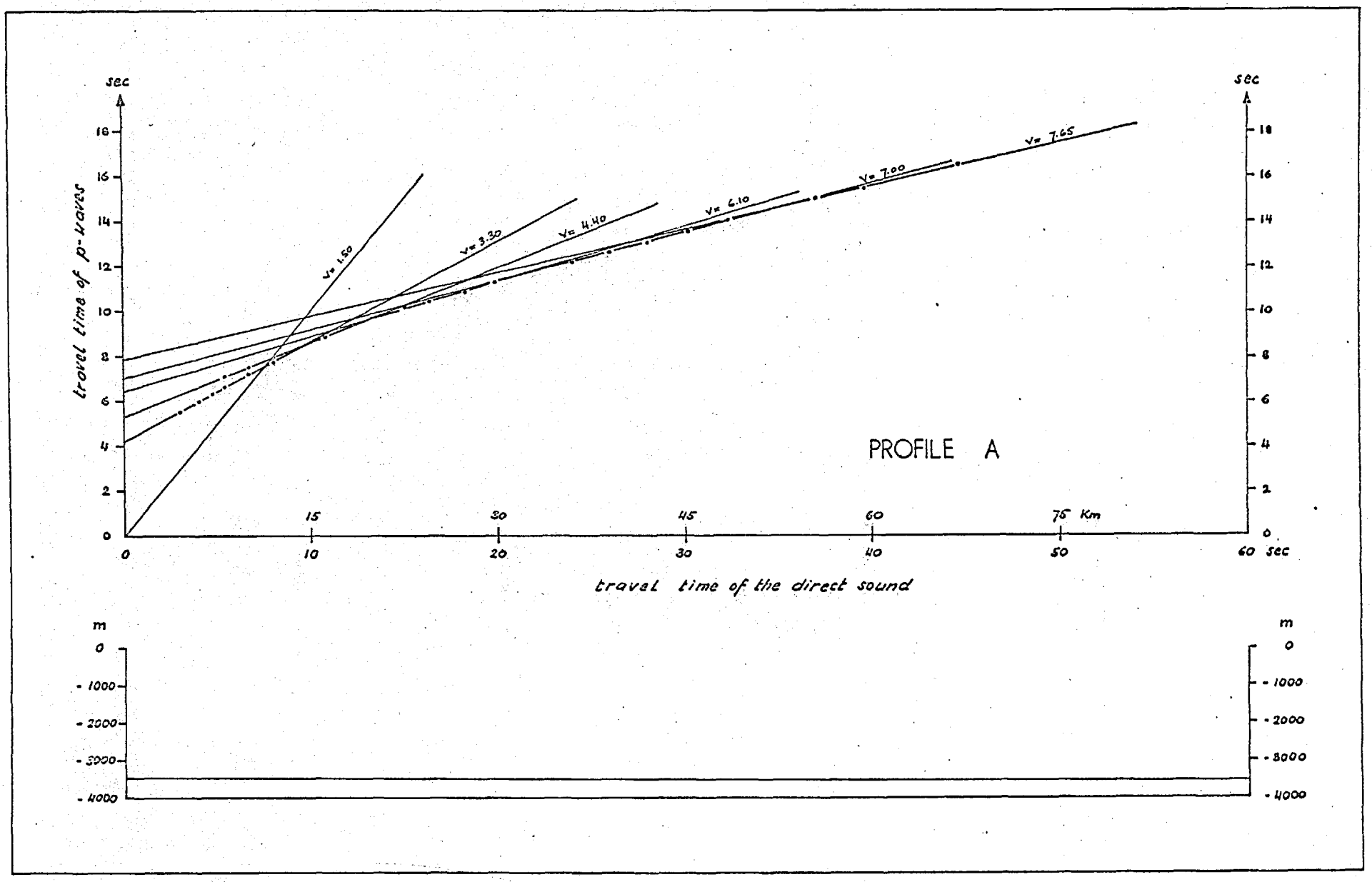
sec
travel time of p-waves
V= 1.50
V= 3.30
V= 4.40
V= 6.10
V= 7.00
V= 7.65
PROFILE A
15
30
45
60
75 Km
0
10
20
30
40
50
60 sec
travel time of the direct sound
m
0
- 1000
- 2000
- 3000
- 4000

Fig.14

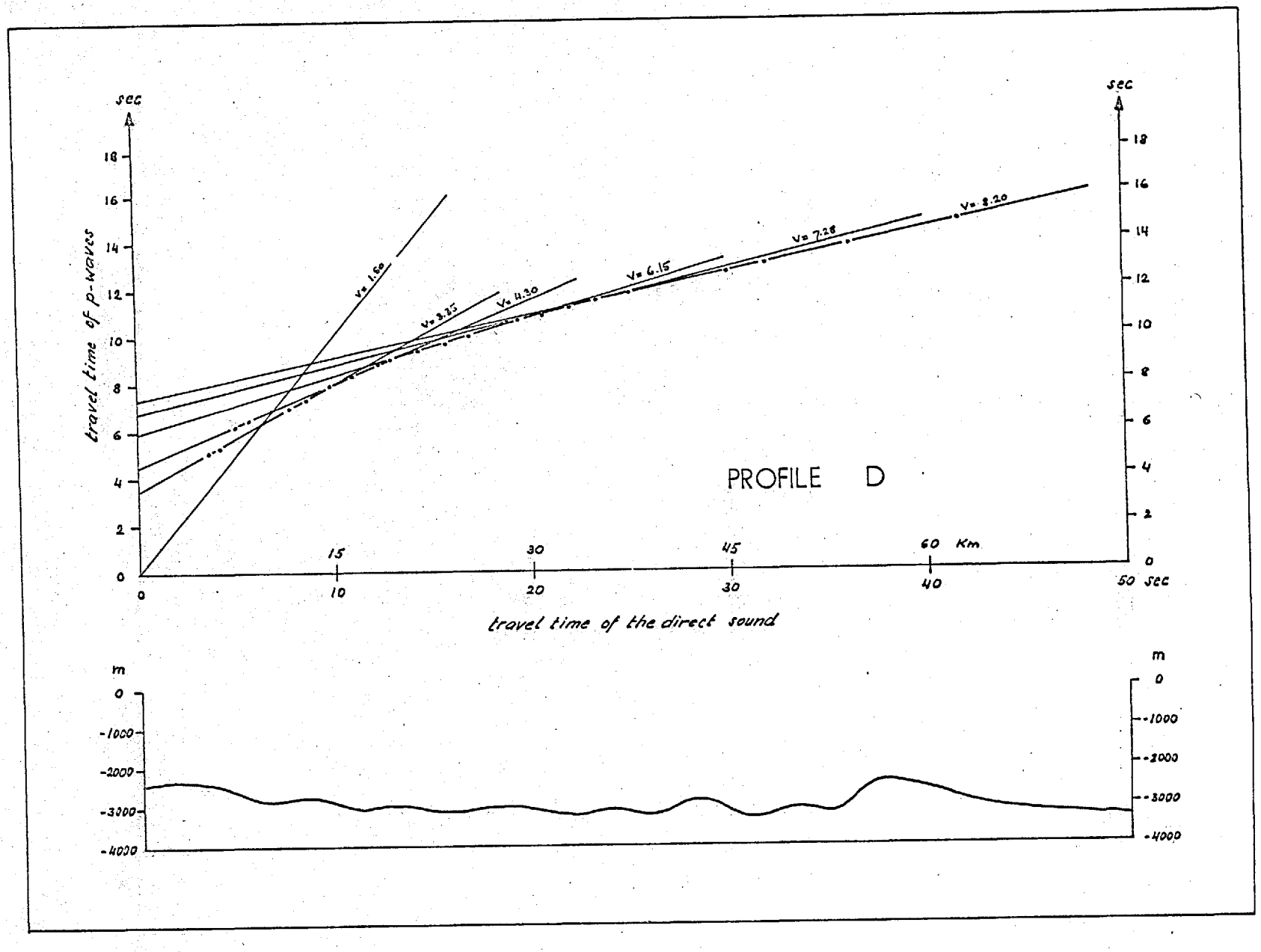
sec
travel time of p-waves
V= 1.69
V= 3.75
V= 4.30
V= 6.15
V= 7.28
V= 8.20
PROFILE D
15
30
45
60 Km
10
20
30
40
50 sec
travel time of the direct sound
m
0
-1000
-2000
-3000
-4000

Fig.15

and 7.65 km/sec were detected. Arrivals from distant shots were very weak because of the insensitivity of the recording system .. An airgun profile close by (Fig. 6) did not show any sign of low-velocity sediments (HINZ, 1967) which were not accounted for when calculating the thicknesses of the beds. Table I shows the velocities, thicknesses and depths of the refractors.

3.2.1.2 Profile D

The first arrivals of Profile D were very significant and yielded a reliable time-distance graph (Fig. 15). Consequently it was used as the key profile for interpreting the refraction lines. Fig. 16 illustrates the profile with the seismograms plotted at their respective distances from the shot. Five refractors were detected with apparent velocities of 3.00, 3.90, 5.69, 7.04 and 8.12 km/sec. The same assumptions as for profile A were used for calculating the thicknesses, shown in Table II.

3.2.2 Reversed Profile BC

The profiles B and C were effectively a reversed profile. The seismic arrivals in the profile B were not very clear owing to the fact that the line was shot in very bad weather. However, the time-distance curves showed the characteristic changes in velocity (Fig. 17).

A difficulty arose from the fact that the shallower refractors did not overlap. However, as explained by OFFICER et al.(1959), this difficulty was overcome by having a fairly close agreement of the end-to-end times.

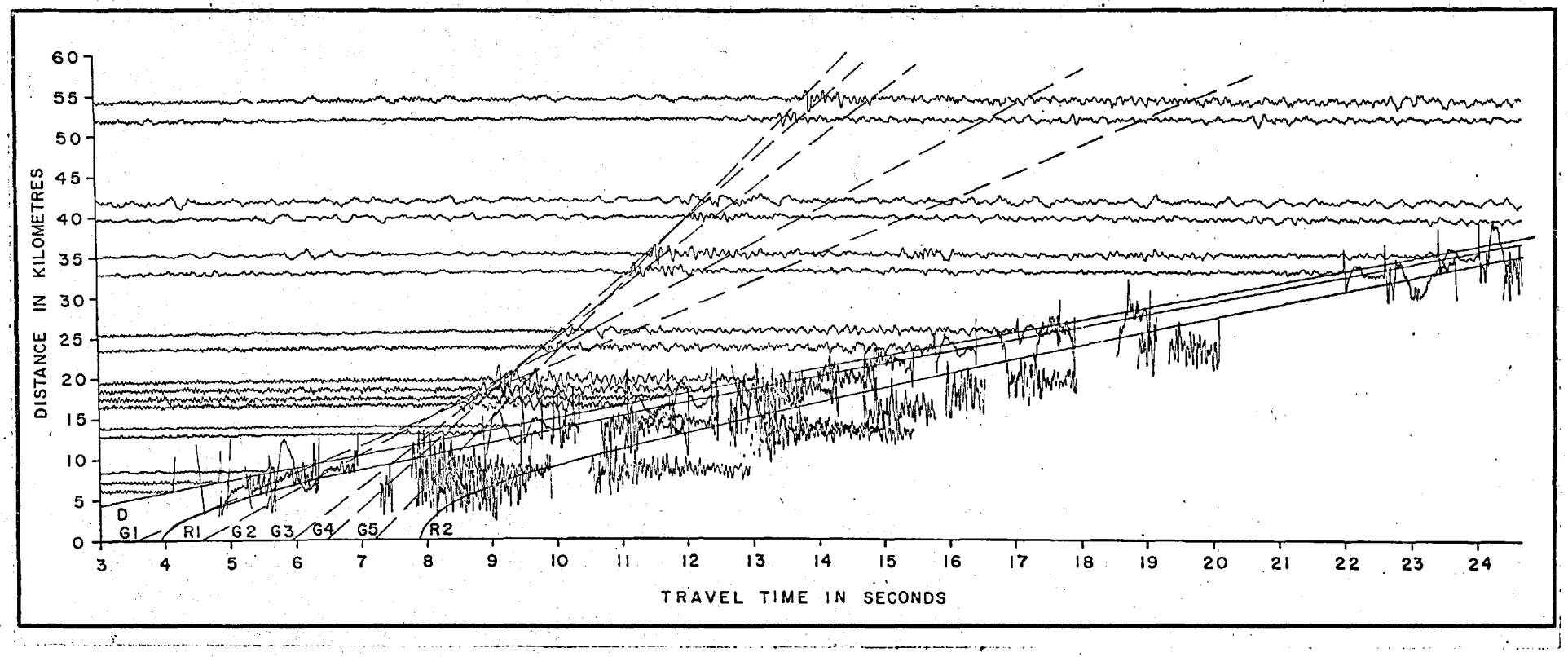
DISTANCE IN KILOMETRES
TRAVEL TIME IN SECONDS
D
G1
R1
G2
G3
G4
G5
R2

Fig.16

Table I

Velocity km/sec	Thickness km	Depth km
1.50	3.54±0.03	0
3.35±0.02	2.14±0.24	3.54±0.03
4.42±0.06	2.41±0.44	5.68±0.25
6.00±0.09	3.50±0.71	8.09±0.50
7.05±0.08	3.16±1.17	11.59±0.87
7.65±0.08		14.75±1.45

Table II

Velocity km/sec	Thickness km	Depth km
1.50	2.81±0.15	0
3.00±0.11	1.99±0.59	2.81±0.15
3.90±0.11	3.02±0.64	4.80±0.61
5.69±0.09	2.94±0.88	7.82±0.88
7.04±0.17	3.51±1.24	10.76±1.25
8.12±0.09		14.27±1.62

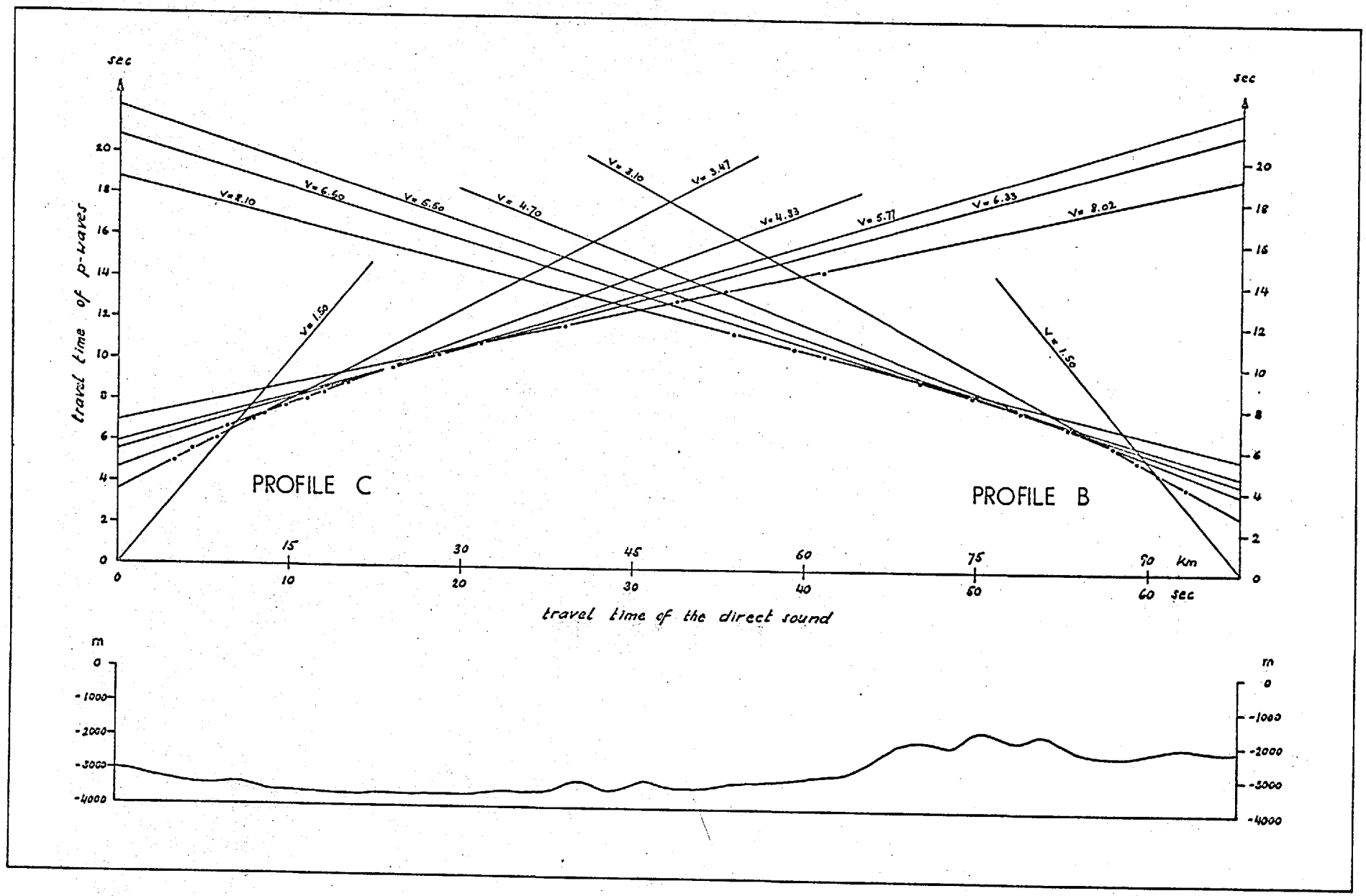
sec
travel time of p-waves
V= 8.10
V= 6.69
V= 5.50
V= 4.70
V= 3.10
V= 3.47
V= 4.33
V= 5.77
V= 6.33
V= 8.02
V= 1.50
V= 1.50
PROFILE C
PROFILE B
0 15 30 45 60 75 90 km
0 10 20 30 40 50 60 sec
travel time of the direct sound
m
0
-1000
-2000
-3000
-4000

Fig.17

Table III

Profile B

Velocity km/sec	Thickness km	Depth km
1.50	2.59±0.14	0
3.15±0.13	1.40±0.80	2.59±0.14
4.24±0.67	3.73±1.01	3.99±0.81
5.64±0.28	1.45±1.28	7.72±1.30
6.72±0.38	2.87±1.64	9.17±1.82
8.10±0.57		12.04±2.45

Profile C

Velocity km/sec	Thickness km	Depth km
1.50	3.37±0.09	0
3.30±0.07	1.70±0.33	3.37±0.09
4.75±0.04	2.20±0.69	5.07±0.34
5.77±0.23	1.71±1.26	7.27±0.77
6.60±0.10	3.25±1.45	8.98±1.48
8.01±0.29		12.23±2.07

Five refractors were detected having the following apparent velocities

	V_1	V_2	V_3	V_4	V_5	
Profile B	3.15	4.24	5.64	6.72	8.10	km/sec
Profile C	3.30	4.75	5.77	6.60	8.00	km/sec

Calculations of the refractors' thicknesses were made for the two-dimensional multilayer case with dipping beds according to WEBER's method (in RYBACH, 1962). Table III shows the velocity, thickness and depth of various layers.

3.3 Interpretation of the John Murray Work

Standard interpretational techniques to determine the crustal structure could not be applied to the refraction data obtained from the John Murray expedition, because unlike the standard pattern, recording stations were located on various islands while shots were fired in the surrounding sea. A method had to be devised which would account for this configuration.

It was arrived at by comparing observed travel times with theoretical ones, computed for various structural models which were based on geological data of marine volcanoes. In order to avoid many theoretical travel time plots being produced until one matched the observed travel times, a least-squares method was devised. It automatically computed the thickness of various layers after all other parameters influencing travel times were eliminated, i.e. the slope of an island, the velocity of the refractors, dips of interfaces and the shot-detector distances.

Hence differences between calculated and observed travel times were assumed to be caused only by variations in the thicknesses of the refractors. In order to find the best fitting set of thicknesses Z_i these differences had to be minimised:

$$E^2 = \sum_{r=1}^{n} \left[T_r^c - T_r^o\right]^2 \qquad (1)$$

where T_r^c = calculated time for refractor r

T_r^o = observed time for refractor r

To reduce the error E^2, equation (1) is partially differentiated with respect to Z_i and is equated to zero:

$$\frac{\partial E^2}{\partial Z_i} = 0 \qquad \text{for } i=1, \ldots n \qquad (2)$$

Calculation of the Z_i is hence reduced to the problem of solving a set of simultaneous linear equations of the type of equation (2). Let the travel times of the P - waves for a five layer case be

$$\begin{aligned} T_1^c &= a_1 z_1 + b_1 \\ T_2^c &= a_2 z_1 + b_2 z_2 + c_2 \\ T_3^c &= a_3 z_1 + b_3 z_2 + c_3 z_3 + d_2 \\ T_4^c &= a_4 z_1 + b_4 z_2 + c_4 z_3 + d_3 z_4 + f_1 \end{aligned} \qquad (3)$$

Substituting equation (3) in equation (1) yields:

$$\begin{aligned} E^2 = &\left[a_1 z_1 + b_1 - T_1^o\right]^2 \\ &+ \left[a_2 z_1 + b_2 z_2 + c_2 - T_2^o\right]^2 \\ &+ \left[a_3 z_1 + b_3 z_2 + c_3 z_3 + d_2 - T_3^o\right]^2 \\ &+ \left[a_4 z_1 + b_4 z_2 + c_4 z_3 + d_3 z_4 + f_1 - T_4^o\right]^2 \end{aligned} \qquad (4)$$

Equation (4) was differentiated according to (2) and the following expressions were obtained:

$$\frac{\partial E}{\partial z_1} = \alpha_1 z_1 + \beta_1 z_2 + \gamma_1 z_3 + \delta_1 z_4 + \varepsilon_1 = 0$$
$$\frac{\partial E}{\partial z_2} = \beta_1 z_1 + \beta_2 z_2 + \gamma_2 z_3 + \delta_2 z_4 + \varepsilon_2 = 0$$
$$\frac{\partial E}{\partial z_3} = \gamma_1 z_1 + \gamma_2 z_2 + \gamma_3 z_3 + \delta_3 z_4 + \varepsilon_3 = 0$$
$$\frac{\partial E}{\partial z_4} = \delta_1 z_1 + \delta_2 z_2 + \delta_3 z_3 + \delta_4 z_4 + \varepsilon_4 = 0 \qquad (5)$$

where the $\alpha_i, \beta_i, \gamma_i$ and δ_i are functions of a_i, b_i, c_i, d_i and f_i.

The coefficients of equation (5) are calculated for all the shot points of one profile and added together. In a matrix notation, this can be expressed as

$$\underbrace{\begin{bmatrix} \sum \alpha_1 & \sum \beta_1 & \sum \gamma_1 & \sum \delta_1 \\ \sum \beta_1 & \sum \beta_2 & \sum \gamma_2 & \sum \delta_2 \\ \sum \gamma_1 & \sum \gamma_2 & \sum \gamma_3 & \sum \delta_3 \\ \sum \delta_1 & \sum \delta_2 & \sum \delta_3 & \sum \delta_4 \end{bmatrix}}_{A} \times \underbrace{\begin{bmatrix} z_1 \\ z_2 \\ z_3 \\ z_4 \end{bmatrix}}_{Z} = \underbrace{\begin{bmatrix} \sum -\varepsilon_1 \\ \sum -\varepsilon_2 \\ \sum -\varepsilon_3 \\ \sum -\varepsilon_4 \end{bmatrix}}_{E} \qquad (6)$$

An inversion of matrix A enables the z_i to be determined:

$$Z = A^{-1} \times E$$

or

$$z_i = \sum_{r=1}^{n} A_{ir}^{-1} \times E_r \qquad (7)$$

The coefficients of the matrices A and E were determined with the use of a digital computer for various models.

This least squares procedure has various advantages over the conventional intercept time methods, which are

i) authentic observed travel times are used in the computations instead of extrapolated theoretical ones;

ii) all the thicknesses are fitted simultaneously to the travel times so that the overall error is diminished to a minimum;

iii) no errors computed from the shallower refractors are transferred to the deeper ones, thus giving more accurate thicknesses and depths of individual refractors;

iv) the results obtained from the least squares fit are final, thus obviating the necessity of a master curve.

3.3.1 Model A

While constructing model A, the following geophysical results obtained on various volcanic islands were taken into consideration. RAITT (1954, 1957) found a crustal structure consisting of four layers for some of the atolls in the Marshall Islands. The core of the atolls is built up of material with a velocity of 5.5 - 6.15 km/sec, overlain by a layer with a velocity of 3.5 - 4.75 km/sec. These two layers are in turn covered with material having a velocity of 3.0 - 3.5 km/sec. The crest of the atoll consists of a low velocity layer of 2.4 - 2.6 km/sec. With the exception of the topmost layer, the refractors are almost parallel to one another and follow the topographic relief.

FURUMOTO and WOOLLARD (1965) found a similar structure for some of the islands of the Hawaiian archipelago where the upper layers with velocities of 3.7 - 4.2 km/sec and 5.0 - 6.4 km/sec follow the bathymetry quite closely.

Under major rift zones, mantle-like material with a velocity of about 7.5 km/sec is observed at the shallow depth of 5-6 km.

The Koolau volcano in the Hawaiian Islands consists chiefly of four layers (FURUMOTO et al.,1965). The upper three again seem to follow the topography from the seabed up to the summit of the volcano.

LAUGHTON et al.(1960) established a crustal model for a seamount north of Madeira where a layer of relatively low velocity covered a "core" of considerably higher velocity.

In a geological study of volcanoes which erupted under the inland iceshield of Iceland, JONES (1966) found that the core of those volcanoes was built up by a steep sided pile of pillow lava buried under a mantle of clastic material and scree. The maximum slopes of the scree were 20°-25° and of the core 30°.

As a result from preliminary investigations and geological data it was clear that the various recording stations were located on the rift zones of the volcanic islands where the mantle-like basement material can be expected to be shallow (FURUMOTO and WOOLLARD,1965). Model A was, therefore, constructed by assuming that the layers found under the ocean were parallel to one another and were the continuation of the structural features of the islands. Fig.18 illustrates the cross-section through the model. The angle DIP depended on the topography of the various islands. The thicknesses of the layers were uniform throughout the model. The beds on the island flanks followed the average slope of the island,parallel to one another, while those under the open sea were horizontal.

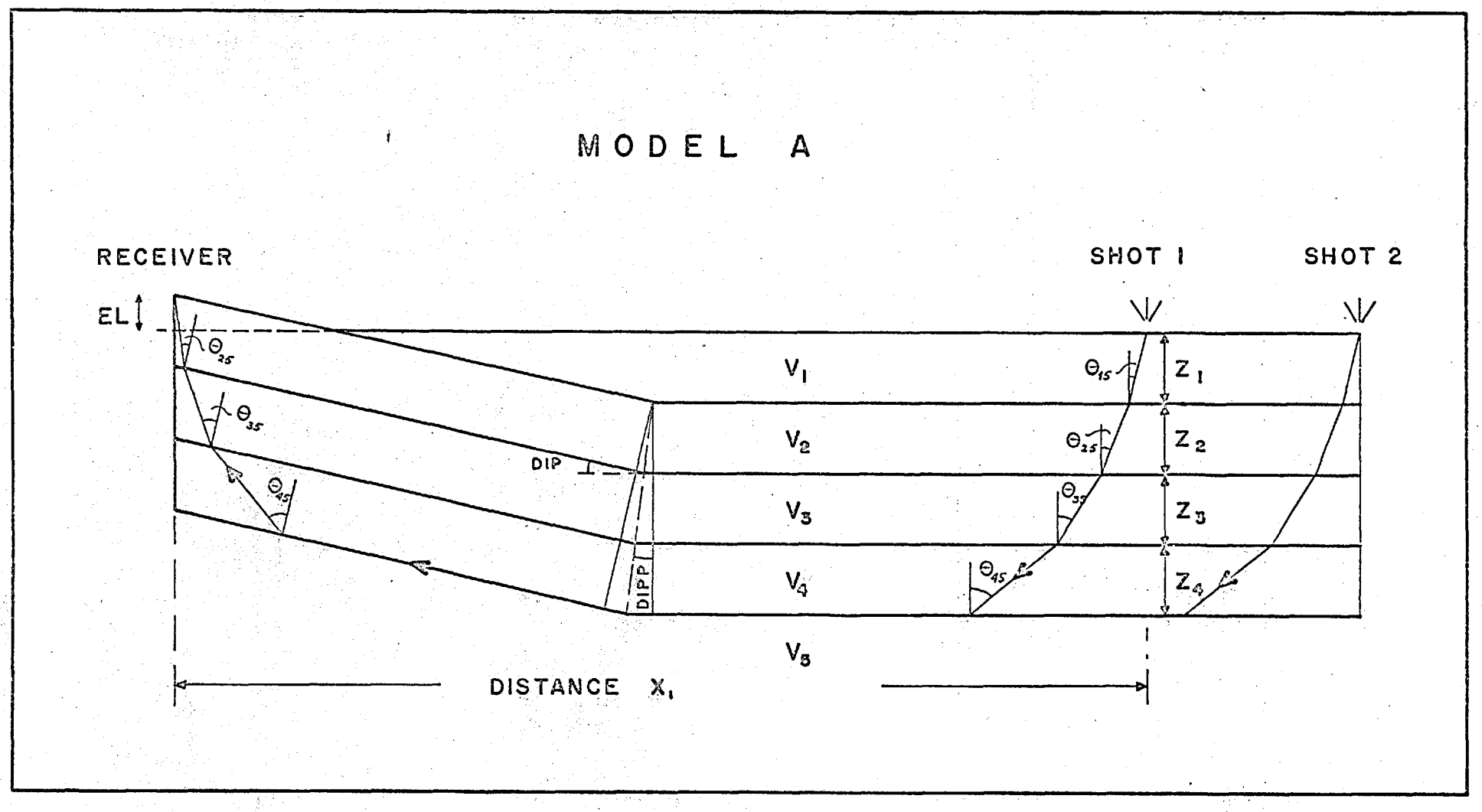
MODEL A
RECEIVER
SHOT 1
SHOT 2
EL
Θ_{25}
Θ_{35}
Θ_{45}
DIP
DIPP
V_1
V_2
V_3
V_4
V_5
Θ_{15}
Θ_{25}
Θ_{35}
Θ_{45}
Z_1
Z_2
Z_3
Z_4
DISTANCE X_1

Fig.18

The individual travel times for four refractors were:

$$T_1 = \left(\frac{\cos\theta_{12}}{V_1} + \frac{1 - \cos DIP}{\sin DIP \, V_2}\right) z_1 + \frac{x}{V_2} + \frac{EL(1 - \cos DIP)}{\sin DIP \cdot V_2}$$

$$T_2 = \left(\frac{\cos\theta_{13}}{V_1} + \frac{1 - \cos DIP}{\sin DIP \cdot V_3}\right) z_1 + \left(\frac{2\cos\theta_{23}}{V_2} + \frac{2\tan DIPP}{V_3}\right) z_2 + \frac{x}{V_3} + \frac{EL(1 - \cos DIP)}{\sin DIP \cdot V_3}$$

$$T_3 = \left(\frac{\cos\theta_{14}}{V_1} + \frac{1 - \cos DIP}{\sin DIP \cdot V_4}\right) z_1 + \left(\frac{2\cos\theta_{24}}{V_2} + \frac{2\tan DIPP}{V_4}\right) z_2 + \left(\frac{2\cos\theta_{34}}{V_3} + \frac{2\tan DIPP}{V_4}\right) z_3 + \frac{x}{V_4} + \frac{EL(1 - \cos DIP)}{\sin DIP \cdot V_4}$$

$$T_4 = \left(\frac{\cos\theta_{15}}{V_1} + \frac{1 - \cos DIP}{\sin DIP \cdot V_5}\right) z_1 + \left(\frac{2\cos\theta_{25}}{V_2} + \frac{2\tan DIPP}{V_5}\right) z_2 + \left(\frac{2\cos\theta_{35}}{V_3} + \frac{2\tan DIPP}{V_5}\right) z_3 + \left(\frac{2\cos\theta_{45}}{V_4} + \frac{2\tan DIPP}{V_5}\right) z_4 + \frac{x}{V_5} + \frac{EL(1 - \cos DIP)}{\sin DIP \cdot V_5}$$

where DIP = average slope on island

DIPP = DIP/2

EL = elevation of the recording stations

Z_i = thicknesses of the refractors as variables

V_i = velocities of refractors

$\sin \theta_{ik} = V_i/V_k$

The above formulae are valid only for points at distances

$$x \geq \frac{z_1 + EL}{\tan DIP} + \sum_{i=1}^{k} z_i \cdot \tan\theta_{i,i+1} - \sum_{i=2}^{k} z_i \cdot \tan DIPP$$

3.3.2 Model B and Model C

These two models were constructed to interpret the travel times recorded at Vilaflor on Tenerife, because model A did not fit them properly. When constructing these models, geophysical results obtained on some volcanoes in the Hawaiian islands were taken into consideration.

ADAMS and FURUMOTO (1965) carried out a refraction survey over the Koolau volcano in Hawaii and found a "plug-like" body with a velocity of 7.6 km/sec buried under only 1.6 km of material with a velocity of 4.63 km/sec. This body had a circular shape with an upper radius of 4 km.

STRANGE et al. (1965) computed a structural model of the Koolau volcano which corresponded with the observed gravity anomaly. They assumed a cylindrical "high density body" of 3.2 g/cc with an upper radius of 4 km increasing stepwise to an 8 km radius at a depth of 13 km.

MACFARLANE and RIDLEY (1968) assumed a similar "high density body" to explain the Bouguer anomaly over Tenerife in the Canary Islands. This body had an upper radius of 12 km and extended from 2 km to 16 km depth.

In a recent geological survey of the island of La Palma in the Canaries, MIDDLEMOST (1969) found a basal complex in the Caldera de Taburiente which consisted of mafic and ultramafic rocks (olivine-rich basalts, dunites etc.)

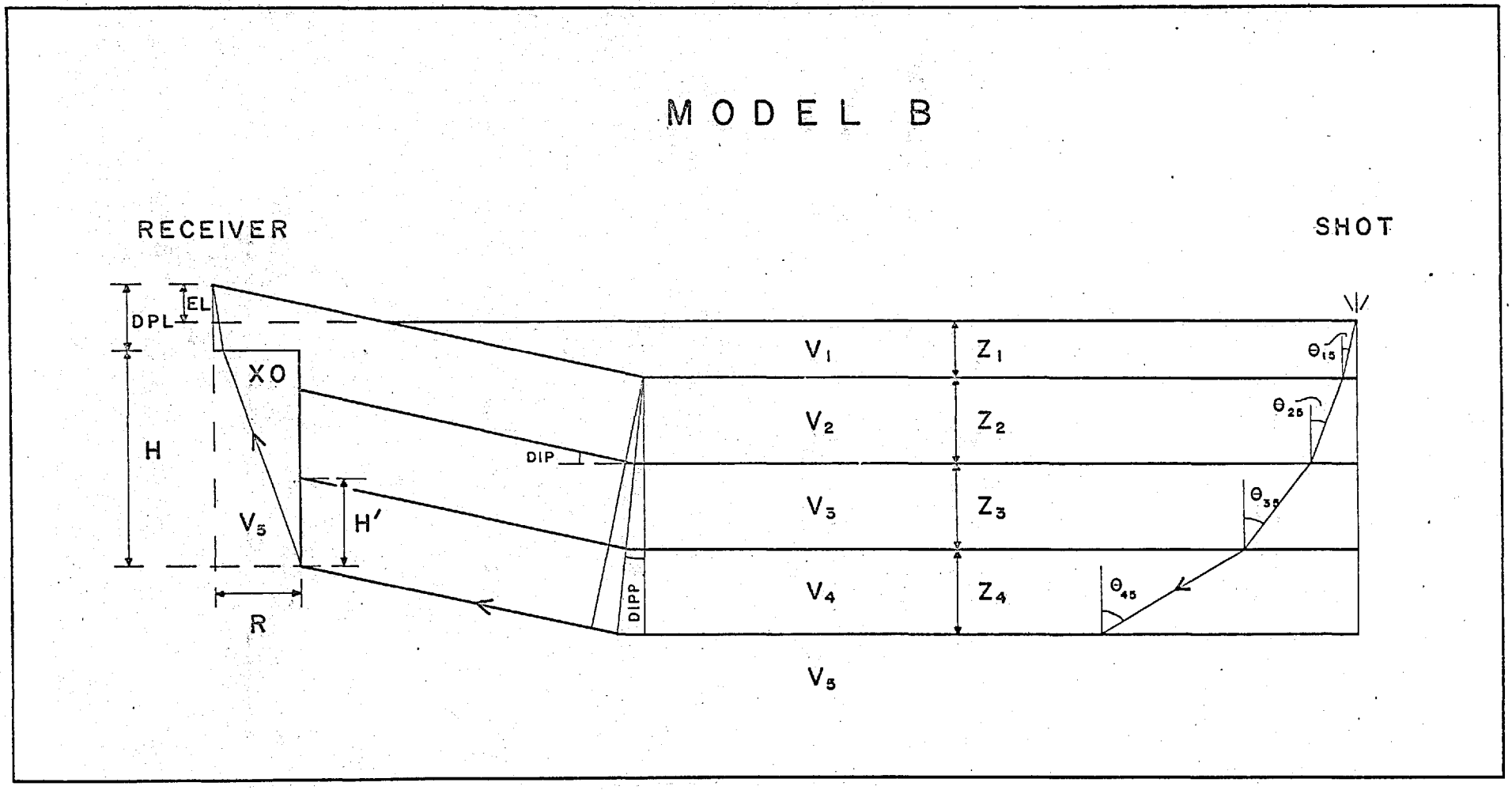
MODEL B
RECEIVER
SHOT
DPL
EL
XO
H
H'
V5
R
DIP
DIPP
V1
V2
V3
V4
V5
Z1
Z2
Z3
Z4
θ15
θ25
θ35
θ45

Fig.19

and which most probably represented the surface of a "high density body".

The recording station of Vilaflor was at an altitude of 1210 metres and approximately 10 km inshore, close to the centre of the Bouguer anomaly. The travel times were therefore expected to be influenced by the "high density body" underneath. But to account for the totally unknown structure of this body, more assumptions had to be made than were desirable.

Since this "plug" was expected to be present at a shallow depth, model B was constructed so that this body penetrated all the layers of model A under the island. Fig. 19 shows this model where the "plug" is assumed to be cylindrical and to have a velocity equal to that of the basement layer.

The travel times for four refractors were:

$$T_1 = \left(\frac{\cos\Theta_{12}}{V_1} + \frac{1 - \cos DIP}{\sin DIP \cdot V_2}\right) z_1 + \frac{x}{V_2} + \frac{EL(1 - \cos DIP)}{\sin DIP \cdot V_2}$$

$$T_2 = \left(\frac{\cos\Theta_{13}}{V_1} + \frac{1 - \cos DIP}{\sin DIP \cdot V_3}\right) z_2 + \left(\frac{\cos\Theta_{23}}{V_2} + \frac{2\tan DIPP - \tan DIP}{V_3} - \frac{AL2}{\sin DIP \cdot \cos^2 DIP \cdot V_5 \cdot DN2} + \frac{V_3}{\sin DIP \cdot \cos DIP \cdot V_5^2 \cdot DN2}\right) z_2 +$$

$$\left(DPL \left\{ \frac{V_2(1 - DN2)}{DE2\ V_5^2\ DN2} - \frac{V_3}{\sin DIP\ V_5^2\ DN2} + \frac{1}{DE2\ V_2} + AL2 \left(\frac{1}{\sin DIP \cos DIP \cdot V_5 \cdot DN2} - \frac{V_2}{\cos DIP \cdot V_5 V_3 \cdot DE2 \cdot DN2} \right) \right\} \right)$$

$$\frac{x}{V_3} + \frac{EL(1 - \cos DIP)}{\sin DIP \cdot V_3}$$

$$T_3 = \left(\frac{\cos\Theta_{14}}{V_1} + \frac{1 - \text{cosDIP}}{\text{sinDIP } V_4}\right)z_1 + \left(\frac{\cos\Theta_{24}}{V_2} + \frac{2\text{tanDIPP} - \text{tanDIP}}{V_4} - \right.$$

$$\left.\frac{AL3}{DN3\ \text{sinDIP}\ \cos^2\text{DIP}\ V_5} + \frac{V_4}{\text{sinDIP}\ \text{cosDIP}\ V_5^2\ DN3}\right)z_2 +$$

$$\left(\frac{\cos\Theta_{34}}{V_3} + \frac{2\text{tanDIPP} - \text{tanDIP}}{V_4} - \frac{AL3}{\text{sinDIP}\ \cos^2\text{DIP}\ V_5\ DN3}\right. +$$

$$\left.\frac{V_4}{\text{sinDIP}\ \text{cosDIP}\ V_5^2\ DN3}\right)z_3 + \left(\text{DPL}\left\{\frac{V_2(1 - DN3)}{DE3\ V_5^2\ DN3} - \right.\right.$$

$$\frac{V_4}{\text{sinDIP}\ V_5^2\ DN3} + \frac{1}{DE3\ V_2} + AL3\left(\frac{1}{\text{sinDIP}\ \text{cosDIP}\ V_5\ DN3} - \right.$$

$$\left.\left.\left.\frac{V_2}{\text{cosDIP}\ V_4 V_5 DE3\ DN3}\right)\right\}\right) + \frac{x}{V_4} + \frac{EL(1 - \text{cosDIP})}{\text{sinDIP}\ V_4}$$

$$T_4 = \left(\frac{\cos\Theta_{15}}{V_1} + \frac{1 - \text{cosDIP}}{\text{sinDIP}\ V_5}\right)z_1 + \left(\frac{\cos\Theta_{25}}{V_2} + \frac{2\text{tanDIPP} - \text{tanDIP}}{V_5}\right)z_2 +$$

$$\left(\frac{\cos\Theta_{35}}{V_3} + \frac{2\text{tanDIPP} - \text{tanDIP}}{V_5}\right)z_3 + \left(\frac{\cos\Theta_{45}}{V_4} + \frac{2\text{tanDIPP} - \text{tanDIP}}{V_5}\right)z_4 +$$

$$\frac{x}{V_5} + \frac{EL(1 - \text{cosDIP})}{\text{sinDIP}\ V_5} - \frac{R}{\text{cosDIP}\ V_5} + \frac{H}{V_5 \cos\left(\arctan\frac{XO}{H}\right)} +$$

$$\frac{DPL}{V_2 \cos\left(\arctan\frac{R - XO}{DPL}\right)}$$

where $AL2 = \sqrt{1 - \sin^2\text{DIP}\,\frac{V_5^2}{V_3^2}}$

$AL3 = \sqrt{1 - \sin^2\text{DIP}\,\frac{V_5^2}{V_4^2}}$

$DE2 = \sqrt{1 - \frac{V_2^2}{V_5^2} + \sin^2\text{DIP}\,\frac{V_2^2}{V_3^2}}$ $\qquad DN2 = 1 - \frac{AL2\ V_3}{\text{cosDIP}\ V_5}$

$DE3 = \sqrt{1 - \frac{V_2^2}{V_5^2} + \sin^2\text{DIP}\,\frac{V_2^2}{V_4^2}}$ $\qquad DN3 = 1 - \frac{AL3\ V_4}{\text{cosDIP}\ V_5}$

R,XO and H are as shown in Fig. 20.

Z_i = variable thicknesses

DPL = depth to the plug

V_i = velocities of the refractors

DIP = average slope of the topography

As in the case of model A, the above formulae were valid only for points beyond the foot of the island.

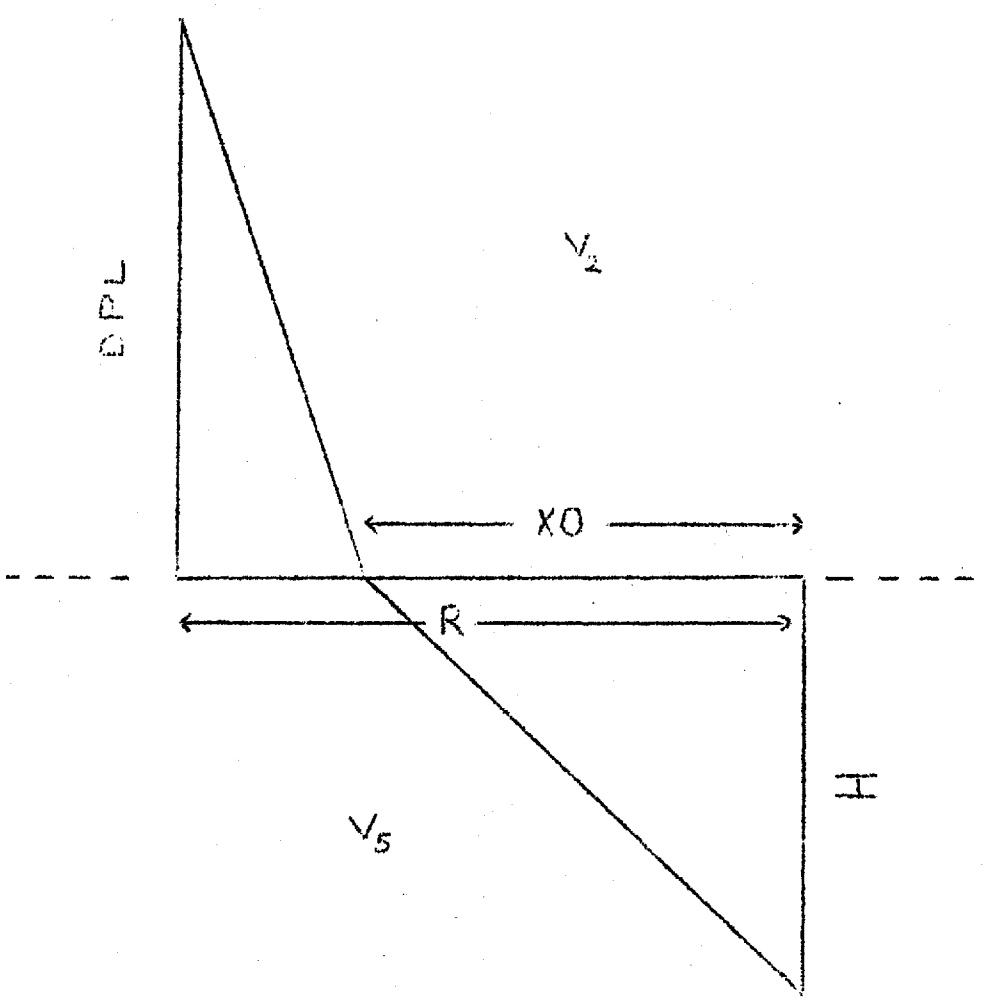

Fig.20

The terms with (arctan XO/H) and arctan (R-XO/DPL) in the expression for T_4 had to be determined before a least squares fitting was possible. Fig. 20 shows the ray path from the lower boundary of the plug to the receiver. The total travel time is

$$T(XO) = T_1 + T_2 = \frac{\sqrt{H^2 + XO^2}}{V_5} + \frac{\sqrt{DPL^2 + (R-XO)^2}}{V_2} \qquad (1)$$

where XO is the only variable. To satisfy Fermat's principle, T(XO) must be a minimum or dT/dXO = 0:

$$\frac{dT}{dXO} = \frac{XO}{V_5\sqrt{H^2 + XO^2}} + \frac{-(R-XO)}{V_2\sqrt{DPL^2 + (R-XO)^2}} = 0 \qquad (2).$$

and transformed is

$$\frac{XO}{V_5\sqrt{H^2 + XO^2}} = \frac{R - XO}{V_2\sqrt{DPL^2 + (R-XO)^2}} \qquad (3)$$

It is evident that equation (3) is Snell's law. The solution of equation (3) for XO required the solution of a polynomial of fourth order.

A computer programme was written to calculate the values of XO for various sets of R and H, both expressed as functions of DPL. Only one of the four roots had a physical significance, namely when the positive value of XO was smaller than R.

The correct values of Z_i were obtained for two conditions, namely when for a definite value of DPL the radius R was

$$R = \frac{(Z_2 + Z_3) \cdot V_4}{\sin DIP.\cos^2 DIP} + DPL \left(\frac{V_2}{V_5 DE3} - \frac{V_4}{\sin DIP.V_5} \right) \frac{AL3}{DN3}$$

and Z_n equal to H', where

$H' = H.\cos DIP + DPL.\cos DIP - R.\sin DIP - (Z_2 + Z_3)$.

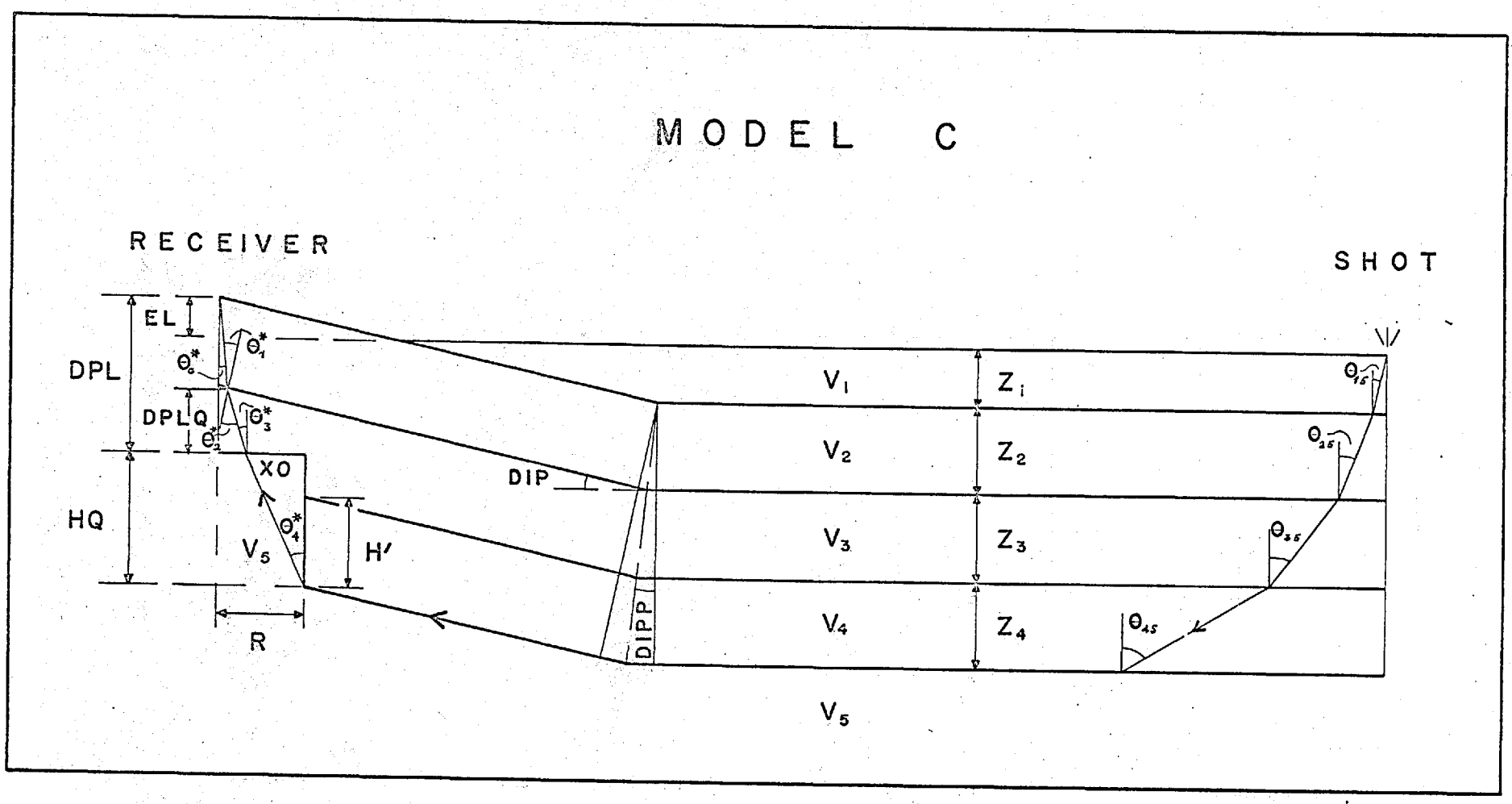
MODEL C
RECEIVER
SHOT
EL
DPL
DPLQ
HQ
XO
R
H'
DIP
DIPP
V1
V2
V3
V4
V5
Z1
Z2
Z3
Z4

Fig.21

This calculation was implemented for various values of DPL. However, these two conditions were never satisfied and, consequently, the model failed to fit the travel times of Vilaflor.

Because the depth of the plug could not be depressed below Z_2 without violating the original assumptions, this model had to be replaced.

Model C, as shown in Fig. 21, had the same "plug" which intruded all but the uppermost layer in the island. The following travel times were calculated for four refractors:

$$T_1 = \left(\frac{\cos\Theta_{12}}{V_1} + \frac{1 - \cos DIP}{\sin DIP \cdot V_2}\right) z_1 + \frac{x}{V_2} + \frac{EL(1 - \cos DIP)}{\sin DIP \cdot V_2}$$

$$T_2 = \left(\frac{\cos\Theta_{13}}{V_1} + \frac{1 - \cos DIP}{\sin DIP \cdot V_3}\right) z_1 + \left(\frac{2\cos\Theta_{23}}{V_2} + \frac{2\tan DIPP}{V_3}\right) z_2 + \frac{x}{V_3} + \frac{EL(1 - \cos DIP)}{\sin DIP \cdot V_3}$$

$$T_3 = \left(\frac{\cos\Theta_{14}}{V_1} + \frac{1 - \cos DIP}{\sin DIP \cdot V_4}\right) z_1 + \left[\frac{\cos\Theta_{24}}{V_2} + \frac{2\tan DIPP - \tan DIP}{V_4}\right.$$
$$\frac{\tan\alpha_4}{\cos^2 DIP \cdot V_4 \cdot Q3} + \frac{1}{\cos\alpha_4 \cdot \cos DIP \cdot V_5 \cdot Q3} + \frac{1}{\cos\alpha_1 \cdot V_1} +$$
$$\frac{\tan\alpha_3}{\cos\alpha_1}(\sin\alpha_2 - \cos\alpha_2)\left\{\frac{1}{\sin\alpha_4 \cdot V_5 \cdot Q3} + \frac{1}{V_3(\sin\alpha_3 - \cos\alpha_3 \cdot \tan\alpha_2)} - \right.$$
$$\left.\left.\frac{1}{\cos DIP \cdot V_4 \cdot Q3} - \frac{1}{\sin\alpha_4 \cdot V_5}\right\}\right] \cdot z_2 + \left(\frac{\cos\Theta_{34}}{V_3} + \frac{2\tan DIPP' - \tan DIP}{V_4} - \right.$$
$$\left.\frac{\tan\alpha_4}{\cos^2 DIP \cdot V_4 \cdot Q3} + \frac{1}{\cos\alpha_4 \cdot \cos DIP \cdot V_5 \cdot Q_3}\right) z_3 + \frac{x}{V_4} + \frac{EL(1 - \cos DIP)}{\sin DIP \cdot V_4} +$$
$$DPL\left\{\frac{\tan\alpha_4 - \tan\alpha_3}{\cos DIP \cdot V_4 \cdot Q3} - \frac{1}{\cos\alpha_4 \cdot V_5 \cdot Q3} + \frac{\tan\alpha_3 - \tan\alpha_2}{V_3 \cdot (\sin\alpha_3 - \cos\alpha_3 \cdot \tan\alpha_2)} + \right.$$
$$\left.\tan\alpha_3\left(\frac{1}{\sin\alpha_1 \cdot V_5 \cdot Q3} - \frac{1}{\sin\alpha_4 \cdot V_5}\right)\right\}$$

$$T_4 = \left(\frac{\cos\theta_{15}}{V_1} + \frac{1 - \cos DIP}{\sin DIP \cdot V_5}\right)z_1 + \left(\frac{\cos\theta_{25}}{V_2} + \frac{2\tan DIPP}{V_5} - \frac{\tan\theta_1^*}{\cos\theta_1^* \cdot V_2}\right)z_2 + \left(\frac{\cos\theta_{35}}{V_3} + \frac{2\tan DIPP}{V_5}\right)z_3 + \left(\frac{\cos\theta_{45}}{V_4} + \frac{2\tan DIPP}{V_5}\right)z_4 + \frac{x}{V_5} + \frac{EL(1 - \cos DIP)}{\sin DIP \cdot V_5} + \frac{HQ}{\cos(\arctan\frac{XO}{HQ}) \cdot V_5}(1 - \sin(\theta_4^* + DIP)) + \frac{DPLQ}{\cos(\arctan\frac{RQ-XO}{DPLQ})}\left(\frac{1}{V_3} - \frac{\sin\theta_2^*}{V_5}\right)$$

where $\sin\alpha_4 = \sqrt{1 - \sin^2 DIP \frac{V_5^2}{V_4^2}}$

$$\sin\alpha_3 = \sin\alpha_4 \cdot \frac{V_3}{V_5}$$

$$\sin\alpha_2 = \sin(\arcsin(\sin\alpha_4 \frac{V_3}{V_5}) + DIP)$$

$$\sin\alpha_1 = \sin\alpha_2 \frac{V_2}{V_3}$$

$$Q3 = 1 - \tan DIP \cdot \tan\alpha_4$$

$$\sin\theta_1^* = \frac{V_2}{V_3}\sin(\arctan\frac{RQ-XO}{DPLQ} + DIP)$$

$$\sin\theta_2^* = \sin(\arctan\frac{RQ-XO}{DPLQ} + DIP)$$

$$\sin(\theta_4^* + DIP) = \sin(\arctan\frac{XO}{HQ} + DIP)$$

As for model B, a table of values for XO was computed for various sets of RQ and HQ as functions of DPLQ.

The Z_i were fitted to the travel times so that the following conditions were satisfied

$$RQ = R - \frac{Z_2 \cdot \sin\theta_0^*}{\cos\theta_1^*}$$

$$DPLQ = DPL - \frac{Z_2 \cdot \cos\theta_0^*}{\cos\theta_1^*}$$

$$H' = HQ.\cos DIP + DPL.\cos DIP - R.\sin DIP - (Z_2 + Z_3)$$

where $\theta_0^* = \theta_1^* - DIP$ and θ_1^* as in Fig. 21. and

$$R = \left[DPL(\tan\alpha_3 - \tan\alpha_4) + Z_2 \left(\frac{1}{\cos DIP} + \frac{\tan\alpha_3 (\sin\alpha_2 - \cos\alpha_2)}{\cos\alpha_1}\right) + Z_3 \frac{1}{\cos DIP} \right] \cdot \frac{1}{Q_3}$$

This was done for a variety of assumed depths of the plug and the model fitted the travel times in every case.

3.3.3 Model D

On visual examination a displacement of Profile E's time-distance curve was observed. This could be caused by a fault and Model D was constructed to fit the observed travel times. It was basically the same as Model A, as shown in Fig. 22, since the horizontal beds were vertically displaced at the fault.

Assuming a vertical thrust, the thicknesses of the horizontal beds were modified to $(Z_i - dZ_i)$ on the eastern side of the fault. Since the Z_i were computed on the undisturbed part of the profile from Model A, the new thicknesses could be determined from the formulae

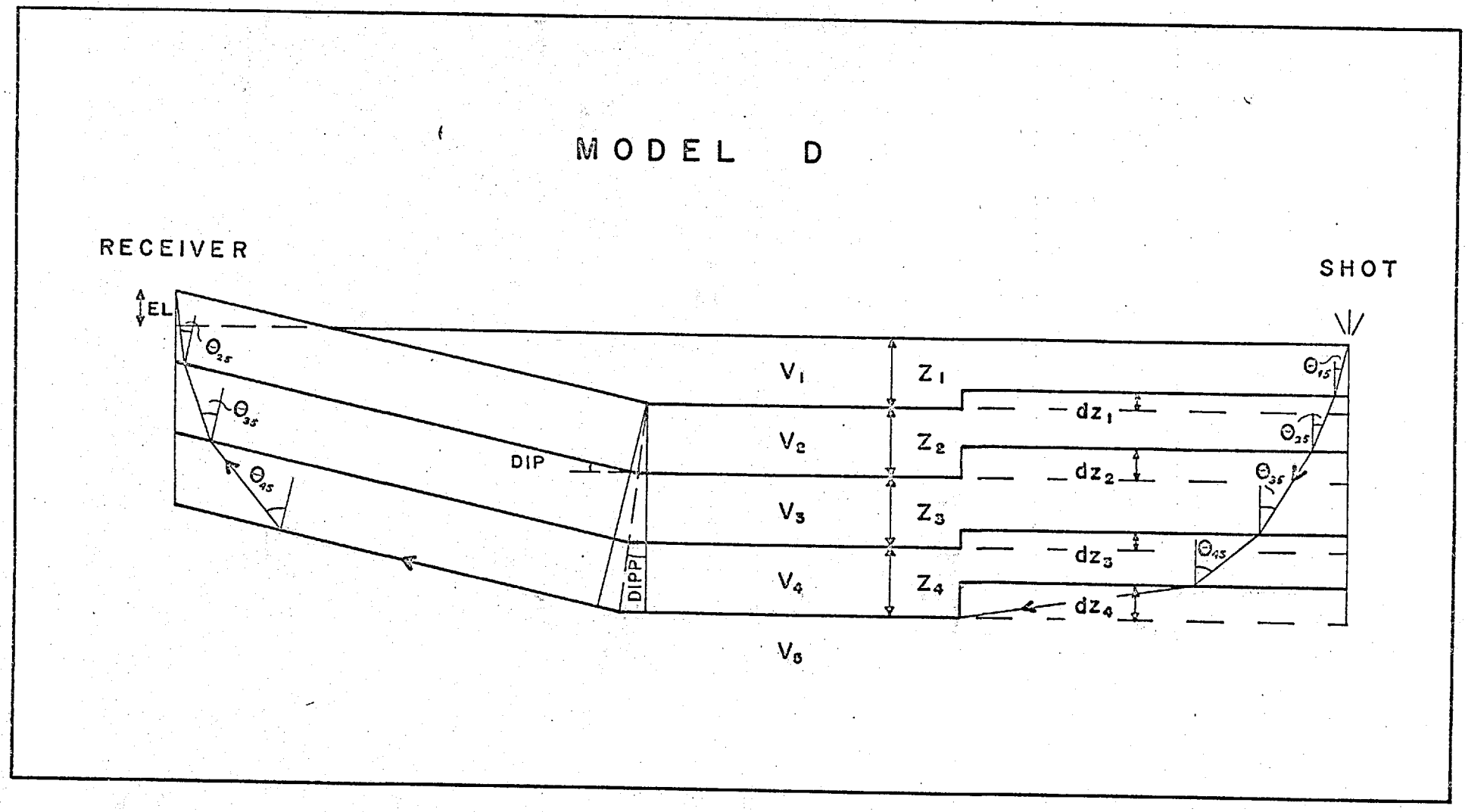
MODEL D
RECEIVER
SHOT
EL
DIP
DIPP
V1
V2
V3
V4
V5
Z1
Z2
Z3
Z4
dz1
dz2
dz3
dz4

Fig.22

$$T_1 = \left(\frac{\cos\Theta_{12}}{V_1} + \frac{1 - \cos DIP}{\sin DIP . V_2}\right) z_1 - \frac{\cos\Theta_{12}}{V_1} dz_1 + \frac{x}{V_2} + \frac{EL(1 - \cos DIP)}{\sin DIP . V_2}$$

$$T_2 = \left(\frac{\cos\Theta_{13}}{V_1} + \frac{1 - \cos DIP}{\sin DIP . V_3}\right) z_1 + \left(\frac{\cos\Theta_{23}}{V_2} - \frac{\cos\Theta_{13}}{V_1}\right) dz_1 + \left(\frac{2\cos\Theta_{23}}{V_2} + \frac{2\tan DIPP}{V_3}\right) z_2 - \frac{\cos\Theta_{23}}{V_2} dz_2 + \frac{x}{V_3} + \frac{EL(1 - \cos DIP)}{\sin DIP . V_3}$$

$$T_3 = \left(\frac{\cos\Theta_{14}}{V_1} + \frac{1 - \cos DIP}{\sin DIP . V_4}\right) z_1 + \left(\frac{\cos\Theta_{24}}{V_2} - \frac{\cos\Theta_{14}}{V_1}\right) dz_1 + \left(\frac{2\cos\Theta_{24}}{V_2} + \frac{2\tan DIPP}{V_4}\right) z_2 + \left(\frac{\cos\Theta_{34}}{V_3} - \frac{\cos\Theta_{24}}{V_2}\right) dz_2 + \left(\frac{2\cos\Theta_{34}}{V_3} + \frac{2\tan DIPP}{V_4}\right) z_3 - \frac{\cos\Theta_{34}}{V_3} dz_3 + \frac{x}{V_4} + \frac{EL(1 - \cos DIP)}{\sin DIP . V_4}$$

$$T_4 = \left(\frac{\cos\Theta_{15}}{V_1} + \frac{1 - \cos DIP}{\sin DIP . V_5}\right) z_1 + \left(\frac{\cos\Theta_{25}}{V_2} - \frac{\cos\Theta_{15}}{V_1}\right) dz_1 + \left(\frac{2\cos\Theta_{25}}{V_2} + \frac{2\tan DIPP}{V_5}\right) z_2 + \left(\frac{\cos\Theta_{35}}{V_3} - \frac{\cos\Theta_{25}}{V_2}\right) dz_2 + \left(\frac{2\cos\Theta_{35}}{V_3} + \frac{2\tan DIPP}{V_5}\right) z_3 + \left(\frac{\cos\Theta_{45}}{V_4} - \frac{\cos\Theta_{35}}{V_3}\right) dz_3 + \left(\frac{2\cos\Theta_{45}}{V_4} + \frac{2\tan DIPP}{V_5}\right) z_4 - \frac{\cos\Theta_{45}}{V_4} dz_4 + \frac{x}{V_5} + \frac{EL(1 - \cos DIP)}{\sin DIP . V_5}$$

where the dz_i are variables and the z_i input values.

3.3.4. Model E

This model was constructed to fit the travel times recorded on Tenerife for profile F because they were displaced at a certain distance from the recording station as shown in Fig.25. Assuming a vertical thrust similarly to Model D, Model C was adapted to Model E (Fig.23), in which the horizontal beds of Model C were vertically displaced by the amounts dz_i which were computed from the formulae

$$T_1 = \left(\frac{\cos\Theta_{12}}{V_1} + \frac{1 - \cos DIP}{\sin DIP . V_2}\right) z_1 - \frac{\cos\Theta_{12}}{V_1} dz_1 + \frac{x}{V_2} + \frac{EL(1 - \cos DIP)}{\sin DIP . V_2}$$

$$T_2 = \left(\frac{\cos\Theta_{13}}{V_1} + \frac{1 - \cos DIP}{\sin DIP . V_3}\right) z_1 + \left(\frac{\cos\Theta_{23}}{V_2} - \frac{\cos\Theta_{13}}{V_1}\right) dz_1 + \left(\frac{2\cos\Theta_{23}}{V_2} + \frac{2\tan DIPP}{V_3}\right) z_2 - \frac{\cos\Theta_{23}}{V_2} dz_2 + \frac{x}{V_3} + \frac{EL(1 - \cos DIP)}{\sin DIP . V_3}$$

$$T_3 = \left(\frac{\cos\Theta_{14}}{V_1} + \frac{1 - \cos DIP}{\sin DIP . V_4}\right) z_1 + \left(\frac{\cos\Theta_{24}}{V_2} - \frac{\cos\Theta_{14}}{V_1}\right) dz_1 + \left(\frac{\cos\Theta_{24}}{V_2} + \frac{2\tan DIPP - \tan DIP}{V_4} - \frac{\tan\alpha_4}{\cos^2 DIP . V_4 . Q3} + \frac{1}{Q3 . \cos\alpha_4 \cos DIP V_5} + \frac{1}{\cos\alpha_1 . V_2} - \frac{(\sin\alpha_2 - \cos\alpha_2) . \tan\alpha_3}{Q3 . V_4 . \cos DIP . \cos\alpha_1} + \frac{(\sin\alpha_2 - \cos\alpha_2) . \tan\alpha_3}{Q3 . \sin\alpha_4 . V_5 . \cos\alpha_1} - \frac{(\sin\alpha_2 - \cos\alpha_2) . \tan\alpha_3}{\sin\alpha_4 . \cos\alpha_1 . V_5} + \frac{(\sin\alpha_2 - \cos\alpha_2) . \tan\alpha_3}{V_3 (\sin\alpha_3 - \cos\alpha_3 \tan\alpha_2) \cos\alpha_1}\right) z_2 +$$

$$\left(\frac{\cos\theta_{34}}{V_3} - \frac{\cos\theta_{24}}{V_2}\right) dz_2 + \left(\frac{\cos\theta_{34}}{V_3} + \frac{2\tan DIPP - \tan DIP}{V_4} - \frac{\tan\alpha_4}{\cos^2 DIP \cdot V_4 \cdot Q3} + \frac{1}{Q3 \cdot \cos\alpha_4 \cdot \cos DIP \cdot V_5}\right) z_3 + \frac{x}{V_4} + \frac{EL(1 - \cos DIP)}{\sin DIP \cdot V_4}$$

$$+ DPL\left(\frac{\tan\alpha_4 - \tan\alpha_3}{\cos DIP \cdot V_4 \cdot Q3} - \frac{1}{\cos\alpha_4 \cdot V_5 \cdot Q3} + \frac{\tan\alpha_3}{Q3 \cdot \sin\alpha_4 \cdot V_5} - \frac{\tan\alpha_2}{\sin\alpha_4 \cdot V_5} + \frac{\tan\alpha_5 - \tan\alpha_2}{V_3(\sin\alpha_3 - \cos\alpha_3 \tan\alpha_2)}\right)$$

$$T_4 = \left(\frac{\cos\theta_{15}}{V_1} + \frac{1 - \cos DIP}{\sin DIP \cdot V_5}\right) z_1 + \left(\frac{\cos\theta_{25}}{V_2} - \frac{\cos\theta_{15}}{V_1}\right) dz_1 +$$

$$\left(\frac{\cos\theta_{25}}{V_2} + \frac{2\tan DIPP}{V_5} - \frac{\tan\theta_1^*}{V_5} + \frac{1}{\cos\theta_1^* \cdot V_2}\right) z_2 +$$

$$\left(\frac{\cos\theta_{35}}{V_3} - \frac{\cos\theta_{25}}{V_2}\right) dz_2 + \left(\frac{\cos\theta_{35}}{V_3} + \frac{2\tan DIPP}{V_5}\right) z_3 +$$

$$\left(\frac{\cos\theta_{45}}{V_4} - \frac{\cos\theta_{35}}{V_3}\right) dz_3 + \left(\frac{\cos\theta_{45}}{V_4} + \frac{2\tan DIPP}{V_5}\right) z_4 -$$

$$\frac{\cos\theta_{45}}{V_4} dz_4 + \frac{x}{V_5} + \frac{EL(1 - \cos DIP)}{\sin DIP \cdot V_5} +$$

$$\frac{HQ}{\cos\left(\arctan\frac{XO}{HQ}\right) \cdot V_5}\left(1 - \sin(\theta_4^* + DIP)\right) +$$

$$\frac{DPLQ}{\cos\left(\arctan\frac{RQ - XO}{DILQ}\right)}\left(\frac{1}{V_3} - \frac{\sin\theta_2^*}{V_5}\right)$$

where the dz_i are the variables and the z_i are input values.

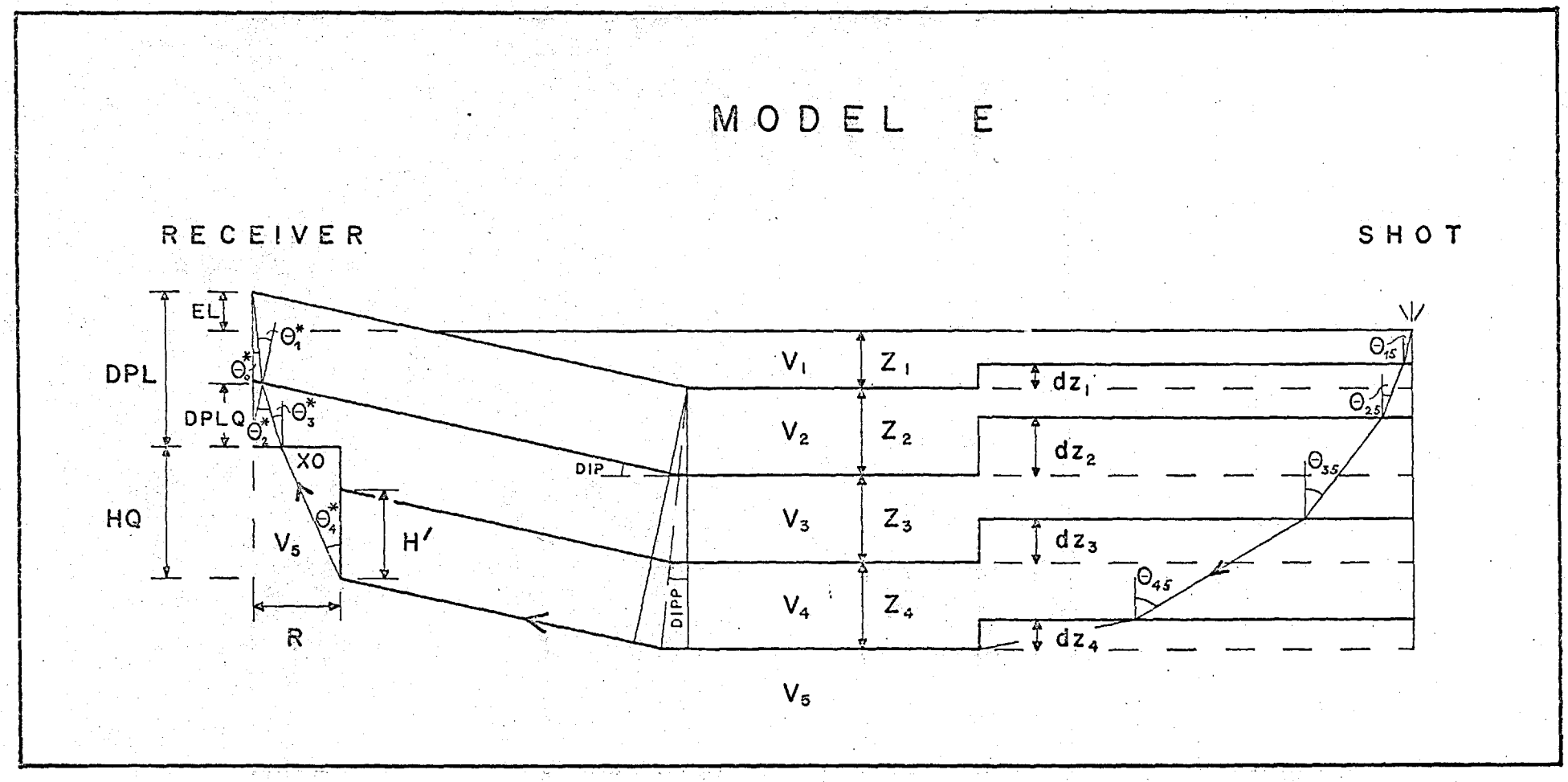
MODEL E
RECEIVER
SHOT
EL
DPL
DPLQ
HQ
XO
R
H'
DIP
DIPP
V1
V2
V3
V4
V5
Z1
Z2
Z3
Z4
dz1
dz2
dz3
dz4

Fig.23

3.4 Results of the John Murray Work

The time-distance curves of the profiles E, F, G, H and I were interpreted using one of the models of section 3.3.

3.4.1 Line E

The time-distance curve is shown in Fig. 24. Since very few shots were fired for this line, only a limited number of points were available for constructing the time-distance graph. As shown earlier, most of the noise was eliminated from the records with the digital processing, giving a good definition of the arrivals. The travel time curves could therefore be drawn with fair accuracy.

Second and later arrivals were also used to construct the travel time curves for all the shallower refractors. Four layers were detected with velocities of 3.25 km/sec, 4.18 km/sec, 5.24 km/sec and 7.48 km/sec.

On most traces "ghost arrivals" were observed immediately following the first arrival. The time-lag was between 150-260 milliseconds. On observation, it was noticed that the time-lags had direct dependence on the size of the charge and hence the depth of detonation. Subsequently, as shown below, this assumption was proved to be correct and the time-lags were used to compute the depth of the shot from the formula:

$$T = \frac{2\cos\theta_{ik} \cdot Z}{V_i}$$

where $\sin \theta_{ik} = V_i/V_k$

Z = depth of shot

T = delay time

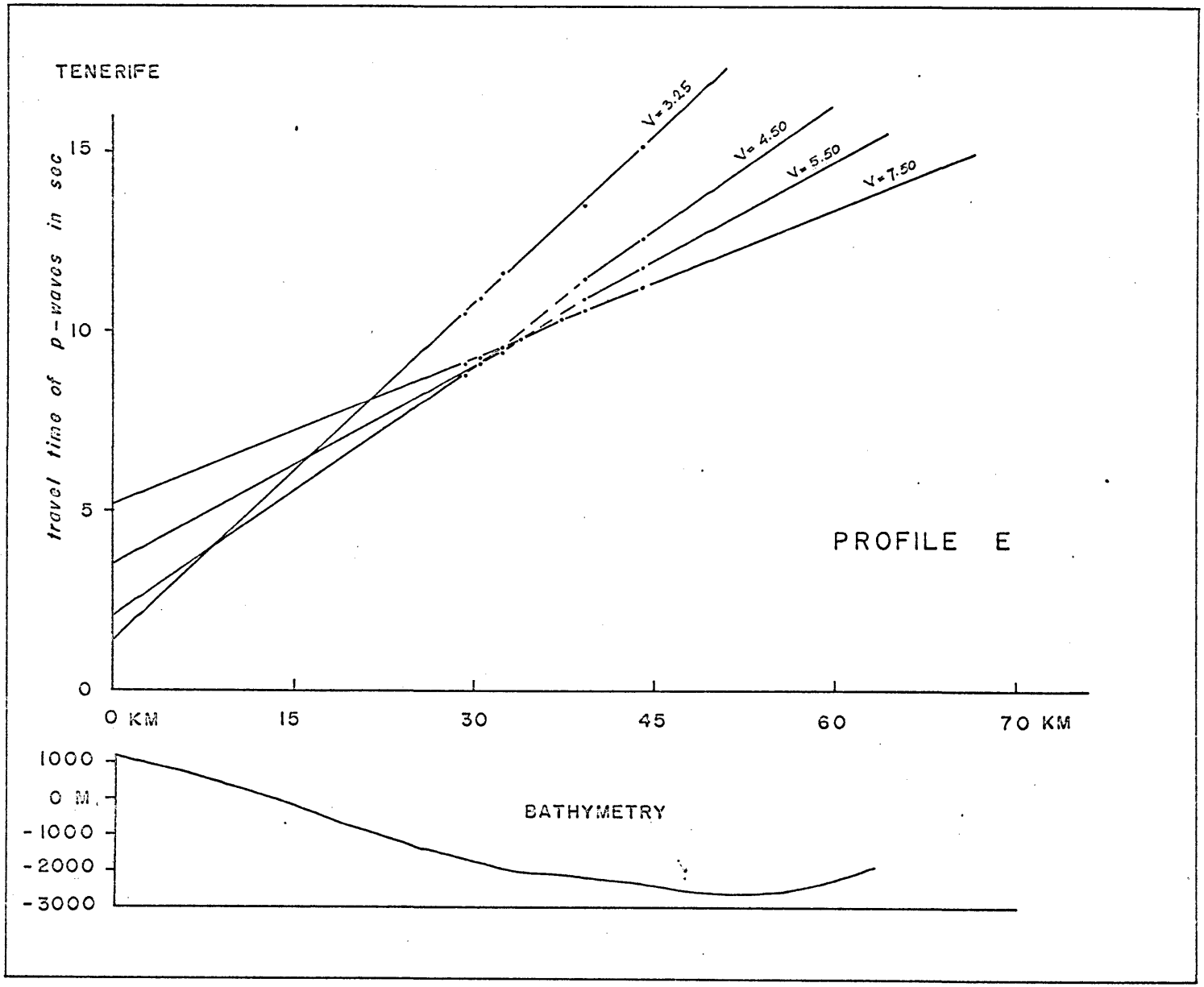
TENERIFE
travel time of p-waves in sec
15
10
5
0
V=3.25
V=4.50
V=5.50
V=7.50
PROFILE E
0 KM
15
30
45
60
70 KM
1000
0 M.
-1000
-2000
-3000
BATHYMETRY

Fig.24

For a velocity constrast of 0.2 a depth of 115 m was computed from the time delay of 150 milliseconds. This corresponded well with the 112.5 m computed from the sinking rate of the 50 lb charge. The "ghost" arrival occurring for a 100 lb charge was delayed by 260 milliseconds and its depth calculated as 200 m. Again, this corresponded well with the depth of 210 m computed from its sinking rate. These "ghost" arrivals disappeared with charges smaller than 50 lb.

Because profile E was recorded at Vilaflor, models B and C were used for interpreting the western half of the line. But as both these models failed to fit the travel times, it was concluded that the plug did not extend far enough beyond Vilaflor to influence them. Consequently, model A was used to interpret the western part of the line. As mentioned in section 3.3.3, model D served for the eastern side of the profile and the thicknesses are shown, together with velocities and depths on both sides of the profile, in Table IV.

3.4.2 Line F Recorded on Tenerife

The time-distance curve (Fig. 25) could be constructed with a fair degree of accuracy from the arrivals obtained from the digitally processed records. The graph showed a time displacement at a distance of 37.7 km from the recording station. The first arrivals were P-waves refracted at the upper boundary of the 7.4 km/sec layer. Later arrivals enabled two shallower refractors with the velocities of 4.20 and 5.45 km/sec to be detected. For proper depth calculations, a shallower refractor with a velocity of 3.20 km/sec was assumed. "Ghost" arrivals

Table IV

West of the fault

Velocity km/sec	Thickness km	Depth km
1.50	2.30±0.31	0
3.20±0.14	1.85±0.20	2.30±0.31
4.55±0.09	3.63±0.32	4.15±0.37
5.50±0.11	4.47±0.41	7.78±0.49
7.50±0.09		12.25±0.64

East of the fault

Velocity km/sec	Thickness km	Depth km
1.50	2.30±0.31	0
3.20±0.14	2.39±0.27	2.30±0.31
4.55±0.09	2.70±0.29	4.69±0.41
5.50±0.11	5.75±0.44	7.39±0.50
7.50±0.09		13.14±0.67

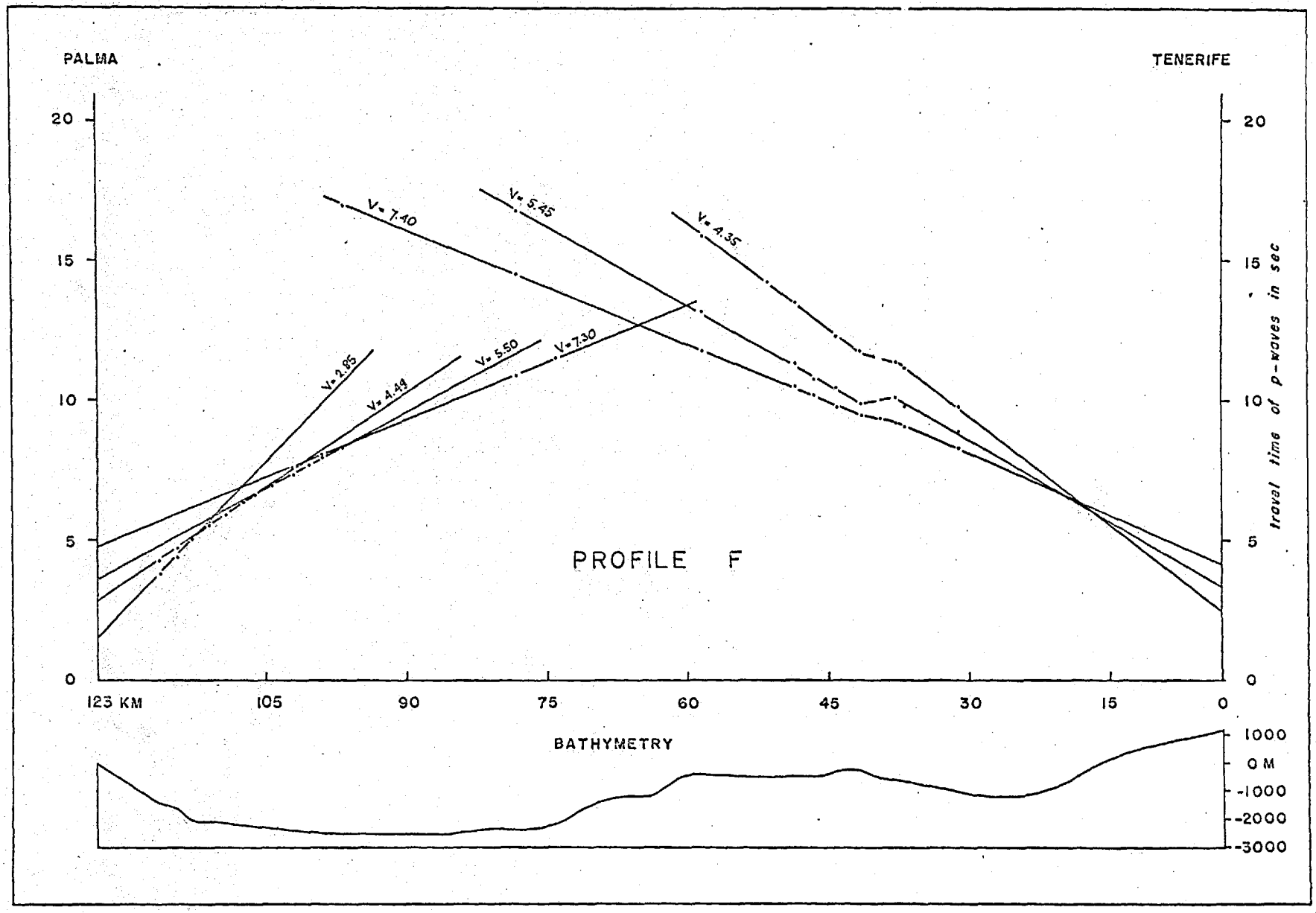
PALMA
TENERIFE
20
15
10
5
0
V= 7.40
V= 5.45
V= 4.35
V= 2.85
V= 4.49
V= 5.50
V= 7.30
PROFILE F
123 KM
105
90
75
60
45
30
15
0
travel time of p-waves in sec
BATHYMETRY
1000
0 M
-1000
-2000
-3000

Fig.25

Table V

West of the fault

Velocity km/sec	Thickness km	Depth km
1.50	(2.30)	0
(3.20)	1.80 ± 0.21	2.30
4.20 ± 0.07	2.56 ± 0.27	4.10 ± 0.21
5.45 ± 0.11	3.09 ± 0.36	6.66 ± 0.34
7.40 ± 0.10		9.74 ± 0.50

East of the fault

Velocity km/sec	Thickness km	Depth km
1.50	(2.30)	0
(3.20)	1.97 ± 0.23	2.30
4.20 ± 0.07	3.31 ± 0.31	4.27 ± 0.23
5.45 ± 0.11	1.39 ± 0.39	7.58 ± 0.39
7.40 ± 0.10		8.97 ± 0.55

were again used to verify the depths of the shots and were confirmed in every case.

Model C was used to interpret the eastern side of the fault and model E for the western part of the profile. The depth of the plug was construed to be 4.7 km because this value gave a depth to the 7.4 km/sec refractor which corresponded best with the one obtained from the La Palma side of the profile. Both these depths had to be equal since the travel time branches overlapped. Table V displays the thicknesses, velocities and depths of the refractors on both sides of the fault.

3.4.3 Line F Recorded on La Palma

The time-distance graph is shown in Fig. 25. Only very few later arrivals could be observed since all of the geophones were heavily damped. Four refractors were detected with velocities of 2.85, 4.49, 5.50 and 7.30 km/sec. Whereas the velocity control was fair for the upper layers, it was poor for the 7.3 km/sec refractor because only two first arrivals were observed.

Model A was used to interpret the travel times. The thicknesses, velocities and depths of the individual refractors are shown in Table VI.

3.4.4 Line G

The small number of 9 shots fired for this line enabled only the upper crustal layers to be detected. The time-distance graph is shown in Fig. 26. The velocities of the refractors were 3.25, 4.35 and 5.35 km/sec respectively. Model A was used to calculate the thicknesses of the refractors

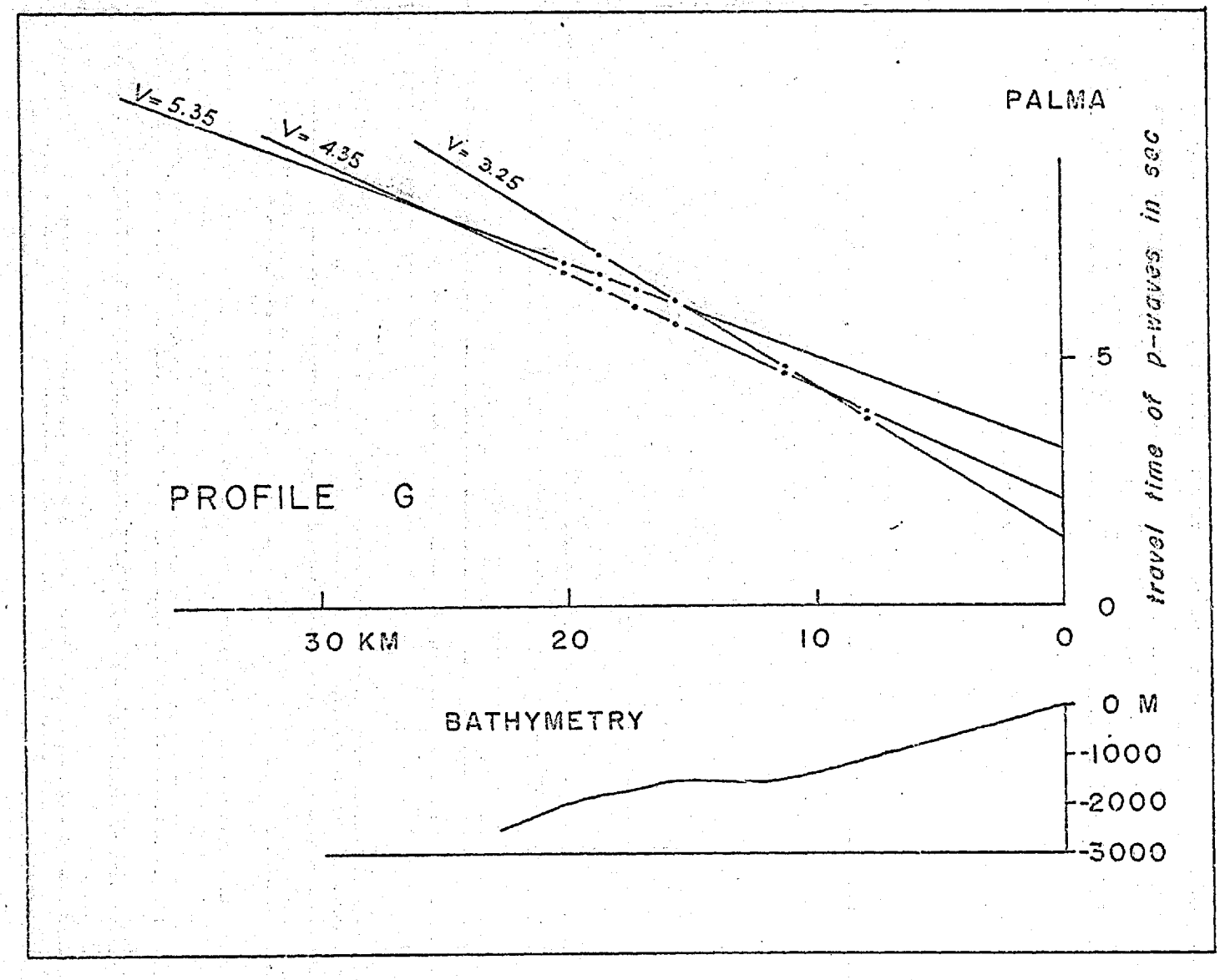
V= 5.35
V= 4.35
V= 3.25
PALMA
PROFILE G
30 KM
20
10
0
5
0
travel time of p-waves in sec
BATHYMETRY
0 M
-1000
-2000
-3000

Fig.26

Table VI

Velocity km/sec	Thickness km	Depth km
1.50	2.34±0.60	0
2.85±0.12	2.26±0.61	2.34±0.60
4.49±0.15	1.77±0.54	4.60±0.86
5.50±0.09	3.52±0.50	6.37±1.01
7.20±0.38		9.88±1.13

Table VII

Velocity km/sec	Thickness km	Depth km
1.50	2.23±0.33	0
3.25±0.15	1.53±0.41	2.23±0.33
4.35±0.16	2.93±0.37	3.76±0.53
5.35±0.55		6.69±0.64

and these are shown with the appropriate velocities and depths in Table VII.

3.4.5 Line H

Only three upper crustal layers were detected. The travel times are shown in Fig. 27, and the refractors' velocities were 3.16, 4.25 and 5.71 km/sec. Model A was used to compute the thicknesses of the refractors, shown with the velocities and depths in Table VIII.

3.4.6 Line I

The time-distance curve, as shown in Fig. 27, is not very reliable since only five shots were fired on this line. Three refractors were constructed with velocities of 3.56, 4.55 and 5.66 km/sec. The thicknesses, computed from model A, are shown together with their depths in Table IX.

3.5 Interpretation of Lines A and D with Model F

Since the least squares method developed in section 3.3 proved to be very successful, it was thought worthwhile to re-interpret lines A and D with the same technique. The results obtained for the intercept time method and the least squares method for each profile gave a comparison of the accuracy of both techniques.

Therefore, model F was constructed assuming a multi-layer case with plane and horizontal interfaces. Table X shows the thicknesses, velocities and depths of the refractors of profile A and profile D computed from the two methods. The computed depths are within their error limits, but the errors

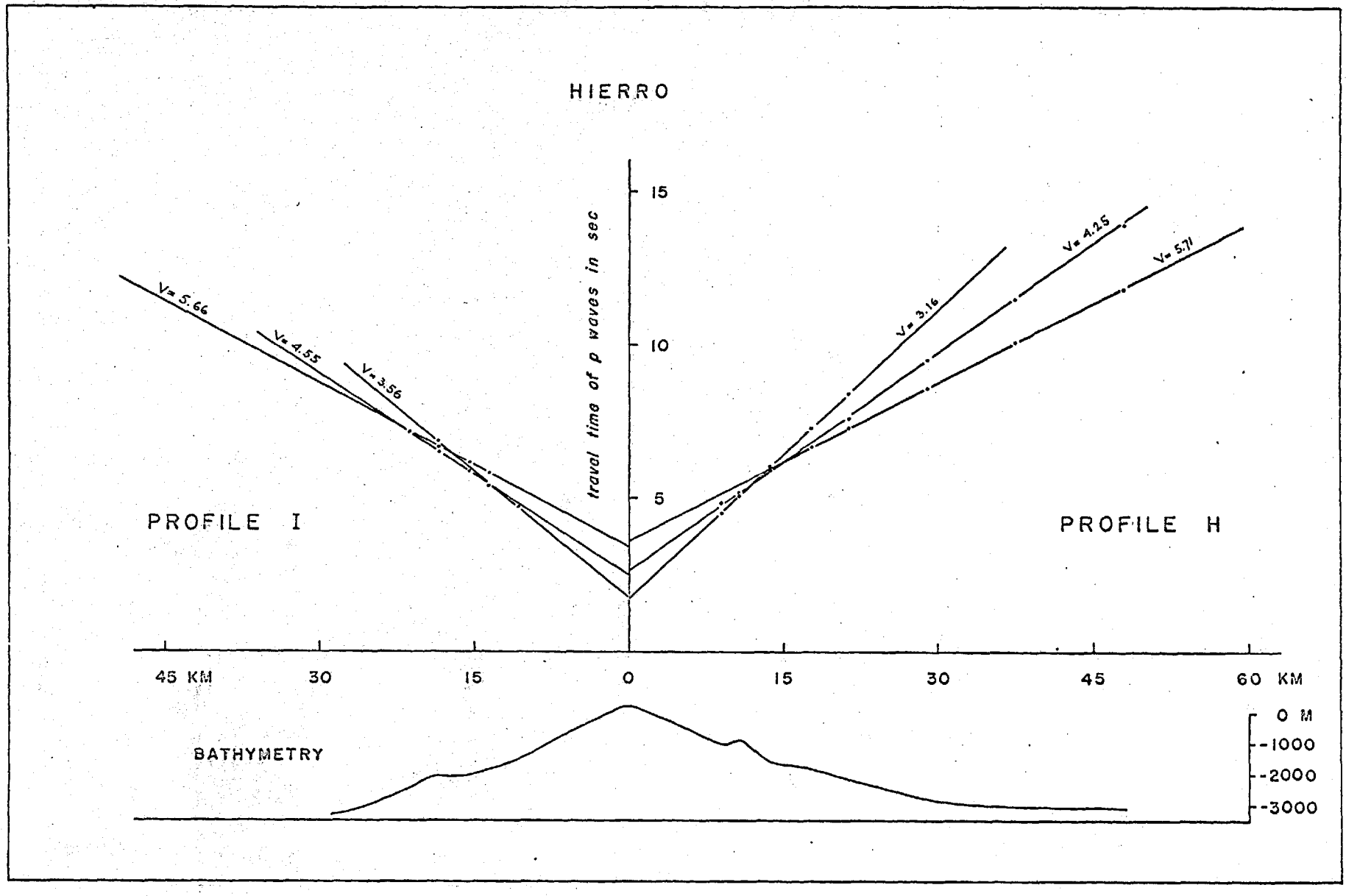
HIERRO
travel time of p waves in sec
15
10
5
V= 5.66
V= 4.55
V= 3.56
V= 3.16
V= 4.25
V= 5.71
PROFILE I
PROFILE H
45 KM
30
15
0
15
30
45
60 KM
BATHYMETRY
0 M
-1000
-2000
-3000

Fig.27

Table VIII

Velocity km/sec	Thickness km	Depth km
1.50	2.62 ± 0.10	0
3.16 ± 0.02	2.05 ± 0.24	2.62 ± 0.10
4.25 ± 0.08	1.96 ± 0.31	4.67 ± 0.26
5.71 ± 0.07		6.63 ± 0.40

Table IX

Velocity km/sec	Thickness km	Depth km
1.50	2.75 ± 0.77	0
3.56 ± 0.37	1.87 ± 1.05	2.75 ± 0.77
4.55 ± 0.16	2.53 ± 0.36	4.62 ± 1.30
5.66 ± 0.19		7.15 ± 1.35

Table X

Profile A

Velocity km/sec	Thickness km		Depth km	
	Intercept	Least squares	Intercept	Least squares
1.50	3.54±0.03	3.53±0.05	0	0
3.35±0.02	2.14±0.24	2.16±0.27	3.54±0.03	3.53±0.05
4.42±0.06	2.41±0.44	2.47±0.38	5.68±0.25	5.69±0.27
6.00±0.09	3.50±0.71	3.28±0.33	8.09±0.50	8.16±0.47
7.05±0.08	3.16±1.17	3.56±0.19	11.59±0.87	11.44±0.57
7.65±0.08			14.75±1.45	15.00±0.60

Profile D

Velocity km/sec	Thickness km		Depth km	
	Intercept	Least squares	Intercept	Least squares
1.50	2.81±0.15	2.78±0.32	0	0
3.00±0.11	1.99±0.59	1.93±0.54	2.81±0.15	2.78±0.32
3.90±0.11	3.02±0.64	3.12±0.61	4.80±0.61	4.71±0.63
5.69±0.09	2.94±0.88	2.80±0.41	7.82±0.88	7.83±0.88
7.04±0.17	3.51±1.24	3.24±0.31	10.76±1.25	10.63±0.97
8.12±0.09			14.27±1.62	13.87±1.02

are much larger for the intercept time method than for the least squares method. The latter is therefore the better technique.

3.6 Continuous Reflection Records

The profiles gave a fair picture of the distribution of low velocity sediments since they were recorded in various parts of the island group.

3.6.1 Airgun Profile La Palma - Gomera - Hierro

This profile started on the northern side of the Canaries ridge at 28°44'30"N, 17°33'W just above the North Canary Basin (Fig. 28). On most of the profile, hyperbolic echoes and occasional discontinuous layering was observed. On the southernmost side of the ridge a continuous sub-bottom echo appeared from 27°45'N, 17°32'30"W onwards. It had a time delay of 60 milliseconds, increasing southwards to 100 milliseconds at 27°38'N, 17°33'W. Therefore, low velocity sediments are present on the southern side of the ridge. They have a thickness ranging from 60 m to 100 m, assuming an average velocity of 2.0 km/sec, whereas the ridge itself is bare of sediment cover.

3.6.2 Sparker Profile Tenerife - Gomera

No penetration could be observed along the slope of Tenerife. In the col between both islands a sub-bottom echo was observed but was rather difficult to follow continuously. The largest penetration was 60 milliseconds, indicating that the bottom consisted, at the most, of 60 m of low velocity sediments in the form of a pocket.

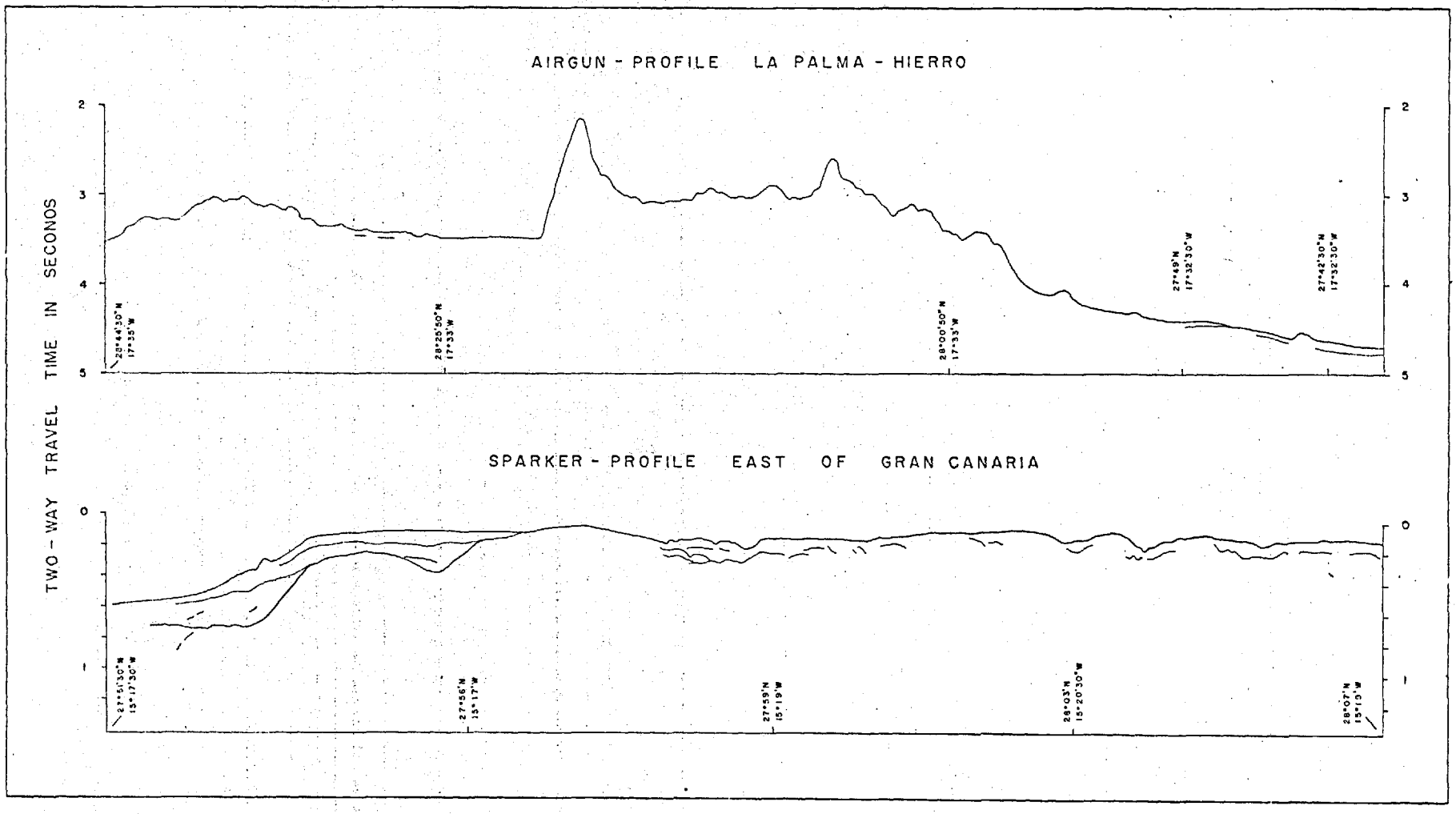
AIRGUN - PROFILE LA PALMA - HIERRO
TWO - WAY TRAVEL TIME IN SECONDS
2
3
4
5
28°44'30"N
17°55'W
28°25'50"N
17°33'W
28°00'50"W
17°33'W
27°49'N
17°32'30"W
27°42'30"N
17°32'30"W
SPARKER - PROFILE EAST OF GRAN CANARIA
0
1
27°51'30"N
15°17'30"W
27°56'N
15°17'W
27°59'N
15°19'W
28°03'N
15°20'30"W
28°07'N
15°13'W

Fig.28

3.6.3 Sparker Profile Tenerife - Gran Canaria

No penetration could be observed along this line. Furthermore, a planned anchoring station on top of the ridge between Tenerife and Gran Canaria had to be abandoned because the anchor threatened to snap, confirming that no low velocity sediment was present on this part of the ridge.

3.6.4 Sparker Profile Parallel to the East Coast of Gran Canaria

This line was located between 27°51'30"N, 15°17'30"W and 28°07'N, 15°19'W (Fig. 28). In the southern part two reflection horizons could be observed above the basement. The first one occurred with a time delay of 60-100 milliseconds below the sea bottom. Assuming a velocity of 2.0 km/sec, the thickness was calculated as 60-100 metres. This layer most probably consists of low velocity sediments.

The second horizon appeared with a time delay of 60-160 milliseconds below the first reflector. This layer probably represents more consolidated sediments and is between 75-200 metres thick assuming a velocity of 2.5 km/sec.

The basement rose stepwise from about 200 metres below the sea bottom at the southern end of the profile to 180 metres at 27°54'N, 15°17'W and reached the surface at 27°56'30"N, 15°17'W. These marked steps are most probably caused by faults and coincide well with located faults further south (HINZ, 1967).

A strongly folded sediment pocket exists between 27°58'N, 15°19'W and 27°59'N, 15°19'W. The sediments are not thicker than 250 metres, assuming a velocity of 3.0 km/sec,

and are quite probably composed of volcanic debris. No low velocity sediment is present there as revealed by the rugged bottom topography.

From 27°59'N, 15°19'W to 28°05'N, 15°20'W only occasional discontinuous layering was observed, indicating a probable volcanic nature of the sea bottom. Between 28°05'N, 15°20'W and the northern end of the line, a disrupted sub-bottom echo appears. The time delay of about 65 milliseconds yields a thickness of 95 metres, assuming a velocity of 3.0 km/sec. This layer probably represents volcanic debris.

3.7 Error Estimation

An estimation of the minimum statistical error of a seismic refraction profile was given by STEINHART and MEYER (1961). Their procedure was adopted here for estimating the errors of the refraction survey.

For the treatment of errors, involved in the approximation of the time-distance plot by straight lines, the assumption is made that only the observed times are affected by errors. This classical least squares model with one variable without error, requires that errors in distance are small compared with errors in time measurement. This condition is usually satisfied in long range work.

3.7.1 Least Squares and Confidence Regions for Line Parameters

For a line $T = t_o + \lambda . x$ from N points (x_i, t_i), the least squares estimates of the parameters are

$$\lambda = \frac{\sum x_i t_i - \frac{\sum x_i \sum t_i}{N}}{\sum x_i^2 - \frac{(\sum x_i)^2}{N}} \qquad (1)$$

$$t_o = \frac{\sum x_i \sum x_i t_i - \sum t_i \sum x_i^2}{(\sum x_i)^2 - N(\sum x_i 2)} \qquad (2)$$

The standard deviations σ_λ and σ_t are required for estimating the uncertainty of the slope and the intercept time respectively. STEINHART and MEYER (1961) use a "best" estimate S_t for σ_t, which is defined as

$$S_t^2 = \frac{\text{Sum of squared residuals}}{N - 2} \qquad (3)$$

for a finite set of data which have been fitted to a line.

Equation (3) can be written in the form

$$S_t^2 = \left\{ \sum t_i^2 - \frac{(\sum t_i)^2}{N} - \frac{(\sum x_i t_i - \frac{\sum x_i \sum t_i}{N})^2}{S_{xx}} \right\} \frac{1}{N-2} \qquad (4)$$

where $S_{xx} = \sum x_i^2 - \frac{(\sum x_i)^2}{N}$

The equation for the "best" estimate S_λ for σ_λ is obtained as

$$S_\lambda^2 = \frac{S_t^2}{S_{xx}} \qquad (5)$$

where S_{xx} as in (4).

It is important to know how significant their "best" estimates are. STEINHART and MEYER (1961) use a probability statement in the form of Student's t-distribution for this purpose and obtain the following expressions for the variances:

$$\text{Var}(\lambda) = \pm S_\lambda \cdot \tau_{N-2} \qquad (6)$$

where Var (λ) = variance of the slope

S_λ = as in (5)

τ_{N-2} = Student's t-distribution with N-2 degrees of freedom

and

$$\text{Var}(t) = \pm \mathcal{T}_{N-2} \cdot S_t \left[\frac{1}{N} - \frac{\bar{x}^2}{S_{xx}} \right]^{\frac{1}{2}} \qquad (7)$$

where Var (t) = variance of the time intercept

S_t = as in (4)

$\mathcal{T}_{N-2}$ = as in (6)

$\bar{x}$ = mean value of the x_i

S_{xx} = as in (4)

3.7.2 Variance of the Computed Depth

Confidence limits are required on the depths obtained from the time-distance graph. The method used is the Taylor expansion method and is applied to the conventional intercept time interpretation both for horizontal layers and for the reversed profile. It was also applied to the least squares fitting technique devised in section 3.3.

3.7.2.1 Horizontal Layering

The equation for the depth of the interface n is

$$D_n = \frac{t_{o,\,n+1}}{2(\lambda_n^2 - \lambda_{n+1}^2)^{\frac{1}{2}}} + \sum_{k=1}^{n-1} h_k \left[1 - \frac{(\lambda_k^2 - \lambda_{n+1}^2)^{\frac{1}{2}}}{(\lambda_n^2 - \lambda_{n+1}^2)^{\frac{1}{2}}} \right] \qquad (8)$$

where t_o, n+1 = intercept time of the line segment with the slope λ_{n+1}

λ_k = slope of line segment k

h_k = thickness of the refractor k

Since (8) is a function of t_o, h_k and λ_k and in turn t_o and h_k are functions of the parameters of the line segments,

equation (7) could be written as

$$Dn = F(\bar{t}_i, \bar{x}_i, \lambda_i) \qquad i = 1,2 \ldots, n+1 \qquad (9)$$

where $\bar{t}_i$ = mean of t_i
$\bar{x}_i$ = mean of x_i
according to the orthogonal form $T = \bar{t} + \lambda(x-\bar{x})$

If the least squares values for these line segments are

$$T = \bar{t}_1 + \lambda_1 (x-\bar{x}_1)$$

$$T = \bar{t}_2 + \lambda_2 (x-\bar{x}_2)$$

$$\vdots$$

$$T = \bar{t}_{n+1} + \lambda_{n+1} (x-\bar{x}_{n+1})$$

an expansion in the region of the experimental values is then

$$Dn = F(\bar{x},\bar{t},\lambda) = F_n + \sum_{i=1}^{n+1} \left(\frac{\partial F}{\partial \bar{x}}\right)_{\bar{x}=\bar{x}_i} (\bar{x} - \bar{x}_i) + \sum_{i=1}^{n+1} \left(\frac{\partial F}{\partial \bar{t}}\right)_{\bar{t}=\bar{t}_i} (\bar{t} - \bar{t}_i)$$
$$+ \sum_{i=1}^{n+1} \left(\frac{\partial F}{\partial \lambda}\right)_{\lambda=\lambda_i} (\lambda - \lambda_i) + \text{higher order terms} \qquad (10)$$

where F_n is the value of D_n calculated from the experimental values. For any set of experimental values a Taylor series expansion of F can be obtained. STEINHART and MEYER (1961) state that D_n is a linear function of the variables $\bar{t}_i$, $\bar{x}_i$ and λ_i to the extent that it is justifiable to neglect higher order terms.

Since the variance of a linear function $F(x, y, z) = a_o + a_1x + a_2y + a_3z$ is given by

$$\text{Var}(a_o + a_1x + a_2y + a_3z) = a_1^2 \cdot \text{Var}(x) + a_2^2 \cdot \text{Var}(y)$$
$$+a_3^2 \cdot \text{Var}(z) + 2a_1a_2\, \text{Covar}(xy) + 2a_1a_3\, \text{Covar}(xz) \qquad (11)$$
$$+2a_2a_3\, \text{Covar}(yz)$$

the variance of D_n can be directly calculated by evaluating the partial derivatives numerically for the range of variation

of the $\bar{x}_i$, $\bar{t}_i$ and λ_i. Since $\bar{x}_i$ is "without error" and the sampling of $\bar{t}_i$ and λ_i is independent, $Var(\bar{x}) = 0$ and the covariances of equation (11) are zero. Thus the variance of D_n may be written as

$$Var(D_n) = \sum_{i=1}^{n+1} A_i^2 \cdot Var(\bar{t}_i) + \sum_{i=1}^{n+1} B_i^2 \cdot Var(\lambda_i) \qquad (12)$$

where $A_i = \frac{\partial D_n}{\partial \bar{t}_i}$, $B_i = \frac{\partial D_n}{\partial \lambda i}$ $(i=1,2 \ldots n+1)$

3.7.2.2 Dipping Layers

In the same way a Taylor expansion may be obtained for dipping layers. Using WEBER's solution for the depth (in RYBACH, 1962), the depth function for the n^{th} layer at the shot end is

$$D_{na} = \frac{t_{o,n+1}}{R_{n;n+1}} - \frac{\sum_{i=1}^{n-1} da_i \cdot R_{i,n}}{R_{n,n+1}} \qquad (13)$$

where $R_{i,k} = \left[(\lambda a_i + \lambda b_i)^2 - (\lambda a_k + \lambda b_k)^2 \right]^{\frac{1}{2}}$

$t_{o,n+1}$ = intercept time for line segment with the slope λ_{n+1} at the distance x=o from the shot

da_i = thickness of the refractor i

Since D_{na} is a function of t_o, da_i, λa_i, and λb_i it can be written as

$$D_{na} = F (\bar{t}_i, \lambda_{ai}, \lambda_{bi}, \bar{x}_i)$$

The Taylor expansion is then similar to 3.7.2.1 and

$$D_{na} = F\left(\bar{t}_i, \bar{x}_i, \lambda a_i, \lambda b_i\right) = F_{na} + \sum_{i=1}^{n+1} \left(\frac{\partial F}{\partial \lambda a}\right)_{\lambda a = \lambda a_i} \left(\lambda a - \lambda a_i\right)$$

$$+ \sum_{i=1}^{n+1} \left(\frac{\partial F}{\partial \lambda b}\right)_{\lambda b = \lambda b_i} \left(\lambda b - \lambda b_i\right) + \sum_{i=1}^{n+1} \left(\frac{\partial F}{\partial \bar{t}}\right)_{\bar{t} = \bar{t}_i} \left(\partial \bar{t} - \partial \bar{t}_i\right)$$

$$+ \sum_{i=1}^{n+1} \left(\frac{\partial F}{\partial \bar{x}}\right)_{\bar{x} = \bar{x}_i} \left(\bar{x} - \bar{x}_i\right) + \text{higher order terms} \qquad (14)$$

The variance of the computed depth can then be obtained as

$$\mathrm{Var}\left(D_{na}\right) = \sum_{i=1}^{n+1} A_i^2 \cdot \mathrm{Var}\left(\bar{t}_i\right) + \sum_{i=1}^{n+1} B_i^2 \cdot \mathrm{Var}\left(\lambda a_i\right) +$$

$$\sum_{i=1}^{n+1} C_i^2 \cdot \mathrm{Var}\left(\lambda b_i\right) \qquad (15)$$

where $A_i = \frac{\partial D_{na}}{\partial \bar{t}_i}$, $B_i = \frac{\partial D_{na}}{\partial \lambda a_i}$, $C_i = \frac{\partial D_{na}}{\partial \lambda b_i}$ $\quad (i = 1,2,\ldots n+1)$

3.7.2.3. Least Squares Fitting of Models

When fitting the z_k to the observed traveltimes, the overall error of the calculations was minimized. The resulting simultaneous linear equations are for a four layer case of the form

$$\begin{aligned}
\alpha_1 z_1 + \beta_1 z_2 + \gamma_1 z_3 + \delta_1 z_4 + \varepsilon_1 &= 0 \\
\beta_1 z_1 + \beta_2 z_2 + \gamma_2 z_3 + \delta_2 z_4 + \varepsilon_2 &= 0 \\
\gamma_1 z_1 + \gamma_2 z_2 + \gamma_3 z_3 + \delta_3 z_4 + \varepsilon_3 &= 0 \\
\delta_1 z_1 + \delta_2 z_2 + \delta_3 z_3 + \delta_4 z_4 + \varepsilon_4 &= 0
\end{aligned} \qquad (16)$$

where $\alpha_1, \beta_1, \beta_2, \gamma_1, \gamma_2, \gamma_3, \delta_1, \delta_2, \delta_3, \delta_4$ are functions of the slopes λ_i.

The only variables contained in the equations (16) are the slopes λ_i of the line segments of the travel time plot. Solving the equations with respect to the z_k yielded the following equations:

$$
\begin{aligned}
z_1 &= F_1(\lambda_i) \\
z_2 &= F_2(\lambda_i) \\
z_3 &= F_3(\lambda_i) \\
z_4 &= F_4(\lambda_i)
\end{aligned}
\qquad (17)
$$

The Taylor expansion is thensimilar to 3.7.2.1 :

$$
\begin{aligned}
z_1 &= F_1 + \sum_{i=1}^{n+1} \left(\frac{\partial F_1}{\partial \lambda}\right)_{\lambda=\lambda_i} (\lambda - \lambda_i) + \text{higher order terms} \\
z_2 &= F_2 + \sum_{i=1}^{n+1} \left(\frac{\partial F_2}{\partial \lambda}\right)_{\lambda=\lambda_i} (\lambda - \lambda_i) + \text{higher order terms} \\
z_3 &= F_3 + \sum_{i=1}^{n+1} \left(\frac{\partial F_3}{\partial \lambda}\right)_{\lambda=\lambda_i} (\lambda - \lambda_i) + \text{higher order terms} \\
z_4 &= F_4 + \sum_{i=1}^{n+1} \left(\frac{\partial F_4}{\partial \lambda}\right)_{\lambda=\lambda_i} (\lambda - \lambda_i) + \text{higher order terms}
\end{aligned}
\qquad (18)
$$

and the variances on the depths were then

$$
\begin{aligned}
\text{Var}(z_1) &= \sum_{i=1}^{n+1} \left(\frac{\partial F_1}{\partial \lambda_i}\right)^2 \cdot \text{Var}(\lambda_i) \\
\text{Var}(z_2) &= \sum_{i=1}^{n+1} \left(\frac{\partial F_2}{\partial \lambda_i}\right)^2 \cdot \text{Var}(\lambda_i)
\end{aligned}
$$

$$\text{Var}\ (z_3) = \sum_{i=1}^{n+1} \left(\frac{\partial F_3}{\partial \lambda_i}\right)^2 \cdot \text{Var}\ (\lambda_i)$$

$$\text{Var}\ (z_4) = \sum_{i=1}^{n+1} \left(\frac{\partial F_4}{\partial \lambda_i}\right)^2 \cdot \text{Var}\ (\lambda_i) \qquad (19)$$

The minimized overall error, i.e. the least squares error of every model was generally less than 2% and was therefore negligible. Consequently, equations (19) were used to determine the errors on the depths computed from the John Murray profiles.

CHAPTER 4

MARINE GRAVITY INVESTIGATION

The seismic data were supplemented by the measurement of the gravitational field around the islands using the sea gravimeter on board F.S. Meteor. As will be shown subsequently, these data used in conjunction with the seismic refraction data provided a clear picture of the crustal structure of the islands and their surrounding areas. Furthermore, the marine gravity data together with the gravity data of some of the islands (MACFARLANE, 1968) permitted a better interpretation of the regional anomalies.

4.1 Data Collection

Variations in the earth's gravitational field were recorded along 2650 line - km in the western part of the Canarian archipelago (Fig. 6). F.S. Meteor's instrument was an Askania sea gravimeter after Graf model GSS2 on a gyro-stabilised platform.

The same navigational technique was applied as that used for seismic refraction (see section 2.1) and the track chart was produced in the vessel's navigation room. The ship's course, speed and the bathymetry were recorded along all of the lines.

In the area of zone A, gravity measurements (lines RR' and SS' in Fig. 6) were made by the Geodetic Institute

of Delft Technological University. This was on board Hr. Neth. Ms. Snellius during the Navado III programme in 1965. The measurements were incorporated in the interpretation, together with gravity data acquired on board H.M.S. Protector by the University of Birmingham Geology Department (line PP' in Fig. 6).

4.2 Data Reduction

Vertical gravitational attraction was recorded continuously in analog form, one scale unit being equal to 104.93 mgal (PLAUMANN, 1967). The value of 25.862 scale units corresponded with an absolute gravity value of 979,386.5 mgal at the base station. This station was located in the harbour of Las Palmas de Gran Canaria at the Muelle Generalissimo Franco. PLAUMANN (1967) established this gravity value using a land-gravimeter to link it with the EASCL station "Gran Canary B".

Points normally taken at half hour intervals (corresponding to 3 to 4 nautical miles) were selected from the analog record, and their absolute gravity values computed from the formula

$$g_m = 979386.5 + (R - 25.862).104.93 \text{ mgal}$$

where g_m = absolute measured gravity

R = reading in scale units.

Two factors influenced those values:

i) the vessel's movements relative to the earth's rotation, and

ii) variation of the gravity field with latitude.

The first influence was accounted for by the Eötvös correction, expressed by WORZEL (1959) as:

$$g = 7.487 \cdot V \cdot \sin\alpha \cdot \cos\phi + \frac{V^2}{240.8} \text{ mgal}$$

where V = ship's speed in knots

α = true course of the vessel

ϕ = geographical latitude.

The second factor was eliminated by subtracting the normal gravity value of each station from the observed value, using the International Gravity Formula (NETTLETON, 1944):

$$gn = 978049.0(1 + 0.0052884 \cdot \sin^2\phi - 0.0000059 \cdot \sin^2 2\phi)$$

where ϕ = geographical latitude

The corrected gravity values became the free-air anomalies g_{fa} and are shown in Fig. 29.

4.3 Bouguer Anomalies

Since the free-air anomalies were still influenced by variations in bottom topography, it was necessary to remove this effect in order to observe abnormalities in the structure of the crust. This correction is known as the Bouguer correction.

In the process of applying this correction, it is common practice to fill the surrounding ocean with material of known density. The choice of this density is not a simple matter and is discussed in section 4.3.2. For each station the simple Bouguer correction was effected by adding to the free-air anomalies the attraction of an infinite sheet of equal thickness as the water layer. This was, of course,

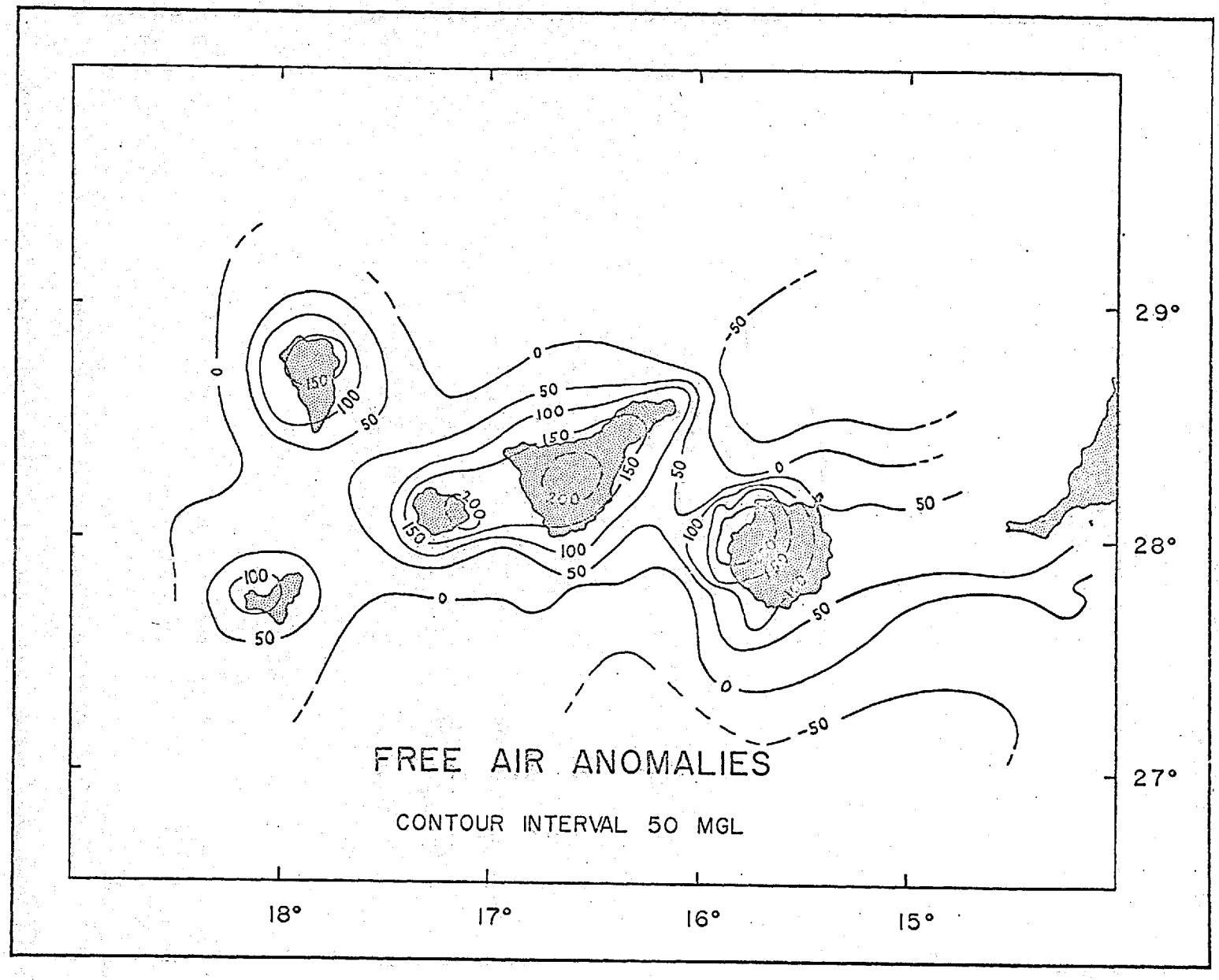
FREE AIR ANOMALIES
CONTOUR INTERVAL 50 MGL
29°
28°
27°
18°
17°
16°
15°
0
50
100
150
200

Fig.29

a rough approximation and in practice the topography differed considerably from this assumed infinite sheet. To avoid large errors, this variation was accounted for by the Terrain correction.

4.3.1 Terrain Correction

A common procedure for calculating the effect of rough terrain is the zone chart method which was presented by HAMMER (1939). But, as it is a very lengthy process, a computer programme was developed to perform these calculations. It determined the vertical attraction of the topography using the formula developed by TALWANI and EWING (1960) for the gravitational effect of a three-dimensional body.

TALWANI and EWING represent the three-dimensional body by contours which are replaced by horizontal, closed, n-sided polygons. The gravitational attraction at each external point is then calculated analytically for each polygon and plotted as a function of the respective depth of the lamina. By interpolation between the depths, the gravitational attractions can be joined by a continuous curve. The total area under this curve represents the total attraction of the body and can be obtained by numerical integration.

The vertical attraction, V, of a lamina per unit thickness was calculated from the formula

$$V = k \cdot \rho \cdot \sum_{i=1}^{n} \left[W \cdot \arccos \left\{ \left(\frac{x_i}{r_i}\right) \cdot \left(\frac{x_{i+1}}{r_{i+1}}\right) + \left(\frac{y_i}{r_i}\right) \cdot \left(\frac{y_{i+1}}{r_{i+1}}\right) \right\} - \arcsin \frac{z \cdot q_i \cdot S}{(p_i^2 + z^2)^{1/2}} + \arcsin \frac{z \cdot f_i \cdot S}{(p_i^2 + z^2)^{1/2}} \right]$$

where S = +1 if p_i positive, S = -1 if p_i negative

W = +1 if m_i positive, W = -1 if m_i negative

x_i, y_i, and x_{i+1}, y_{i+1}, = co-ordinates of two successive vertices of polygon

$$p_i = \frac{y_i - y_{i+1}}{r_{i,i+1}} \cdot x_i - \frac{x_i - x_{i+1}}{r_{i,i+1}} \cdot y_i$$

$$q_i = \frac{x_i - x_{i+1}}{r_{i,i+1}} \cdot \frac{x_i}{r_i} + \frac{y_i - y_{i+1}}{r_{i,i+1}} \cdot \frac{y_i}{r_i}$$

$$f_i = \frac{x_i - x_{i+1}}{r_{i,i+1}} \cdot \frac{x_{i+1}}{r_{i+1}} + \frac{y_i - y_{i+1}}{r_{i,i+1}} \cdot \frac{y_{i+1}}{r_{i+1}}$$

$$m_i = \frac{y_i \cdot x_{i+1} - x_i \cdot y_{i+1}}{r_i - r_{i+1}}$$

$$r_i = + (x_i^2 + y_i^2)^{1/2}$$

$$r_{i+1} = + (x_{i+1}^2 + y_{i+1}^2)^{1/2}$$

$$r_{i,i+1} = ((x_i - x_{i+1})^2 + (y_i - y_{i+1})^2)^{1/2}$$

k = gravitational constant

ρ = density of lamina

The integration procedure used by TALWANI and EWING fitted parabolas to successive sets of three points which determined the area contained between the parabolas and the depth axis. This method was simplified to numerical integration by

the SIMPSON rule provided the laminae were at equi-distant depths: Let V_0, V_1, and V_2 be vertical attractions per unit thickness caused by laminae at depths z_o, z_1, and z_2. The attraction of the body between the planes at z_o and z_2 would be

$$\int_{z_o}^{z_2} V dZ = \frac{z_2 - z_o}{6} \left[V_0 + 4V_1 + V_2 \right]$$

By using successive sets of three points, integration could be achieved for all the contours and the total attraction of the body obtained. The flow chart of the computer programme developed to perform these calculations, is shown in Fig. 30.

The advantages of this method were

i) rapid approximation of the bottom topography represented by contours,

ii) the approximation of the bathymetry could be made as accurately as desired by increasing the number of polygon sides, and

iii) vertical variations in density could be accounted for.

Its disadvantage was the fact that the earth's sphericity could not be taken into consideration. However, the error thus introduced was small (less than 3 mgal). Since it was nearly the same for all the points of observation it did not influence the anomaly picture.

In order to obtain an accurate terrain correction, a new bathymetric map (Fig. 1) was contoured, based on compiled soundings around the Canaries. Isobaths at an equidistance of 250 m, approximated by closed polygons, represented the bottom relief above the 4500 m depth line. The density of

Fig. 30: Flow Chart: Terrain Correction

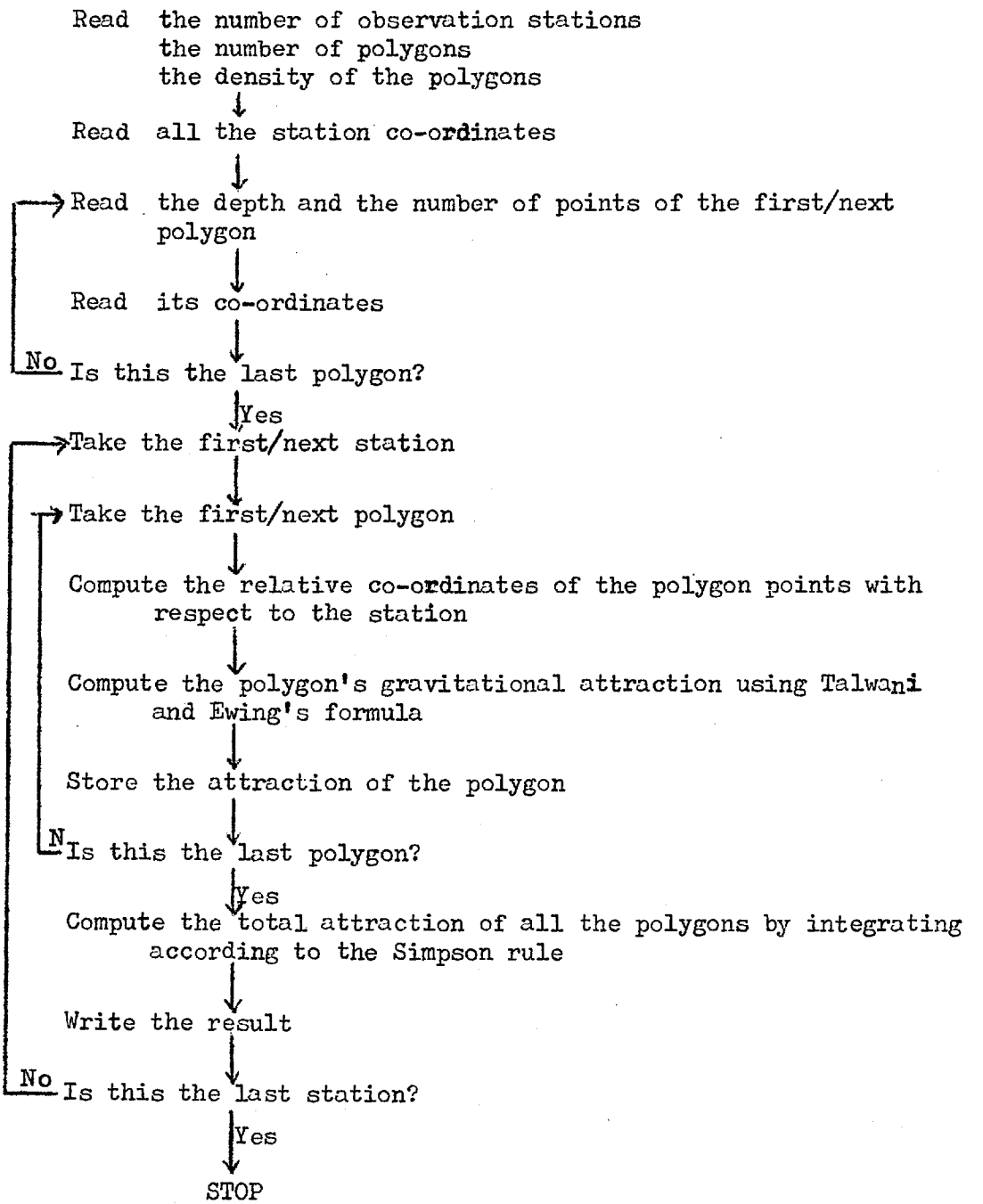

the terrain was taken as 2.40 - 1.03 gm/cc (see section 4.3.2).

The effect of the islands above sea level was determined separately, using the same method and taking the density value as 2.30 gm/cc. The total terrain correction consisted of bathmetric effect plus subaerial effect and the Bouguer anomalies were calculated from the formula

$$g_B = g_{fa} + 2\pi k_o \varsigma h - T$$

where g_{fa} = free-air anomaly

$2\pi k_o \varsigma h$ = simple Bouguer correction

h = thickness of water layer

ς = 2.40 - 1.03 gm/cc

k_o = universival gravity constant

T = total terrain correction

4.3.2 Densities Involved in the Bouguer Correction

When correcting for the mass deficit of the water layer, the crucial problem was choosing the correct density. Densities can be estimated by three different methods, (1) direct measurement of rock samples from the islands, (2) determination from the observed gravity values, and (3) seismic information around the islands.

4.3.2.1 Direct Measurement of Rock Samples

The first method uses sea bottom dredged and surface collected unweathered samples. However, this method yields only an approximate value of the density, because (i) rocks on a volcanic island are heavily weathered, (ii) many intra-flow voids are present, and (iii) much of the lava is vesicular, which reduce the bulk density of an island.

4.3.2.2 Calculation from Observed Gravity Anomalies

One method determines the density along a gravity profile assuming that changes in gravity are caused only by variations in thickness of the underlying formation. This method, due to NETTLETON (1939), selects the correct density as one in which the profile correlates least well with the topography. However, the topography of a volcanic island is closely related to the subsurface structure, violating the conditions for applying NETTLETON's method.

MACFARLANE (1968) developed a method for computing the bulk density of an island after the regional gravitational trend had been removed. This is done by developing by least squares the Bouguer anomalies over an area as polynomials of high order. By choosing a suitable density for the Bouguer correction, the sum of the squares of the residuals are minimised. His results for Tenerife were 2.41 gm/cc, for Hierro 2.36 gm/cc, and for Lanzarote 2.51 gm/cc. The average bulk density of the subaerial part of eleven Atlantic islands was 2.31 gm/cc.

However, the main body of an island is below sea level. Because lavas extruded at some depth in an aquaeous environment consist mainly of pillow basalt or breccias (JONES, 1966; MOORE, 1965; McBIRNEY, 1963), most of the lava tubes and intraflow voids are probably filled with water. Therefore the bulk density is expected to be higher for the submarine part than for the subaerial part of an island. STRANGE et al. (1965) found nearly perfect permeability of lava in the

Hawaiian Islands and a discontinuous change between dry and wet density of 0.2 gm/cc at sea level. MACFARLANE (1968) used a density of 2.4 gm/cc for the island body below sea level, because it yielded a smooth transition in the gravitational trend between the island and the offshore areas.

None of those methods could be applied to the marine gravity data. NETTLETON's (1939) method could not be used for the reasons mentioned earlier, and MACFARLANE's (1968) method required a fairly dense grid of observations which was not available. Furthermore, the bathymetry was not known with sufficient accuracy to enable a precise determination of the densities involved.

4.3.2.3 Estimation from Refraction Seismic Investigations

The bulk density of the islands could be estimated from the observed seismic velocities.

A layer with a compressional wave velocity of 2.85 - 3.56 km/sec was, on the average, 1.95 km thick and formed the upper part of the emerged and submerged island bodies. It was underlain by a layer with a velocity of 3.90 - 4.75 km/sec, with an average thickness of 2.45 km. This one also formed a substantial part of the island bodies above the surrounding ocean floor. The next layer underneath, with a velocity of 5.45 - 6.00 km/sec, only formed part of the island core.

But the seismic evidence has to be treated with some caution when interpreting P-wave velocities in terms of densities, because various factors influencing velocities leave little effect on the densities. As MANGHNANI and

WOOLLARD (1965) have shown, the velocity of vesicular basalt erupted in an oceanic environment is affected by glass content, porosity, permeability and rock structure. Porosity occurs in lavas which erupted not deeper than 800 metres below sea level (MOORE, 1965). However, water filled intraflow voids capable of withstanding high pressures could still be present below 800 metres depth and reduce the P-wave velocity. But the largest reduction in velocity is caused by the glass content. Therefore, NAFE and DRAKE's (1963) velocity-density curve was applied to the observed velocities with some reservations. The range of velocities from 2.85 - 3.56 km/sec, corresponding to the uppermost layer, yielded a density of 2.15 - 2.35 gm/cc. Since this layer is most probably built up by tuffs, clastic material and breccias, an average density of 2.30 gm/cc was chosen for the calculations. The second layer with velocities of 3.90 - 4.75 km/sec, corresponding to densities of 2.35 - 2.55 gm/cc, was interpreted as the glassy and fractured basalt. Therefore, its average density was taken as 2.60 gm/cc, somewhat higher than estimated from NAFE and DRAKE's (1963) curve.

4.3.2.4 Conclusions

Because the largest part of the island bodies is built up by the two upper refractors, the bulk density was expected to lie between 2.30 and 2.60 gm/cc. These values correspond well with MACFARLANE's (1968) estimation of the bulk density of some of the Canary Islands (see 4.3.2.2). For the sake of comparison with MACFARLANE's (1968) work,

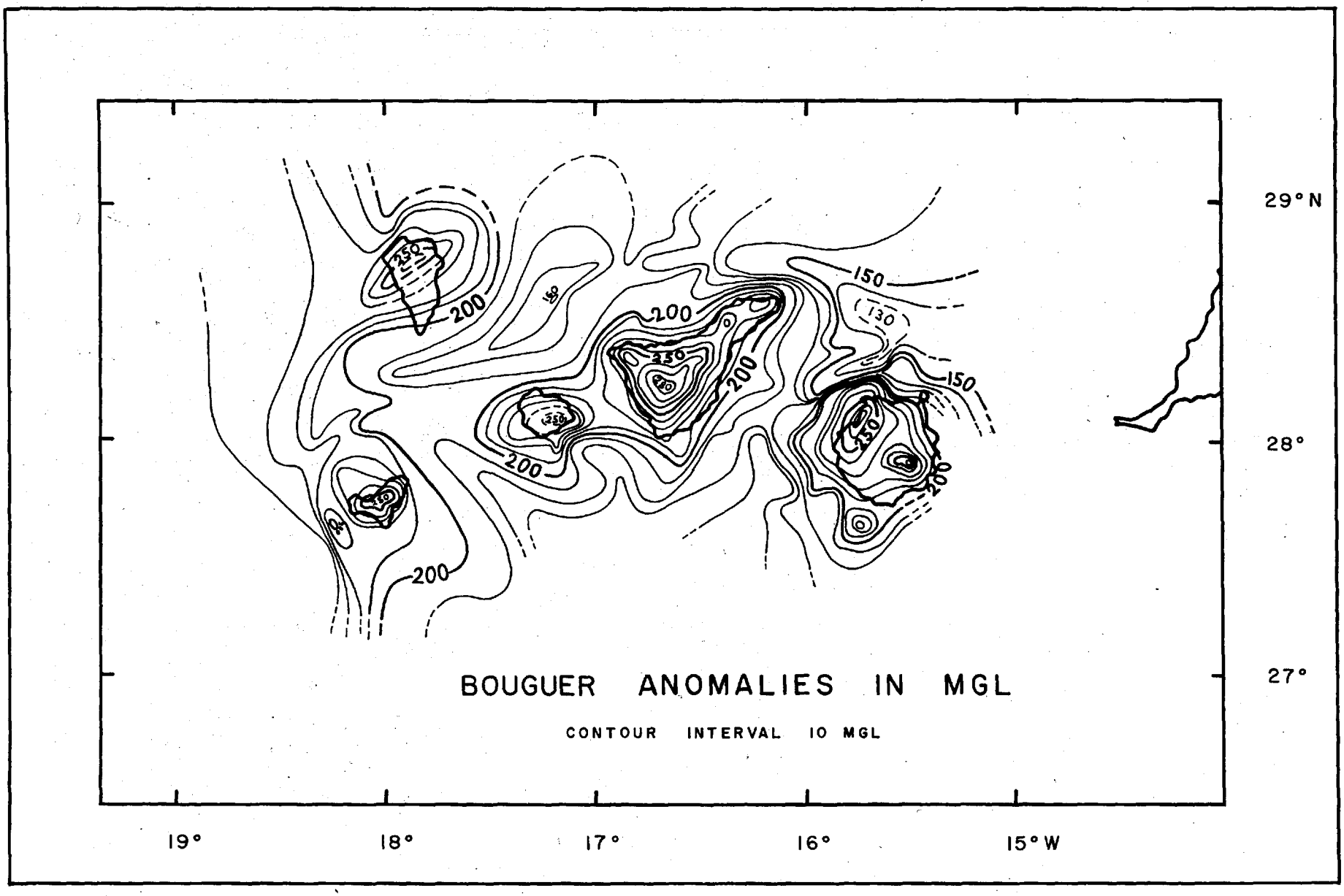
29°N
28°
27°
19°
18°
17°
16°
15°W
150
200
250
BOUGUER ANOMALIES IN MGL
CONTOUR INTERVAL 10 MGL

Fig.31

a density of 2.40 gm/cc for the submarine part of the islands and of 2.30 gm/cc for the subaerial part were chosen for the Bouguer correction. The calculated Bouguer anomalies are shown in Fig. 31 together with the anomaly distribution on the islands as computed by MACFARLANE (1968). It may be noted that very close correlation of the results was achieved between these two independent surveys.

4.4. Calculation of the Depth of the MOHO

The depth to the Mohorovičic Discontinuity, and hence the thickness of the crust, was computed from the free-air anomalies. In principle the same method was used as described by TALWANI et al.(1959), but it was extended to a three-dimensional successive approximation to the depth of the mantle. The extension of this method was justified because the gravity information densely covered an area and because the thickness of the upper crustal layers in the same area had been determined by the refraction survey.

TALWANI's method assumes the area under investigation to be in isostatic balance with the standard oceanic crustal section of WORZEL (1965). Such a section (Fig. 32) consists of 4.9 km of water of density 1.03 gm/cc, 0.7 km of sediments with a density of 2.30 gm/cc, 1.7 km of "layer 2" of density 2.55 gm/cc and 4.2 km of "layer 3" of density 2.90 gm/cc, underlain by the mantle with a density of 3.40 gm/cc. This column is in isostatic balance with the sea-level continental column 33 km high with a mean density of 2.90 gm/cc (Fig. 32).

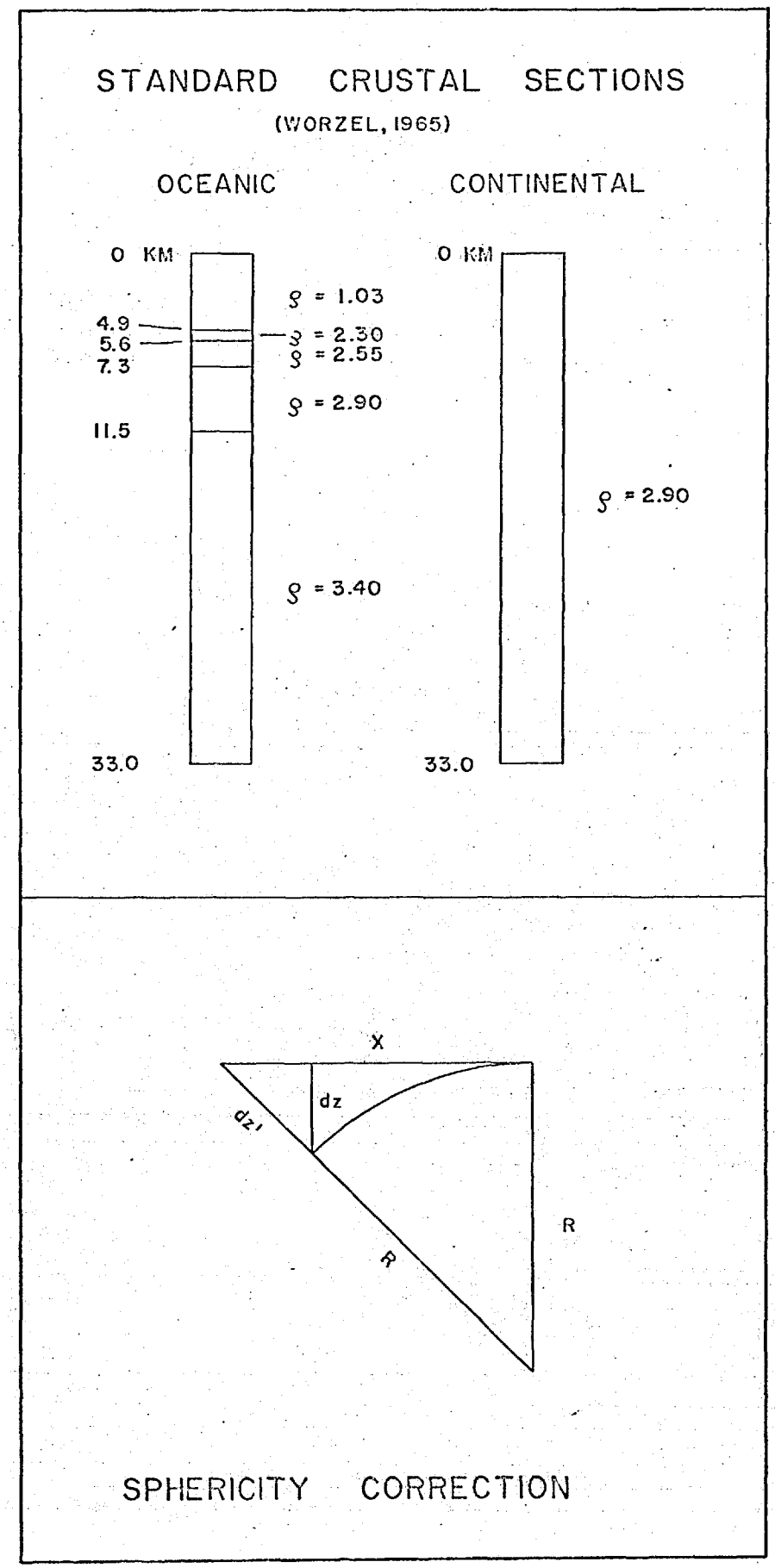
STANDARD CRUSTAL SECTIONS
(WORZEL, 1965)
OCEANIC
CONTINENTAL
0 KM
4.9
5.6
7.3
11.5
33.0
ρ = 1.03
ρ = 2.30
ρ = 2.55
ρ = 2.90
ρ = 3.40
0 KM
33.0
ρ = 2.90
X
dz
dz'
R
R
SPHERICITY CORRECTION

Fig.32

When computing the gravitational effect of each layer, the value of the density was taken as the difference between the density of the layer and the mean density of the continental column:

$$\Delta\rho_i = \rho_i - 2.90 \text{ gm/cc} \qquad i=1,\ldots n$$

The effect of all of the upper layers was computed and subtracted from the free-air value of each station. The resulting gravity value, termed "crustal anomaly", had to be equal to the gravitational attraction of the basement and mantle. By adjusting the depth of the basement - mantle interface, the residual anomaly could be reduced to zero and the depth of the MOHO determined.

4.4.1 Computing Technique

The method of TALWANI and EWING (1960) for computing the gravitational attraction of a three-dimensional body of arbitrary shape, used for the Terrain correction, could not be applied here for the following reasons:

i) the interfaces between individual layers were not planes and the application of TALWANI and EWING's (1960) technique became very complicated. It was unsuitable as it is based on the attraction of plane horizontal laminas.

ii) The "depth of the MOHO" calculations involved a crustal section extending radially 200 km from each station. Consequently, the earth's curvature became significant. TALWANI and EWING's method could not account for this influence.

Therefore a new computing technique was developed, based on the attraction of a right rectangular prism. The layers were

approximated by prisms of various sizes, heights and densities. NAGY (1966) presented a formula for the attraction of a right rectangular prism, which is completely contained in one of the four xy-quadrants, as

$$
\begin{aligned}
V = k \cdot \rho \Big\{ & x_2 \cdot \ln\left(y_2 + \sqrt{x_2^2 + y_2^2 + z_1^2} \right) - \\
& x_1 \cdot \ln\left(y_2 + \sqrt{x_1^2 + y_2^2 + z_1^2} \right) + \\
& y_2 \cdot \ln\left(x_2 + \sqrt{x_2^2 + y_2^2 + z_1^2} \right) - \\
& y_2 \cdot \ln\left(x_1 + \sqrt{x_1^2 + y_2^2 + z_1^2} \right) - \\
& z_1 \cdot \arcsin \frac{z_1^2 + y_2^2 + y_2 \sqrt{x_2^2 + y_2^2 + z_1^2}}{\left(y_2 + \sqrt{x_2^2 + y_2^2 + z_1^2} \right) \cdot \sqrt{y_2^2 + z_1^2}} + \\
& z_1 \cdot \arcsin \frac{z_1^2 + y_2^2 + y_2 \sqrt{x_1^2 + y_2^2 + z_1^2}}{\left(y_2 + \sqrt{x_1^2 + y_2^2 + z_1^2} \right) \cdot \sqrt{y_2^2 + z_1^2}} - \\
& x_2 \cdot \ln\left(y_1 + \sqrt{x_2^2 + y_1^2 + z_1^2} \right) + \\
& x_1 \cdot \ln\left(y_1 + \sqrt{x_1^2 + y_1^2 + z_1^2} \right) - \\
& y_1 \cdot \ln\left(x_2 + \sqrt{x_2^2 + y_1^2 + z_1^2} \right) + \\
& y_1 \cdot \ln\left(x_1 + \sqrt{x_1^2 + y_1^2 + z_1^2} \right) + \\
& z_1 \cdot \arcsin \frac{z_1^2 + y_1^2 + y_1 \sqrt{x_2^2 + y_1^2 + z_1^2}}{\left(y_1 + \sqrt{x_2^2 + y_1^2 + z_1^2} \right) \cdot \sqrt{y_1^2 + z_1^2}} - \\
& z_1 \cdot \arcsin \frac{z_1^2 + y_1^2 + y_1 \sqrt{x_1^2 + y_1^2 + z_1^2}}{\left(y_1 + \sqrt{x_1^2 + y_1^2 + z_1^2} \right) \cdot \sqrt{y_1^2 + z_1^2}}
\end{aligned}
$$

$$z_1 \cdot \arcsin \frac{z_1^2 + y_1^2 + y_1\sqrt{x_1^2 + y_1^2 + z_1^2}}{\left(y_1 + \sqrt{x_1^2 + y_1^2 + z_1^2}\right) \cdot \sqrt{y_1^2 + z_1^2}} -$$

$$x_2 \cdot \ln\left(y_2 + \sqrt{x_2^2 + y_2^2 + z_2^2}\right) +$$

$$x_1 \cdot \ln\left(y_2 + \sqrt{x_1^2 + y_2^2 + z_2^2}\right) -$$

$$y_2 \cdot \ln\left(x_2 + \sqrt{x_2^2 + y_2^2 + z_2^2}\right) +$$

$$y_2 \cdot \ln\left(x_1 + \sqrt{x_1^2 + y_2^2 + z_2^2}\right) +$$

$$z_2 \cdot \arcsin \frac{z_2^2 + y_2^2 + y_2\sqrt{x_2^2 + y_2^2 + z_2^2}}{\left(y_2 + \sqrt{x_2^2 + y_2^2 + z_2^2}\right) \cdot \sqrt{y_2^2 + z_2^2}} -$$

$$z_2 \cdot \arcsin \frac{z_2^2 + y_2^2 + y_2\sqrt{x_1^2 + y_2^2 + z_2^2}}{\left(y_2 + \sqrt{x_1^2 + y_2^2 + z_2^2}\right) \cdot \sqrt{y_2^2 + z_2^2}} +$$

$$x_2 \cdot \ln\left(y_1 + \sqrt{x_2^2 + y_1^2 + z_2^2}\right) -$$

$$x_1 \cdot \ln\left(y_1 + \sqrt{x_1^2 + y_1^2 + z_2^2}\right) +$$

$$y_1 \cdot \ln\left(x_2 + \sqrt{x_2^2 + y_1^2 + z_2^2}\right) -$$

$$y_1 \cdot \ln\left(x_1 + \sqrt{x_1^2 + y_1^2 + z_2^2}\right) -$$

$$\left.\begin{aligned} &z_2 \cdot \arcsin \frac{z_2^2 + y_1^2 + y_1\sqrt{x_2^2 + y_1^2 + z_2^2}}{\left(y_1 + \sqrt{x_2^2 + y_1^2 + z_2^2}\right) \cdot \sqrt{y_1^2 + z_2^2}} + \\ &z_2 \cdot \arcsin \frac{z_2^2 + y_1^2 + y_1\sqrt{x_1^2 + y_1^2 + z_2^2}}{\left(y_1 + \sqrt{x_1^2 + y_1^2 + z_2^2}\right) \cdot \sqrt{y_1^2 + z_2^2}} \end{aligned}\right\}$$

where x_1, y_1, z_1 are the co-ordinates of the prism close to the station and x_2, y_2, z_2 are the co-ordinates on the far side of the prism. k_o is the universal gravity constant and ρ the density.

Three cases were distinguished: (1) the prism was completely contained in one of the four quadrants; (2) the prism crossed either the x-axis or the y-axis; and (3) the prism crossed both axes. Case (1) was a straight-forward computation from the above formula. Cases (2) and (3) required the prism to be split into subprisms, which were completely contained in one of the xy-quadrants. This reduced the computation to case (1). The z-values were always positive causing no problems. The total attraction of the upper crustal layers were obtained by adding the effects of individual prisms.

4.4.2 Sphericity Correction

When computing the attraction of a layer up to a radius of 200 km it was essential to correct for the earth's curvature.

The derivation of the formula used to lower the depth co-ordinates of the prisms was as follows (see Fig. 32):

The true correction $dz' = \sqrt{R^2 + x^2} - R$

could be replaced by dz with an error smaller than 1% for $R = 6368$ km and $x \leq 200$ km. The above expression could be transformed to

$$dz = \sqrt{R^2 + x^2} - R$$

and $$\frac{dz}{R} = 1 + x^2/2R^2 - x^4/8R^4 + x^6/24R^6 - \ldots - 1$$

or $$dz \approx x^2/2R \quad \text{neglecting terms in } 1/R^4 \text{ and over.}$$

Hence the depth co-ordinates of a prism at a distance x from the station were adjusted according to

$$Z' = Z + X^2/2R$$

or $$Z' = Z + 0.0000785 \cdot X^2$$

where z and x are in kilometres.

4.4.3 Successive Approximation

Because the effect of the water layer had already been determined when computing the Bouguer correction, the free-air anomalies were modified to

$$g_{mf} = g_{fa} + 2\pi k_o \cdot \varrho \cdot h - T$$

where ϱ = density of water - 2.90 gm/cc =-1.87 gm/cc

h = depth of water

T = terrain effect for a density of -1.87 gm/cc

The attraction of the upper crustal layers was computed for each station and subtracted from its modified free-air value, yielding the Crustal Anomaly. For this calculation, the densities of the upper refractors were assumed to be 2.30 gm/cc, 2.60 gm/cc and 2.70 gm/cc and the thicknesses of the layers were determined from seismic information.

Before the depth of the MOHO could be computed, the problem of the varying density of the basement had to be solved. It was seen that the basement velocities obtained for different refraction profiles varied significantly. For example, profiles B and C had revealed a velocity of 6.60 - 6.72 km/sec, profiles A and D one of 7.05 km/sec and profiles E and F velocities of 7.3 - 7.5 km/sec. Using NAFE and DRAKE's velocity-density curve, the basement's density was assessed to be 2.90 gm/cc

under B and C, and 3.1 gm/cc under A, D, E and F.

Obviously, the few seismic lines could not define the area accurately where the basement was denser, and its boundary had hence to be assumed. Beside the seismic evidence another source of information was gained by calculating a first approximation to the depth of the mantle. This was effected, assuming the basement to consist of material of uniform density and to be an infinite Bouguer sheet, with the formula

$$DM = 33 \left(\frac{\Delta\rho_M}{\Delta\rho_M - \Delta\rho_B}\right) - \frac{CA}{41.91\ (\Delta\rho_M - \Delta\rho_B)}$$

where $\Delta\rho_M$ = 0.5 gm/cc

$\Delta\rho_B$ = density of basement - 2.90 gm/cc

CA = crustal anomaly

DM = depth of the MOHO

These calculations showed that the MOHO dipped from the ocean basins towards the island ridge. At the foot of the ridge this trend was converted to an upward slope. This change in slope was assumed to result from mass deficiency. This trend, together with seismic evidence, was used to determine the boundary of the denser basement.

Once the area of the denser basement was defined, the depth of the MOHO under each station was successively approximated by computing the gravitational effect of the basement plus the mantle and subtracting it from the crustal anomaly of each station. The residual anomaly R was used to correct the depth of the basement-mantle interface according to DM' = DM - d where $d = \frac{R}{2\pi k_o\ (\Delta\rho_M - \Delta\rho_B)}$

and where

DM' = new depth of the MOHO

DM = old depth of the MOHO

This interface was adjusted for prisms lying within a radius of 20 km from a station in the western region and within 40 km in zone A.

After the depth of the MOHO had been calculated for every station and the prisms' depths were adjusted, the attraction of the modified basement and mantle was recomputed. The new residual anomaly served for a re-adjustment of the depth of the MOHO.

It was found that the root mean square of the residuals, calculated after each approximation, diminished very slowly after the fourth cycle. It approached the accuracy of the data and little would have been gained by repeating the cycle. Fig. 33 shows the flow chart of the computer programme.

4.4.4 Advantages and Disadvantages of the Method

The advantages of the method can be tabulated below:

i) the prism method is a very versatile tool, because it can be applied to any structure with lateral and vertical variations in density,

ii) the approximation of a three-dimensional body can be made as accurately as desired by increasing the number of prisms,

iii) when computing the gravitational attraction of a large portion of the crust, the sphericity of the earth can

Fig. 33: Flow Chart: Depth of MOHO

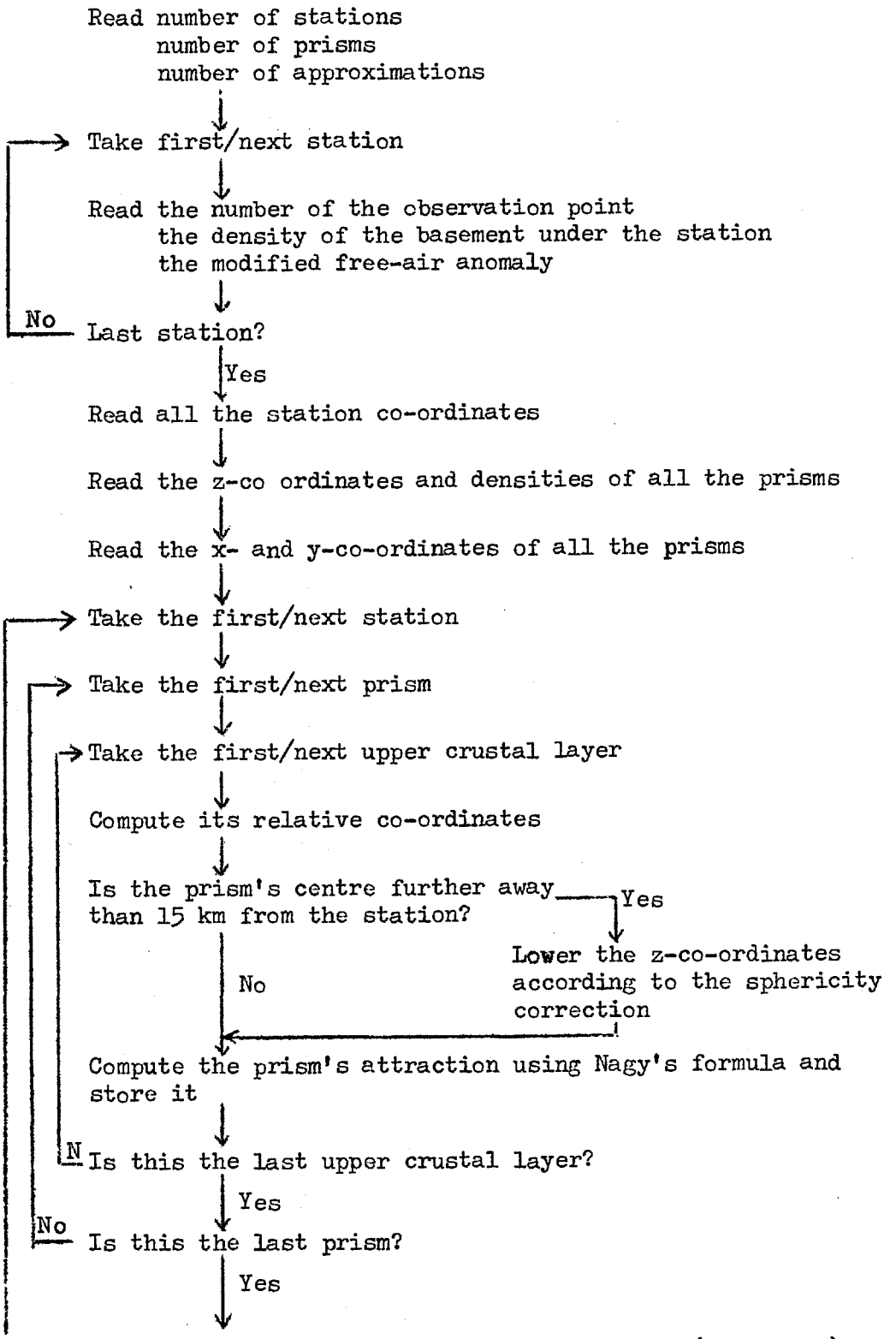

(Continued)

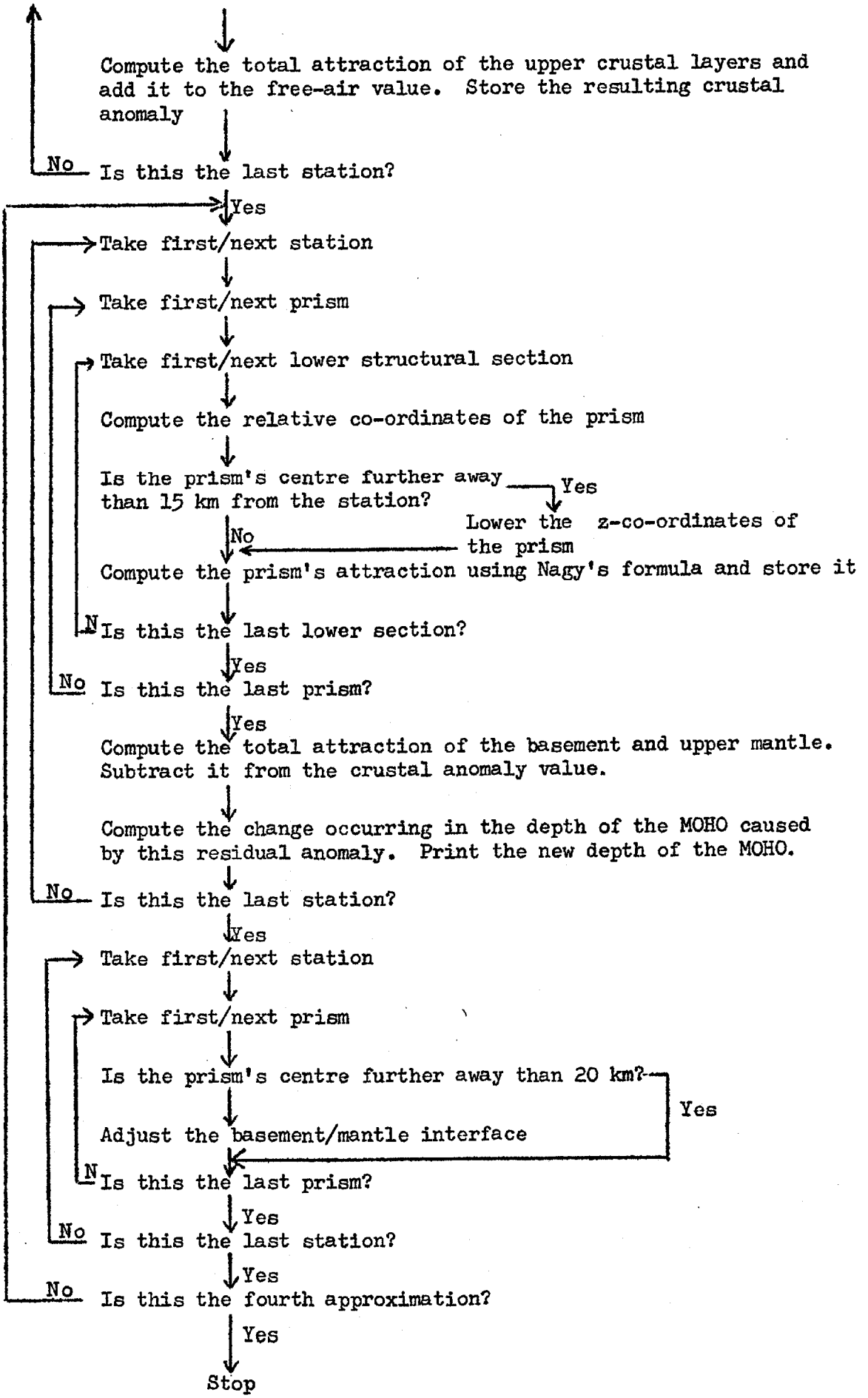
Compute the total attraction of the upper crustal layers and add it to the free-air value. Store the resulting crustal anomaly
No
Is this the last station?
Yes
Take first/next station
Take first/next prism
Take first/next lower structural section
Compute the relative co-ordinates of the prism
Is the prism's centre further away than 15 km from the station?
Yes
Lower the z-co-ordinates of the prism
No
Compute the prism's attraction using Nagy's formula and store it
N
Is this the last lower section?
Yes
No
Is this the last prism?
Yes
Compute the total attraction of the basement and upper mantle. Subtract it from the crustal anomaly value.
Compute the change occurring in the depth of the MOHO caused by this residual anomaly. Print the new depth of the MOHO.
No
Is this the last station?
Yes
Take first/next station
Take first/next prism
Is the prism's centre further away than 20 km?
Yes
Adjust the basement/mantle interface
N
Is this the last prism?
Yes
No
Is this the last station?
Yes
No
Is this the fourth approximation?
Yes
Stop

be taken into consideration, and

iv) any variation in thickness of a layer can be easily accounted for.

Disadvantages: To avoid errors, the adjustment of the basement-mantle interface has to be done on a large scale, involving a great number of prisms. These in turn influence the required computing time and in the present case 0.15 minutes were needed for one approximation and one station. The depth of the MOHO for all the stations in the Canaries was calculated in 240 minutes.

Accuracy of the method: WORZEL's (1965) standard oceanic crustal section was recomputed on the basis of the three-dimensional method. The depth of the MOHO was established at 10.6 km which was 0.9 km shallower than the "standard" depth of 11.5 km in oceanic areas.

4.4.5 Results

Fig. 34 shows the depth of the MOHO in the vicinity of the Canary Islands. As can be seen, there is a close agreement between the depths computed from gravity and seismic information:

	Depth of the MOHO	
	from seismic	from gravity
Profile B	12.0 ± 2.5 km	13.0 ± 1.0 km
Profile C	12.2 ± 2.1 km	13.0 ± 1.0 km
Profile A	15.0 ± 0.6 km	15.5 ± 1.0 km
Profile D	13.9 ± 1.0 km	15.0 ± 1.0 km

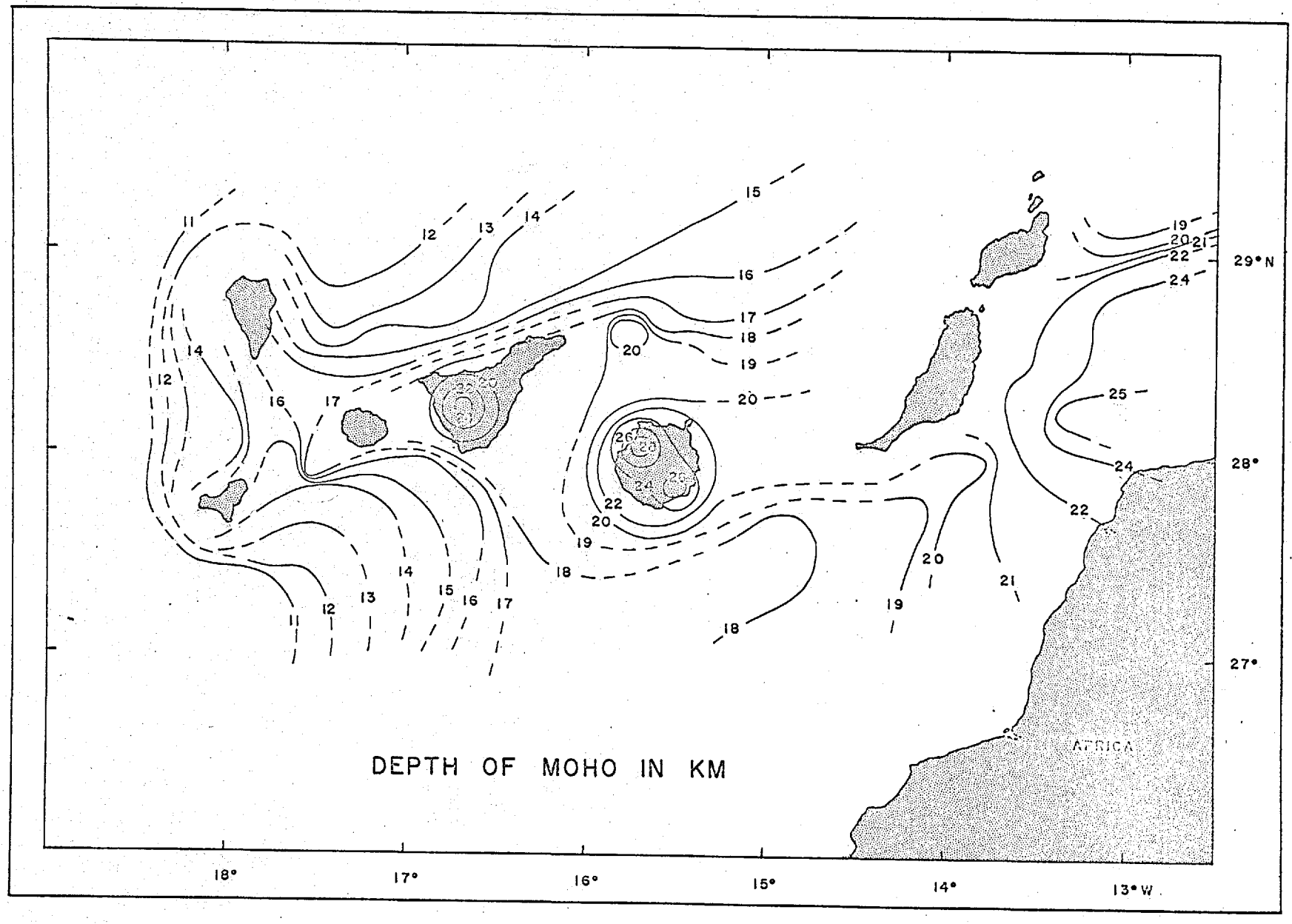

Fig.34

It may be noted that the depths are well within the error limits. However, an error was introduced when assuming the structures of most of the island roots. Since only Tenerife's "plug" and basement were determined fairly accurately, the calculated depths of the MOHO close by the islands are therefore not reliable since the gravitational attraction is influenced by these unknown structures.

4.5 Structural Model for Tenerife

A model was constructed to explain the observed Bouguer anomaly over Tenerife. When constructing the model, five restraints were subjected, (1) the magnitude of the anomaly, (2) the shape of the anomaly, (3) the densities within which the model was to be constructed, (4) the geologically permissible densities, and (5) the maximum depth of the upper boundary of the anomalous body. It was assumed that the structure was radially symmetrical with respect to the vertical axis through the centre of the anomaly.

The structural model was fitted to line AA' (Fig. 35). It was chosen because the field was least disturbed by rift zone effects. The crust was assumed to consist of 4.5 km of material of density 2.3 gm/cc, underlain by a layer 3 km thick of density 2.6 gm/cc. These two layers covered 3 km of material of density 2.7 gm/cc. The basement was 4 km thick and had a density of 2.9 gm/cc.

The structure of the island had been partially determined by seismic measurements where it was suggested that a plug was present at a depth of 4.7 km below Vilaflor

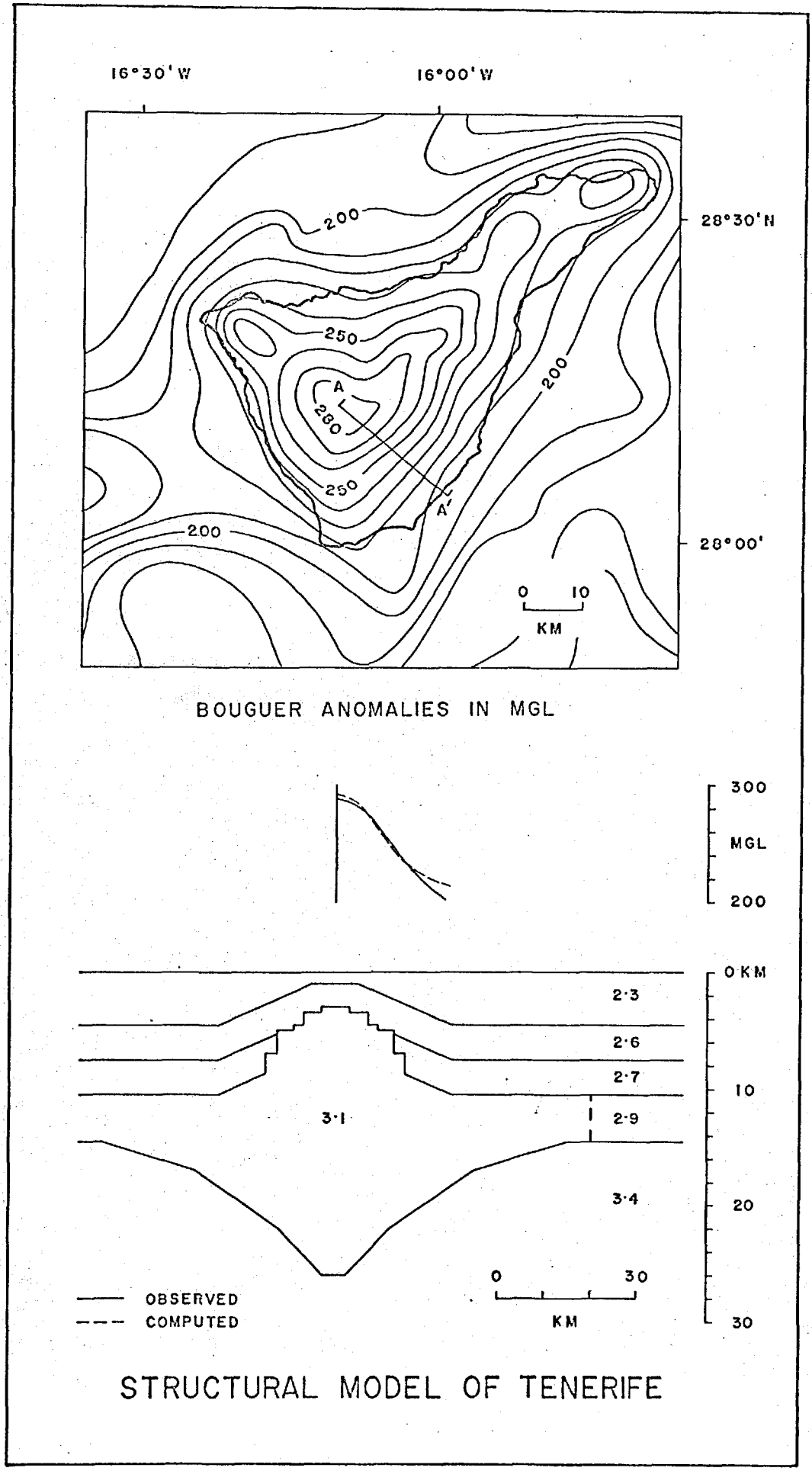
16°30'W
16°00'W
28°30'N
28°00'
200
250
280
A
A'
0 10
KM
BOUGUER ANOMALIES IN MGL
300
MGL
200
0 KM
2·3
2·6
2·7
2·9
3·4
3·1
10
20
30
0 30
KM
OBSERVED
COMPUTED
STRUCTURAL MODEL OF TENERIFE

Fig.35

and that its base had a diameter of 30 km. It was also suggested that the mantle was 14.5 km below the surface of the sea, 50 km from the centre of the anomaly, dipping towards the centre of the island and that the upper crustal layers followed the topography of the island. The upper layers of the island's structure were approximated by truncated cones - a feature similar in shape to an island when the topography above sea level is removed. The density of the basement including the plug was assumed to be 3.1 gm/cc up to a radius of 50 km from the centre of the anomaly and 2.90 gm/cc beyond this limit. Fig. 35 shows one such model which satisfies the above restraints. The MOHO is shown to be locally depressed to 26 km, compensating for the excess mass of the island root.

4.6 Structural Model for Gran Canaria

When constructing this model, similar assumptions were made as for Tenerife. Gran Canaria was approximated by a truncated cone with an upper diameter of 46 km and by assuming that the upper layers followed the island's topography. The crustal layers were assumed to have identical thicknesses and densities to the ones assumed in 4.5, with the exception of the basement. The depth of the MOHO around Gran Canaria had been determined from the free-air anomalies as 18 km and the basement density was assumed to be 3.1 gm/cc to a radius of 100 km from the centre of Gran Canaria and 2.9 gm/cc beyond this limit.

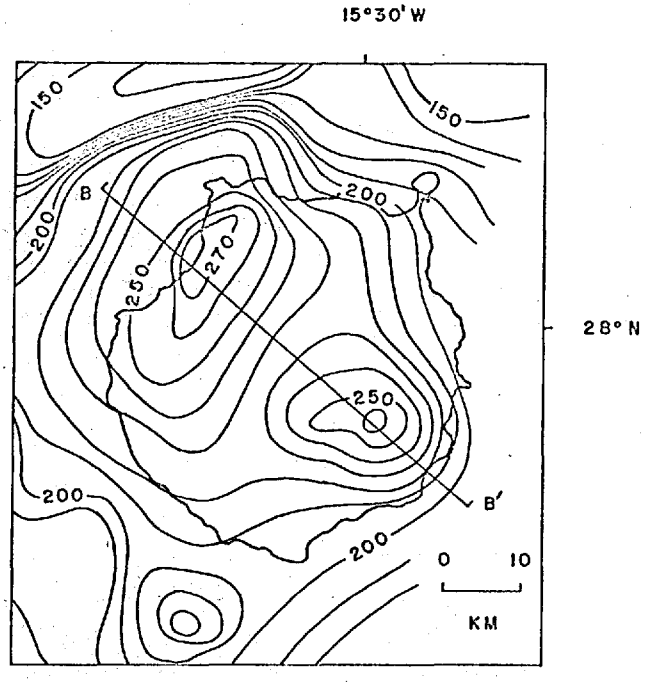

BOUGUER ANOMALIES IN MGL

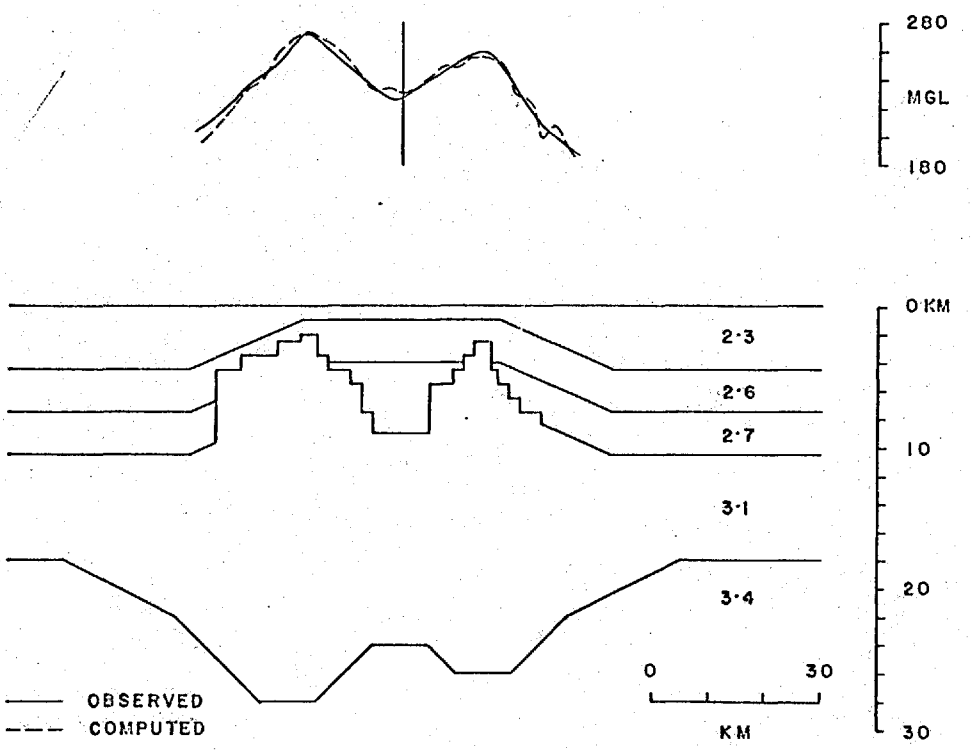

STRUCTURAL MODEL OF GRAN CANARIA

Fig.36

In contrast to the anomaly picture of Tenerife, two Bouguer anomaly highs were observed along line BB'. To explain them, two high-density bodies were assumed and were constructed respecting the five restraints mentioned in 4.5. Fig. 36 shows one possible crustal model where the depth of the MOHO below each body is 28 km, and 26 km respectively.

4.7 Error Consideration

The points where two gravity profiles crossed (Fig. 6) were used to estimate the accuracy of the data.

Repeated measurements at the base station with the ship's gravimeter showed that the instrumental errors were negligible, compared with other sources of error in the gravity values (PLAUMANN, 1967). The main error was introduced by the uncertainty in navigation. At intersections over a flat sea-bottom the average error in the free-air anomaly was $\pm$ 1 mgl. Over a rough bottom topography, such as the island flanks, this figure was substantially larger. The average error in the free-air gravity values, calculated from 12 intersections in various parts of the island group, yielded an error of $\pm$ 6 mgl.

When computing the Bouguer anomalies, another source of error was introduced by the correction for the variations in bottom topography. Since it did not exceed $\pm$ 3 mgl, the accuracy of the Bouguer values is believed to be $\pm$ 7 mgl.

When computing the depth of the MOHO, a variation of 6 mgl in the free-air anomalies displaces the MOHO by not more than 0.5 km. Consequently, the computed depths of the Mohorovičic Discontinuity are believed to be accurate to $\pm$ 1 km.

CHAPTER 5

DISCUSSION OF THE RESULTS

The seismic and gravity surveys in the Canaries have yielded some information on the structure of the crust in this area. Regional and local crustal trends have been established. The geophysical results have been correlated with geological and petrological data and the relevant conclusions are discussed in the following sections.

5.1 Seismic Velocities

The P-wave velocities encountered in the Canary Islands can be correlated with geological and petrological data to determine the local crustal structure.

Since the Canaries are volcanic islands and the different measured velocities represent layers of differing composition, it is appropriate to review ideas of the structure of marine volcanoes.

From a geological study of intra-glacial volcanoes in Iceland, JONES (1966) suggested that volcanic eruptions in deep water are characterised by quiet effusions of lava. The associated rocks consist mainly of pillow lavas and breccias forming steep ridges or piles. Gravitational collapse of pillow lavas produces breccias and clastic material which surround these ridges or piles. The growing pile of lava causes the sea to shoal and the character of the eruptions changes. In shallow water the outflow of lava is explosive,

producing mainly vitric tuff. The feeder system intrudes the core of pillow lavas and this results in a dyke injection into the body of the island.

NAYUDU (1962) proposed a three-stage development of submarine volcanoes. Fissures in the crust enable fluid lava to erupt and to form tuffs and breccias. As this pile grows, it is intruded by later magma which forms dykes, sills and laccolith-like structures within the mound. Extruding magma forms, as in the first stage, tuffs and breccias. This sequence, if repeated, results in a structure consisting of a core with a high proportion of solid lava, surrounded by tuffs, breccias and clastic material.

Both hypotheses suggest that island cores consist of a high proportion of solid lava, surrounded by a mantle of pillowy lava and breccias and an outer layer of tuff and clastic material.

Refraction surveys in the vicinity of oceanic islands have revealed structures which correspond well with the above geological hypotheses. RAITT (1954,1957) found that some atolls in the Marshall Islands consist chiefly of four layers: the core is built up of material with a P-wave velocity of 5.5-6.15 km/sec, possibly representing an intrusive basaltic core. It is covered by a layer with a velocity of 3.5-4.75 km/sec which is inferred to be vesicular and fractured basalt. Those layers are in turn buried under material of 3.0-3.35 km/sec. Drill cores show that it is mostly tuff and volcanic debris, but rare calcareous material was also found. The uppermost layer has a velocity

of 2.4-2.6 km/sec and was inferred to be sedimentary.

RAITT (unpublished) made similar observations in two other surveys north of Guadeloupe Island and north of Hawaii. In both cases a positive feature with P-wave velocities close to 6 km/sec underlies material with a velocity of 4 km/sec. The relief of the 4 km/sec layer was in all cases considerable.

Investigating the island of Bermuda, OFFICER et al. (1952) suggested that the island is the truncated cone of a volcano, capped by some 200 metres of volcanic debris and chalky limestone. The top of the cone was thought to be amygdaloidal basalt becoming increasingly compact with depth to P-wave velocities of 5.5 km/sec,

The velocities encountered in the Canaries can be successfully compared with the refraction surveys in the Hawaiian arch and the Hawaiian Ridge (FURUMOTO and WOOLLARD, 1965). The velocities fall into five groups as shown below:

	P-wave velocities in km/sec		
	Hawaiian arch	Hawaiian Ridge	Canaries
Group 1	2.15	2.68	2.85-3.56
Group 2	4.20	3.65	3.90-4.75
Group 3	5.56-6.41	4.96	5.35-6.00
Group 4	6.82-7.01	7.15	6.60-7.50
Group 5	7.97-8.68	8.20	7.65-8.12

The geological significance of each of these groups is discussed in the following paragraphs.

5.1.1 Group 1: 2.85-3.56 km/sec

These velocities were found on every profile and represent the first refractor. The thickness of this layer varies between 1.40 and 2.90 km. It may represent NAYUDU's (1962) and JONES' (1966) clastic zone. The velocities are too high to be associated with unconsolidated sediments.

5.1.2 Group 2: 3.90-4.75 km/sec

These velocities, associated with the second refractor, were observed on all the profiles. The thickness of this layer varies from 1.77 km to 3.73 km and large variations in velocities seem to be characteristic. RAITT (1954, 1957) found the velocities ranging between 3.50-4.75 km/sec and FURUMOTO and WOOLLARD (1965) between 3.65-4.20 km/sec. A large variety of rocks could be attributed to these velocities.

However, this layer most probably represents the pillow basalt. This view is in accordance with geological hypotheses. The considerable variations in thickness of this refractor may have been caused by uneven outflow of lava. The wide range of velocities found for this layer are probably due to the heterogeneity of the material.

MANGHNANI and WOOLLARD (1965) investigated factors which influence velocities in basalts. They found that two factors lowered the velocity, viz. (i) the amount of interstitial glass present and (ii) the porosity, whereas the velocity increased with the olivine content. Only small variations of these three factors were necessary to cause

considerable changes in the observed velocities.

RAITT (1954) gave further evidence for the volcanic composition of this layer. He correlated the observed velocities of 3.50-4.75 km/sec on Bikini Atoll with drilled samples of vesicular basalt. OFFICER et al.(1952) obtained a similar result on Bermuda where the solid basaltic cone of the volcano had a shell of amygdaloidal basalt.

Some sedimentary rocks show P-wave velocities which are also compatible with those observed. For geological reasons it seems highly improbable, however, that a sedimentary layer would occur so close to the island core because:

i) the location of this layer is such, that it is buried under tuff and clastic material. As the exposed part of Hierro is less than 1.5 MY old (ABDEL-MONEM et al., 1967) an impossibly high sedimentation rate would have been necessary to obtain the observed thickness of 3.73 km.

ii) Since possible sources of sediment are (a) the islands themselves, (b) the African continent and (c) direct sedimentation from the sea, a gradual decrease in sediment thickness should be expected away from the continent and the islands. But no relationship of this kind was observed.

iii) Outflowing lava would have affected any autochthonous sediment present at the time of eruption. Hence signs of altered and remobilised sediment should be found among the Canarian rocks and their chemical composition. However, geological data did not reveal any indications for this (see section 5.5).

Therefore it is very improbable that this layer consists of sediment alone.

5.1.3 Group 3: 5.35-6.00 km/sec

The velocities observed for the third refractor are compatible with velocities of the oceanic layer 2. RAITT (1963) found average values of 5.14 ± 0.6 km/sec for the Eastern North Atlantic and of 4.89 ± 0.6 km/sec for the Western North Atlantic. A wide variety of rock types including sediments and volcanics can be attributed to observed velocities of the oceanic layer 2.

Advocating a sedimentary nature of this layer, EMILIANI (1965) suggested that it consisted of carbonates of possibly lower Cretaceous age in the Carribean and Bahamas.

However, the nature of this layer does not seem to be uniform under the oceans. RAITT (1963) argued that it had a volcanic composition near some groups of Pacific islands and atolls. Experimental drilling at a possible Mohole site in Guadeloupe Bay off California indicated a basaltic nature of layer 2 (HESS, 1965). OFFICER et al.(1952) correlated the refractor with a velocity of 5.52 km/sec, observed on Bermuda, with drilled samples of compact basalt.

Experimental work on the variations of velocity with temperature and pressure of some basic igneous rocks (HUGHES and MAURETTE, 1957) yielded values of 5.5-5.7 km/sec for basalt at a depth of 8 km. MANGHNANI and WOOLLARD (1965) showed that Hawaiian basalts of low porosity had velocities ranging between 4.8-6.0 km/sec. HILL (1957) measured P-wave velocities on basalts and found them to be well within the range attributable to layer 2.

Therefore it is plausible to view the third refractor in the Canaries as representing massive basalt. This interpre-

tation closely agrees with the geological hypotheses inferring that the centres of islands have a high proportion of solid lava in the form of dykes, sills and laccolith-like structures. Furthermore, the average depth of this layer of 6.75 km under the Canaries ridge and 7.75 km under the island flanks correlates well with the experimental data of HUGHES and MAURETTE (1957).

5.1.4 Group 4: 6.60-7.50 km/sec

These velocities are associated with the basement layer, the lowest crustal layer above the Mohorovičic Discontinuity. In contrast to all the other layers, a correlation between the recording site and the observed velocity is evident. In the west of the Canaries, the velocities are 6.60-6.72 km/sec. In the adjacent ocean basins north and south of the Canaries ridge, they are 7.05 km/sec, whereas under the island ridge itself velocities of 7.3-7.5 km/sec are observed.

Velocities of 6.60-6.72 km/sec are typical of the oceanic layer 3. RAITT (1963) found average velocities of 6.56 ± 0.32 km/sec in the Eastern North Atlantic and of 6.70 ± 0.27 km/sec in the Western North Atlantic. The widespread occurrence of this layer under the oceans led EWING and EWING (1959) to call it the "oceanic layer".

HESS (1962) suggested that the oceanic layer consists of partly serpentinised peridotite. This is formed from that part of the upper mantle which is in the active zone of the mid-oceanic ridge crest and which is below the 500°C isotherm. In contradiction to HESS (1962) it was argued by CANN (1968) that the oceanic layer is formed through a

secondary process and is not directly discharged from the mantle. According to CANN (1968), at mid-oceanic ridges, basalts are directly exuded from the mantle. These magmas partly metamorphose some distance away to produce amphibolites which form the oceanic layer. Both hypotheses produce rocks which have velocities compatible with the observed ones (BIRCH, 1960, 1961).

Material of velocity 7.0-7.6 km/sec is generally found under volcanic islands, mid-oceanic ridges and on continental margins (FURUMOTO and WOOLLARD, 1965; EWING and EWING, 1960; LE PICHON et al., 1965, TALWANI et al., 1965; WORZEL, 1965; BELOUSOV, 1967; BLUNDELL and PARKS, 1969). Velocities typical of the oceanic layer 3 are usually absent when the basement consists of material of 7.0-7.6 km/sec.

These basement velocities encountered in Hawaii (FURUMOTO et al., 1965) were interpreted as intruded mantle material, which underwent gravitational differentiation. The rocks thus produced could be olivine-rich basalts and dunites. This is consistent with experimental results, where very olivine-rich basalts under atmospheric pressure had velocities of up to 7.0 km/sec (MANGHNANI and WOOLLARD, 1965). HUGHES and MAURETTE (1957) measured velocities of 7.2 km/sec for dunite at pressures equivalent to a depth of 10 km.

The rocks in the basement layer under the Canaries ridge can therefore be viewed as being formed by intrusion of mantle-like material into the oceanic layer. This must have been restricted to the area under the Canaries ridge, because the highest basement velocities are confined to that area and

gradually diminish from the axis of the ridge.

Geological evidence supports the hypothesis of an intrusion of mantle-like material into the oceanic layer 3. RIDLEY (1968) pointed out that the bulk of Tenerife's volcanics exhibit a high-pressure mineralogy and therefore must have been formed at a depth of about 35 km. This is well below the depth of the MOHO around Tenerife (Fig. 34). The subsequent vulcanism, characterised by a low-pressure mineralogy, was probably a differentiation from the primary magma (RIDLEY, 1968). This could have resulted in a concentration of dense minerals in the remaining magma. Substantial support to this theory was given by MIDDLEMOST (1969) who found a "basal complex" on La Palma consisting of mafic (olivine-augite basalts) and ultra-mafic rocks (dunites). These rocks correspond excellently with the observed velocities and with the results of MANGHNANI and WOOLLARD (1965) and HUGHES and MAURETTE (1957).

The intrusion of magma into the oceanic layer from the upper mantle, as suggested from petrological data (RIDLEY, 1968), seems, therefore, to be directly associated with the origin of the Canary Islands. It quite satisfactorily explains the decrease in velocity of the basement away from the axis of the Canaries ridge.

The regional trend in the distribution of basement velocity in the Canaries area is of importance. The velocity increases from west to east, towards the African continent. Whereas normal oceanic layer velocities were observed in the ocean basin west of Hierro - La Palma, velocities of 7.05 km/sec were found eastwards of Tenerife - Gomera. This can

be interpreted as a change in crustal character from the oceanic crust in the west to transitional crust eastwards of Tenerife. This suggestion is consistent with the estimations of the depth of the MOHO (see section 5.2).

5.1.5 Group 5: 7.65-8.12 km/sec

These velocities were observed on the four Meteor profiles A, B, C and D. The computed average velocity of 7.97 ± 0.19 km/sec is compatible with upper mantle velocities (RAITT, 1963).

Profiles A and D were shot in opposite directions and revealed velocities of 7.65 km/sec and 8.12 km/sec respectively. Assuming that no lateral changes in velocity and dip are present in the upper mantle, a dip of 3.5° of the MOHO could make those velocities consistent with an upper mantle velocity of 7.9 km/sec. Although one must be cautious when using these assumptions, the downward trend of the MOHO towards the African continent was confirmed by seismic depth estimations and by analyses of the free-air anomalies (see sections 5.2 and 5.4). The value of 3.5° seems, however, to be a locally high dip (Fig. 34).

5.2 Estimation of the Refractors' Thicknesses

The downward trend of the MOHO towards the African continent, suggested from the observed upper mantle velocities, was confirmed by depth estimations. To the west of the Canary Islands the depth of the mantle is about 12 km. It dips towards the east, reaching a depth of 14.2 km south of Gomera-Tenerife and of 14.7 km north of Tenerife-Gran

Canaria. These depths are considerably greater than the "standard" 11.5 km depth of the MOHO in oceanic areas (WORZEL, 1965). The crust can therefore be interpreted to be oceanic west of Hierro-La Palma, and to change its character to a transitional type further to the east. This result closely corresponds with the suggested composition deduced from the increase in basement velocity.

Further evidence for a thickening of the crust towards the African continent is demonstrated by the two faults detected between Gran Canaria and Tenerife (Profile E) and Tenerife and Gomera respectively (Profile F). Both show a downthrow on the southeastern side of about 0.5 km for each interface with the exception of the relative thinning of the second layer towards Gran Canaria and the high basement under Tenerife. It is upwarped by about 1.0 km from the surrounding basement and forms the structural block of Tenerife and Gomera (Fig. 37).

The first and second refractor have no correlation with this increase in crustal thickness towards the African continent. On the contrary, in the second layer a certain decrease of thickness was observed away from the probable lava source, originating from the fractures beneath the islands. This pattern supports the suggested volcanic nature of this layer. Layer 3, representing the massive basalt, and the basement gradually thicken from the west towards the east of the Canaries group. The crustal thickening towards Africa is therefore effected by an accumulation of basalt

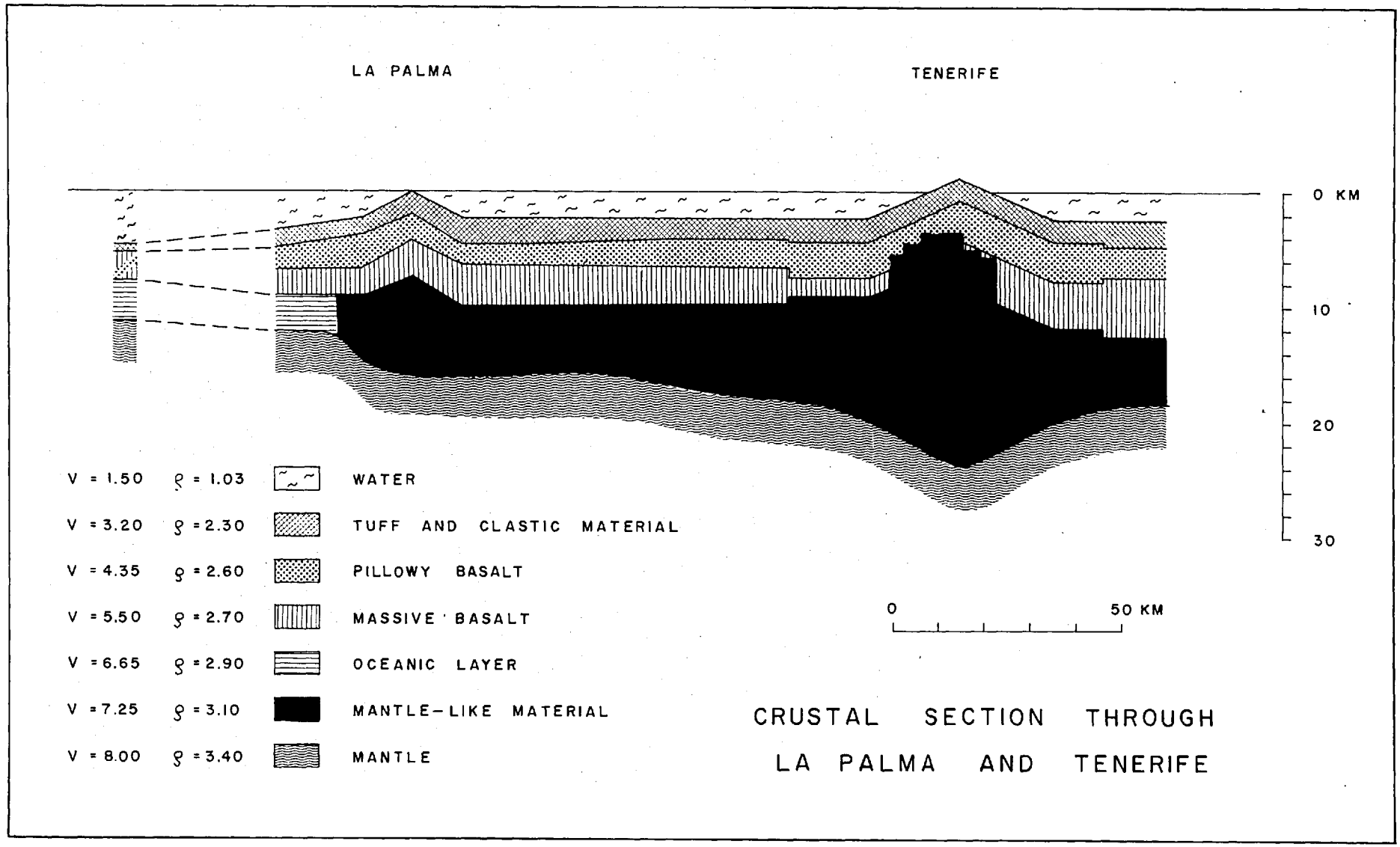
LA PALMA
TENERIFE
0 KM
10
20
30
0
50 KM
V = 1.50 ρ = 1.03 WATER
V = 3.20 ρ = 2.30 TUFF AND CLASTIC MATERIAL
V = 4.35 ρ = 2.60 PILLOWY BASALT
V = 5.50 ρ = 2.70 MASSIVE BASALT
V = 6.65 ρ = 2.90 OCEANIC LAYER
V = 7.25 ρ = 3.10 MANTLE-LIKE MATERIAL
V = 8.00 ρ = 3.40 MANTLE
CRUSTAL SECTION THROUGH
LA PALMA AND TENERIFE

Fig.37

and an intrusion of mantle-like material into the oceanic layer (Fig. 37).

Of special interest is the "high-density body" found under Tenerife. In accordance with the results obtained in the Hawaiian islands (FURUMOTO et al, 1965; MALAHOFF and WOOLLARD, 1966), this plug is at a depth of about 5.5 km below the main caldera. It appears to rise over 6 km from the elevated basement of the Tenerife-Gomera block where it has a diameter of about 30 km (Fig. 35). It is this body which causes the positive Bouguer anomaly over Tenerife. Evidence for similar plugs exist on the other Canary Islands (see section 5.3). It was shown by MIDDLEMOST (1969) that they most probably consist of material very similar to the composition of the basement.

Fig. 37 shows a crustal section from La Palma to Tenerife through the western part of the island group. It was constructed along Profiles G, F and E (Fig. 6) using seismic information and results of computations from free-air anomalies. WORZEL's (1965) standard oceanic crust has been drawn in the west for reference. The transitional character of the crust in the eastern side of the section is evident. In addition, it may be noted that the oceanic layer 2 splits into two distinguishable regions under the island ridge.

5.3 Bouguer Anomalies

The Bouguer Anomaly map (Fig. 31) shows regional and local anomalies. The regional gradient amounts to about 60 mgl from west of La Palma - Hierro to Gran Canaria, yielding an average value of 0.2 mgl/km. This is evidence

for the crust thickening towards the African continent and is consistent with the seismic results (section 5.2).

As was expected, positive anomalies caused by plutonic centres occur over the islands. As might be presumed from the bathymetry (Fig. 1), Gran Canaria, La Palma and especially Hierro seem to be independent islands on the ridge, whereas Tenerife and Gomera lie on the same structural block. It was found in the seismic survey that this structural block consisted of an elevated basement (section 5.2).

The region north of Gran Canaria shows an outstanding feature. Here, the anomaly changes by 138 mgl within 23 km, yielding an average value of 6 mgl/km for the gradient. This is strong evidence for a fault running perpendicularly to the gradient, i.e. NE to SW. The fault located by Profile E between Tenerife and Gran Canaria lies in the same line as this fault and could well be its extension (Fig. 39).

The fault located by Profile F between Tenerife and Gomera coincides with the fracture suggested by MACFARLANE (1968). It strikes NE-SW through Tenerife - Gomera - Hierro and joins a number of positive anomalies (Fig. 39).

Both faults north and south of Tenerife run nearly parallel in NE-SW direction. They are major transcrustal fracture zones which enabled magma to rise to the surface and are the probable cause for the origin of the Canary Islands (see section 5.6). The islands associated with the faults, namely Hierro, Gomera and Tenerife on one hand and Gran Canaria on the other, lie to the southeast

or the downthrown side of the faults. A very similar observation was made by RYALL and BENNETT (1968) on Hawaii. The positive gravity anomalies occurred likewise on the downthrown side of the faults. RYALL and BENNETT (1968) argued that the surface of the downthrown block was affected by a system of secondary cracks and tension fissures. Lava erupting in later cycles followed the shorter route and accumulated on the lower block thus building the bulk of the islands.

Most probably all the western Canary Islands are related to faults in the NE-SW direction. Although there is no geophysical evidence for a fault on La Palma, geological data suggest that the NE-SW striking fault from Santa Cruz to Puerto Naos is the major fracture (MIDDLEMOST, 1969).

Two cases of an association of negative with positive Bouguer anomalies were observed. The trough west of Hierro has a local anomaly of about -20 mgl. The second trough lies northwest of Gran Canaria where the anomalies fall below 140 mgl, yielding a local anomaly of about -30 mgl. It is possible that the mass deficiency, resulting in those negative anomalies, was caused by magma which oozed out at some distance from where it was accumulated. The overlying layers consequently subsided, filling the cauldron with material of lower density. This process may have occurred west of Hierro (see section 5.5.5) but the main cause for the trough northwest of Gran Canaria was probably faulting. A whole portion of the crust may have subsided along the three suggested faults (Fig. 39).

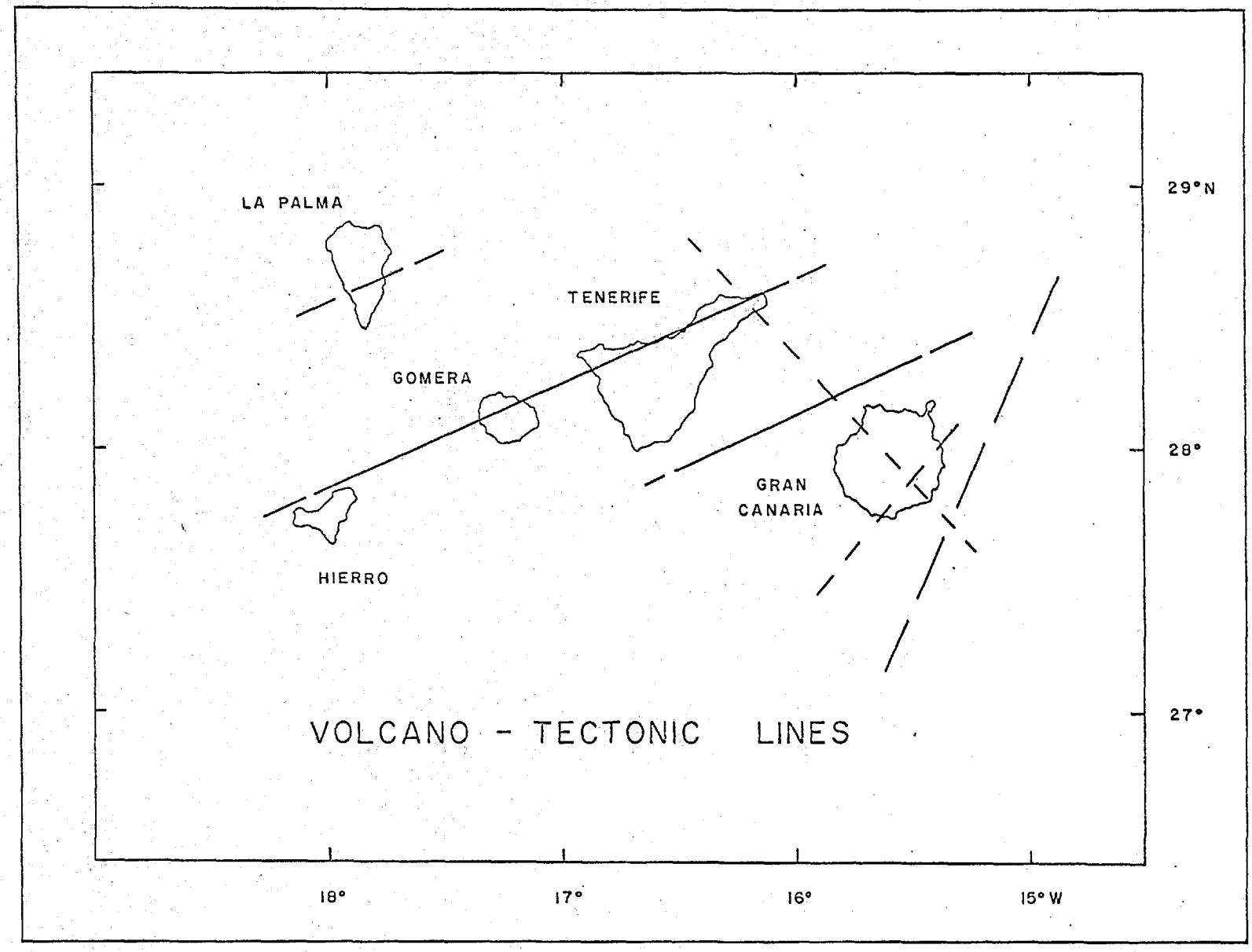
LA PALMA
TENERIFE
GOMERA
GRAN
CANARIA
HIERRO
VOLCANO - TECTONIC LINES
29°N
28°
27°
18°
17°
16°
15° W

Fig.39

There is some evidence for a crustal thickening under the axis of the ridge as displayed by the trough which falls to a value of 160 mgl between La Palma and Tenerife. However, much of its influence is masked by the effect of gravity centres located in the islands.

The Bouguer fields over Tenerife and Gran Canaria obtained by MACFARLANE (1968), together with marine data and seismic information were used to construct structural models (Figs. 35 and 36). Similar models were not calculated for the other islands because their gravity fields were poorly defined and the seismic information was insufficient to reduce the ambiguities substantially.

5.4 Free-Air Anomalies

Although free-air anomalies are affected by changes in bottom topography, they reveal some structural features of the area under investigation.

The high positive free-air anomalies over the island group (Fig. 29) are not associated with an offshore trough of negative anomalies. On the contrary, a gradual change from positive to negative values takes place. This observed pattern suggests that the regional isostatic compensation of the island group is probably on a larger scale than the present observation of the gravity field. Although the gravity survey is inadequate for determining the precise extent of this compensation, the radius of compensation can be estimated from the bathymetry (Fig. 1). The 3500 metres isobath comes close to the continental slope both to the

immediate north and south of the Canaries ridge, forming two basins similar to the Hawaiian deep. The subsidence of the ocean floor may have been caused by the Canaries load, creating a radius of compensation of about 150 km. This is comparable with estimates in the Hawaiian islands (ROSE and BELSHÉ, 1965).

Noticeable negative anomalies (<-50 mgl) occur in the adjacent ocean basins north and south of Gran Canaria. This feature is quite common along continental margins beyond the 2000 metres bathymetric line. It was suggested (WORZEL, 1965) that the mantle may be dipping under the continental block before reaching the edge of the continental margin. According to WORZEL (1965), this is a compensation for the continent extending regionally beyond its boundary. The well-defined negative anomalies around Gran Canaria can be viewed as parts of this belt. They indicate a pronounced dip of the mantle towards the African continent. This result is consistent with the locally high dip of 3.5° estimated from the seismic upper mantle velocities at Profiles A and D (see section 5.1.5).

The free-air anomalies were used to compute the depth of the mantle in the Canaries region as explained in section 4.4. Fig. 34 shows the isobaths of the MOHO. This calculation was also effected for the eastern part of the island group by utilising the gravity profiles PP', RR' and SS' (Fig. 6) in order to show regional trends in crustal structure. But it must be borne in mind that the calculated depths in the eastern region are only approximate values, because few seismic (HINZ, 1967, 1968) and geological data (QUEROL, 1966) were available to restrict the ambiguities.

Three effects can be observed in Fig. 34:

i) a regional crustal thickening resulting in a MOHO depression, graduating from 11-12 km west of the Canaries to 21-22 km under the continental shelf,

ii) a regional compensation for the load of the Canaries ridge,

iii) local compensations for the islands' high-density bodies.

There is a clear indication of a regional compensation of the island ridge in the western part of the archipelago. The cross-section at 17°33' west longitude (Fig. 38) shows that the MOHO dips from 11-12 km under the surrounding ocean basins to 17 km under the island ridge. The same value of 17 km as the shallowest possible depth of the mantle was calculated from seismic measurements (Profile F recorded at Vilaflor) north of Gomera, assuming an upper mantle velocity of 8.0 km/sec.

Local depressions occur under the islands. They are marked by high gradients of the MOHO and have a limited lateral extent. The depths of the MOHO under Tenerife and Gran Canaria were computed from their Bouguer anomalies (Fig. 34).

The local depression north of Gran Canaria is interesting. It may have been caused by subsidence of a complete crustal block as a result of faulting. On the other hand, it may be a non-existent feature arising only from the calculations because no seismic information on the thickness of the upper layers was available and they were assumed to be equal in thickness to the layers under Profile A. But if magma squeezed out at some distance from where it accumulated, as was argued earlier, the resulting collapse of the upper

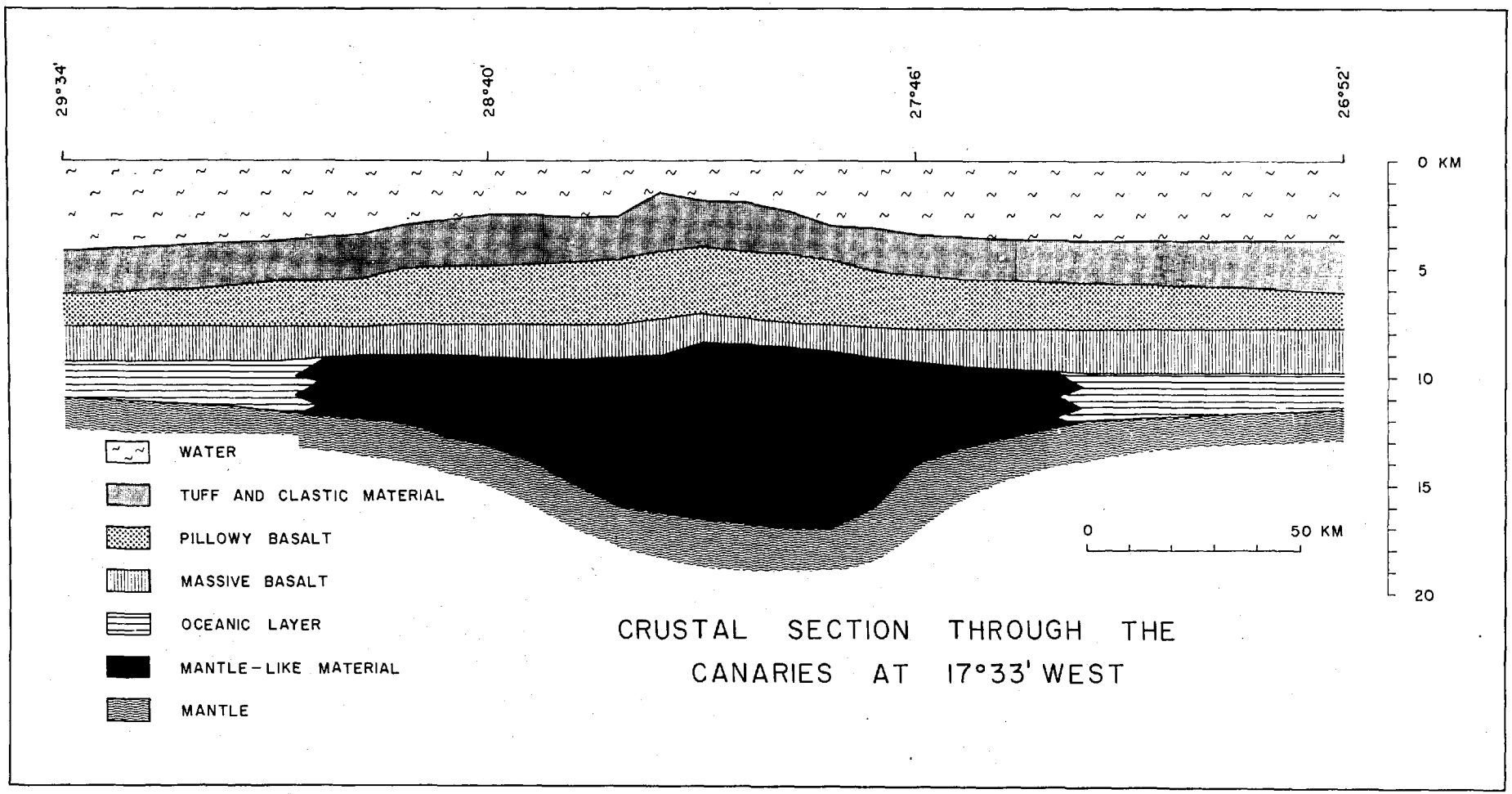
29°34'
28°40'
27°46'
26°52'
0 KM
5
10
15
20
0
50 KM
WATER
TUFF AND CLASTIC MATERIAL
PILLOWY BASALT
MASSIVE BASALT
OCEANIC LAYER
MANTLE-LIKE MATERIAL
MANTLE
CRUSTAL SECTION THROUGH THE
CANARIES AT 17°33' WEST

Fig.38

crustal layers would have altered the thicknesses of the layers with respect to the surrounding structure. The resulting mass deficit would not depress the MOHO.

On examination of Fig. 34 there is a suggestion that the 12 km isobath of the MOHO runs approximately NE-SW parallel to the coastline of Africa to the north and south of the Canaries ridge. Assuming that the four western islands of Hierro, La Palma, Gomera and Tenerife were non-existent, this isobath would probably run between Tenerife and Gran Canaria, dividing the area of the western Canaries into two zones. This pattern could suggest the following points:

i) the area west of this hypothetical line is essentially oceanic in character. The MOHO depression under the ridge is probably caused by a crustal thickening as a result of isostatic compensation for the load of the Canaries ridge, and

ii) in the area east of this line, the MOHO graduates from 12 km to 21-22 km under the continental shelf. This can be viewed as an isostatic compensation for the margins of the African continent.

Therefore, it may be stated that the crust west of this boundary surrounding Tenerife, Gomera, La Palma and Hierro is essentially oceanic. The regional depression under the ridge, accompanied by an increase in basement velocity, is compatible with observations in the Hawaiian islands (FURUMOTO and WOOLLARD, 1965; ROSE and BELSHÉ, 1965).

Since no sign of continental crust could be found in zone B (Fig. 6) it may be concluded that all the five

western Canary islands are independent volcanic edifices and not parts of the African continent, although Gran Canaria lies in the transitional zone between oceanic and continental crust.

5.5 Geology of the Canary Islands

Geological data provide further information about the structure and origin of the Canary Archipelago. They are correlated with the geophysical results of the present survey and discussed below.

5.5.1 Gran Canaria

Gran Canaria is formed by the accumulation of material from several independent volcanic cycles, separated by periods of intense erosion. The tabular basaltic series form the oldest formation at sea level, overlying a core whose age is not known (FUSTER, 1968a). They erupted in the western part of the island between 12-16 MY ago (ABDEL-MONEM et al, 1967) from centres which lay west of the present coastline (HAUSEN, 1962; FUSTER, 1968a). Their character is alkaline with a transition to more salic types and not silica-saturated lavas of tholeiitic type (FUSTER, 1968a). This oldest formation was followed by trachytic-syenitic ignimbrites and tuffs which erupted to the east of the basaltic island. They were probably produced by density differentiation from an alkaline-syenitic magma (FUSTER, 1968a). HAUSEN (1962) believed that this series formed the old nucleus of the island and was a remnant of a pre-Canarian foreland. After an erosive period, a new volcanic cycle produced basic alkaline lavas of phono-

litic type which are 9-14 MY old (ABDEL-MONEM et al, 1967). They built up a great cone in the central part of the island. The fourth cycle was dominated by erosion. Subsequent vulcanism produced basic alkaline lavas and basaltic series in the northwestern part of the island and led HAUSEN (1962) to suggest that a great fault trending NW-SE disrupted Gran Canaria after the phonolitic phase. Later vulcanism piled material on the downthrown block in the northeast. FUSTER (1968a) found no evidence for this fault and suggested an eastward migration of the eruptive centres. Accordingly, Gran Canaria was destroyed in the west and developed towards the east with the passage of time.

The Bouguer anomaly map (Fig. 31) shows two centres of gravity under Gran Canaria and a third one some 15 km SSW of the island. The westernmost centre is associated with a strong gradient in the northwest, suggesting the existence of a fault (see section 5.3). It supports the view that the tabular basaltic series erupted from centres to the west of the present coastline which have since sunk (HAUSEN, 1962; FUSTER, 1968a). There is little geological evidence for a major volcanic source associated with the second gravity centre. It may represent the centre of the phonolitic series because this is the only place where phonolitic lavas lie directly on weathered basalt (HAUSEN, 1962). There is no geological evidence for lavas which could have emerged from the third centre SSW of Gran Canaria. They probably did not reach the present island or were completely eroded after their formation.

FUSTER (1968a) proposed that the trachytes and rhyolites owe their origin to a gravity differentiation in an alkaline - syenitic magma. In HAUSEN's (1962) view they formed part of a pre-Canarian foreland which disintegrated. But there is no geophysical evidence for this pre-Canarian foreland in the western part of the archipelago and HAUSEN's (1962) interpretation is therefore doubtful. Since large sediment accumulations occur to the east of Gran Canaria (HINZ, 1968) which are absent in the west, it is not excluded that the rhyolites and trachytes which should prove a continental origin (HAUSEN, 1962) were probably formed by metasomatic processes from the sediments. This view is compatible with the location of Gran Canaria in the transitional zone between oceanic and continental crust.

5.5.2 Tenerife

The oldest rocks are found in Teno and Anaga peninsulas to the west and northeast of the island, overlying a presumed plutonic basement. They consist of basaltic lava flows and pyroclastics intersected by dykes, plugs and sills of compact basalt (FUSTER, 1968b) which erupted at least 16 MY ago (ABDEL-MONEM et al, 1967). They probably originated from fissures running NE-SW (FUSTER, 1968b) and are probably contemporaneous with similar rocks on Gomera (HAUSEN, 1956), forming a uniform tableland. After an erosional period, the central volcano erupted in a salic phase producing phonolites, trachytes, trachybasalts and pumice which form the bulk of the present island. The last eruptive cycle with olivine

basalts, alkalibasalts and pumice built the twin peaks of Pico Viejo and Pico Teide which form the maximum elevation of 3718 metres in the Atlantic. They grew on the floor of a giant caldera of about 16 km diameter which was produced either by lateral landslipping following subsidence of the underlying magma chamber (RIDLEY, 1968) or by a giant explosion and subsequent collapse (FUSTER, 1968b). A spine of basaltic lavas 1-2 MY old (ABDEL-MONEM et al., 1967), joins the caldera complex with the northeastern peninsula. The lavas are flanked by two major landslides (BRAVO, 1962) interpreted as being due to tectonic processes (HAUSEN, 1956). Vulcanism during the Quaternary produced cinder cones, which have been extinct since the last eruption was recorded in 1909.

The Bouguer anomalies (Fig. 31) show that Tenerife and Gomera most probably have a common basement. It consists of high velocity material and is found roughly 1 km above the surrounding basement layer. The basement may have been formed by an intrusive mixing and gravitational differentiation of mantle-like material into the oceanic layer (Fig. 37). The abundance of mafic and ultramafic nodules in lavas and dykes on Tenerife (BORLEY, 1969) correlates very well with an elevated basement, because the high content of olivine, pyroxene and augite suggests an origin from a similar magma situated not too far below.

As MACFARLANE and RIDLEY (1968) have pointed out, the high Bouguer anomaly over the main crater is not consistent with the suggestion of a collapse caldera. The existence of a

high-density body about 5 km below the caldera floor is favoured.

Positive Bouguer anomalies over the Anaga and Teno peninsulas, together with the NE-SW trend of the basalts which erupted there, led MACFARLANE (1968) to suggest the existence of a tensional axis through Tenerife, Gomera and Hierro. This axis, detected during the seismic survey and interpreted as a fault, showed a downthrow on the southeastern side and was probably the main cause for the origin of Tenerife. Presumably in an early stage of the fault, material erupted to form the Anaga and Teno peninsulas and probably also the area in between. Later, after tectonic movements had taken place, a vast amount of material piled up on the downthrown block through secondary tension fissures and minor faults, forming the bulk of the island.

5.5.3 Gomera

Gomera is a shield volcano which has been partly destroyed by a long cycle of erosion (BRAVO, 1964). The island's nucleus consists of basic and ultrabasic rocks of holocrystalline texture, intruded by a multitude of dykes of varied chemical composition (BRAVO, 1964). Age determinations on a nepheline - syenite intrusion in the basal complex gave an age of 15 MY (ABDEL-MONEM et al, 1967). This basal complex, exposed in the north of the island, was subsequently covered with a thick layer of volcanic agglomerates and a series of oceanic basalts resembling the series of Teno and Anaga peninsulas on Tenerife. After a period of erosion, fissure

eruptions of basalts, some of which are of recent age, accumulated in the southeastern part of the existing island. Volcanic activity on Gomera ceased before the Quaternary (BRAVO, 1964).

The Bouguer anomalies are poorly defined over Gomera because no land survey data were available (Fig. 31). It is therefore not possible to check BRAVO's (1964) statement that "no major feeder pipes are exposed on this island". On the other hand, the occurrence of a basal complex in the north coincides well with the suggested fault through Tenerife - Gomera - Hierro. The similar basaltic series found on Gomera and on Teno and Anaga peninsulas on Tenerife (BRAVO, 1964), suggest that they originated from a common magma or else that they once formed a common platform (HAUSEN, 1956). The high basement found under Tenerife probably extends under Gomera and causes the consistently high Bouguer anomalies observed around both islands.

The genesis of Gomera has a striking similarity to that of Tenerife. Both have an old basement complex in the north and subsequent vulcanism accumulated material in the southeast of their old nuclei. They both seem to have erupted above a major fracture. Tectonic movements caused the southeastern block to subside and subsequent lavas to erupt in the southeast of the existing islands.

5.5.4 La Palma

The bulk of the island is formed by a thick sequence of lavas of ordinary basaltic type (HAUSEN, 1956) which erupted within the last 2 MY (ABDEL-MONEM et al, 1967). They recede

from the Caldera de Taburiente and dip towards the surrounding ocean. These lavas are the remains of a great central volcano, which eroded through the Barranco de las Agustias (HAUSEN, 1961). The floor of the resulting caldera consists of basalts, trachy-basalts and metamorphosed pyroclasts, intruded by nepheline syenites (MIDDLEMOST, 1969). Its basal complex of dunites and olivine-rich basalts was probably formed when the feeder conduits became clogged with dense material (MIDDLEMOST, 1969). The Cumbre Vieja ridge, extending from the caldera to the southern Punta Fuencaliente, is a major rift zone with a probable N-S feeder dyke system below (MIDDLEMOST, 1969). It is built up by basalts with intruded domes of phonolite. The fault, inclining NE-SW from Santa Cruz to Puerto Naos, is the most important one on the island (MIDDLEMOST, 1969).

Very little geophysical data were obtained on La Palma. The gravity field based on marine data (Fig. 31) confirms the presence of a "high-density body" under the Caldera de Taburiente. Unfortunately, no detailed structures can be deduced from the Bouguer anomalies and it is not possible to assess the importance of the NE-SW trending fault for the origin of La Palma.

5.5.5 Hierro

This island is built up by a great series of trachy-basaltic lavas forming an arc open to the northwest, known as "El Golfo". The basalts gently recede from this semi-circle and HAUSEN (1964) considers them to represent the remnants of a great shield volcano. Fractures along "El Golfo" escarpment

caused the northwestern part to subside. The whole of the exposed island probably erupted within the last 1.5 MY (ABDEL-MONEM et al., 1967).

The Bouguer anomalies (Fig. 31) show that the island root has an extension towards the northwest which is consistent with HAUSEN's (1964) suggestion of a giant landslide in this direction.

The Bouguer trough SSW of Hierro and the pronounced dip of lavas in the southern part of the western foreland endorses the earlier suggestion that this trough was created by subsidence of the crust probably due to magma being forced out at some distance from its place of accumulation.

Like Tenerife, Gomera and Gran Canaria, Hierro seems to have been built up on the downthrown side of a major fault. It is an isolated island on the Canaries ridge and the most recent in outcrop.

5.5.6 Summary

On the basis of the studies undertaken, it would be possible to deduce a detailed hypothesis for the origin of the islands.

The islands were formed along major NE-SW fractures in the crust. In the case of Gomera and Tenerife, an old nucleus was formed above a first fracture. Tectonic movements subsequently displaced the southeastern fault block downwards and widened the fracture. Later eruptions contributed to the bulk of the islands on the downthrown block.

Gran Canaria's genesis is more complicated. At first, eruptions formed the nucleus of the island, which was partly destroyed in the west. They were accompanied by a downward movement of the southeastern fault block. New fractures appeared in the east of the old island giving rise to a new eruptive cycle. The downward displacement of the fault block facing Africa and the creation of new faults in the east of the old island can be viewed as a gradual isostatic compensation for the margins of the African continent. Signs of this gradual compensation are found in the sedimentary basins of Spanish Sahara (QUEROL, 1966). The sediments tilt progressively towards the sea with a dip which increases with time, as a result of subsiding basins.

La Palma and Hierro do not show any sign of sequential eruptions and must therefore be quite young. This view is consistent with radiometric determinations of their age (ABDEL-MONEM et al, 1967).

It is quite likely that all of the Canary Islands have a common plutonic basement (FUSTER, 1968c) consisting of rocks similar to the basements of Gomera, La Palma and Fuerteventura. They are probably composed of holocrystalline rocks in the range of alkaline gabbros to peridotites (BRAVO, 1964). Velocities attributable to these rocks (BIRCH, 1960) correspond very well with the basement velocity of 7.3-7.5 km/sec found throughout the Canaries ridge.

The rocks forming the Canaries group belong to the "Atlantic" type, the Na-alkaline series of magmas (HAUSEN, 1956).

Contrasted fractionation split the parent magma into a basic and a salic, phonolitic group with all the transitional types (HAUSEN, 1956). Practically all the lavas are silica-undersaturated with the exception of Gran Canaria's trachytes and rhyolites. These results are consistent with the geo-physical data suggesting that Hierro, La Palma, Gomera and Tenerife are oceanic islands, whereas Gran Canaria lies on a transitional zone.

5.6 Causes for the Origin of the Canary Islands

The present seismic and gravity surveys showed clearly that the western islands of Hierro, La Palma, Gomera and Tenerife are in an area where the crust is essentially oceanic whereas Gran Canaria lies within the transitional zone between oceanic and continental crust. All the islands owe their origin to magma erupting along NE-SW faults and do not form a part of the African continent.

But the question as to where they were formed remains. The tectonic movements which created the faults could have taken place in two areas:

(1) they may have originated on the Mid-Atlantic Ridge and subsequently drifted to their present positions; or

(2) the faults could have been caused by movements of the adjacent continental blocks which means that the islands were initiated in their present positions.

5.6.1 Origin on the Mid-Atlantic Ridge

In a comparative study of islands' age in relation to distances from the mid-oceanic ridges, WILSON (1963) suggested that islands were formed on the ridges and were swept outwards by diverging convection currents. They owe their present positions to the spreading of the ocean floor.

However, the chemical composition of the rocks which formed on mid-oceanic ridges is generally quite different from those formed some distance away (McBIRNEY and GASS, 1967). The rocks on islands near the axis of the ridge are silica-saturated with marked oversaturation of their late differentiates. Islands further from the ridge have undersaturated and sodic rocks with even more undersaturated later differentiates. The degree of silicasaturation is a function of heat-flow and pressure. High heatflow and low pressure, present on mid-oceanic ridges, result in silicasaturation; low heatflow and high pressure produce undersaturated rocks and require a deep generation of the magma. McBIRNEY and GASS (1967) concluded that islands which are at present far from the ridge most probably formed in situ and are related to local zones of magma genesis within the underlying mantle.

Because most of the Canarian rocks are undersaturated and rich in Na-alkaline (HAUSEN, 1956) and display a high pressure mineralogy (RIDLEY, 1968), it seems improbable that they were formed on the Mid-Atlantic Ridge.

GASS (1967) argues that once islands become inactive on the ridge they do not survive as such for long but erode

within periods of 20-25 MY. The remarkable relief of the Canaries, especially Tenerife, is incompatible with this hypothesis and thus with a mid-oceanic origin.

The emerged parts of the western Canary Islands are about 2-16 MY old (ABDEL-MONEM et al., 1967). Their present position, some 2000 km away from the axis of the Mid-Atlantic Ridge, would imply an incredibly high drift rate of 12-100 cm/year for their displacement, if they had formed on the ridge. But it is unlikely that drift rates in the Atlantic have exceeded 6-8 cm/year and the spreading of the ocean floor even ceased several times (LE PICHON, 1968). It therefore does not seem plausible that the Canaries formed on the Mid-Atlantic Ridge.

5.6.2 Connection with the African Continent

The origin of the Canaries may be connected with similar structural trends on the adjacent African continent and this possibility will now be examined.

The northwest African block was submerged in Paleozoic times, forming part of the N-S trending continental flexure (REYRE, 1966). The Hercynian orogeny produced the Moroccøan Meseta and Mauritania which collapsed in early Triassic times, creating various basins. Sediments and salt deposited in them until Lower Lias times when they were uplifted, accompanied by the eruption of basaltic rocks. A period of subsidence followed, resulting in the Rio de Oro and Tarfaya basins and a transgression into the Sahara. It lasted until the end of the Cretaceous time when the Atlas mountains emerged.

Repeated subsidence of the Atlas during Paleocene and Eocene times was connected with a readjustment of the African block (REYRE, 1966). The High Atlas, part of the Lower and Middle Jurassic Tethys basin, were folded in post-Eocene time and again in Miocene (DE SITTER, 1964). At the same time the sea regressed and parts of the sedimentary basins close to the existing continent emerged. Strong volcano-tectonic lines ("transversales" of GLANGEAUD, 1954) striking NE-SW, developed in Burdigalian-Vindobonian (REYRE, 1966): they are the Atlas-Anti Atlas - Canaries, Eglab - Cape Verde, Adamaoua - Sao Thomé - Cameroun and Walvis Ridge - Angola lines. They are usually associated with volcanic provinces which cut through the African block and the adjacent sea floor. The Atlas reached its present height after an uplift during Pliocene.

The NE-SW trend of tectonic lines is the major structural trend in the Atlas mountains and the adjacent border-lands (DUBOURDIEU, 1959). Structures as old as Triassic are dissected by a multitude of NE-SW running faults. The resulting blocks are displaced by shearing movements towards southwest, analogous to a tilted pack of cards (DUBOURDIEU, 1959). The recent catastrophic earthquakes of Agadir in 1960 was a consequence of the forces acting in this region (DUBOURDIEU, 1963). Movements of the continental blocks were probably responsible for the creation of the Atlas mountains and their NE-SW tectonic lines.

In a suggested history of the opening of the Atlantic Ocean, LE PICHON (1968) distinguishes three move-

ments. A first phase started some 120 MY ago, where fast spreading lasted for about 30 MY, terminating in Upper Cretaceous time. North America and Eurasia had moved as a unit, creating a zone of extensional shear between Africa and Eurasia which coincides with the formation of the Tethys geosyncline in North Africa. In Paleocene times the movements resumed and followed another pattern of flow. On this occasion North and South America moved as one unit while Eurasia followed a southeastward trend relative to Africa. Possibly, this movement resulted partly from the opening of the Labrador sea (LE PICHON, 1968) and partly from the rotation of the Iberian Peninsula (WATKINS and RICHARDSON, 1968; VAN DER VOO, 1969). Thus a new zone of shear, connected with compression, occurred in the Lower Tertiary. By Oligocene times the spreading rate had begun to slow down and it stopped altogether in the Miocene Period. These episodes correlate well with the period of maximum compression in the Mediterranean (GLANGEAUD, 1962) when North Africa and Europe came within close contact. In late Miocene a third drift cycle started at a slower rate which followed the same pattern and has continued to the present time.

Comparing the geology of Northwest Africa with the results obtained in the Canaries, the following facts should be noted:

i) The Atlas mountains were first folded in post-Eocene and a second time in Miocene (DE SITTER, 1964). These compressional movements were very probably the result

of a southeastward migration of Europe relative to Africa (LE PICHON, 1968). They correlate well with the period of maximum compression in the Mediterranean (GLANGEAUD, 1962). As a probable consequence of those movements, the Atlas mountains were dissected in a NE-SW direction and volcano-tectonic lines were created.

ii) The oldest rocks sampled on the Western Canary Islands are some 16 MY old (ABDEL MONEM et al, 1967) and are contemporary with the second folding of the Atlas mountains and the forming of the NE-SW tectonic trends.

iii) Probably all of the five western Canary Islands are directly related to faults, striking NE-SW. It is very likely that these form part of REYRE's (1966) Atlas-Canaries volcano-tectonic line and that they are the result of the shear and compressional forces operating in Northwest Africa.

5.6.3 Hypothesis for the Origin of the Western Canary Islands

Although the four western Canary islands of Hierro, La Palma, Gomera and Tenerife are oceanic islands, they did not form on the Mid-Atlantic Ridge. The same is true for Gran Canaria, which lies in the transitional zone between oceanic and continental crust. On the contrary, they formed along NE-SW faults which were presumably established by the Lower Miocene as a probable result of shear and compressional forces in Northwest Africa. Alkaline magma was generated at

some depth in the Upper Mantle and erupted along these fractures, commencing in the east and later extending towards the west. Downward displacement of the fault blocks facing Africa were the probable result of an isostatic compensation for the margins of the African continent.

CHAPTER 6

CONCLUSIONS

The seismic refraction and gravity surveys in the western Canaries were aimed at resolving the problem of the islands' origin.

No sign of continental crust could be found in the western area of the Canarian archipelago and therefore the hypotheses which associate the Canary Islands with either the mythological continent Atlantis or with a pre-Canarian sub-continent gain no support. Neither can the western islands be part of the Atlas Mountains nor of the African continent. However, the geophysical data available at present for the easternmost islands of Fuerteventura and Lanzarote are inadequate for determining their crustal structure precisely. The depth of the MOHO in that area does not exclude the eastern islands from being continental.

Some hypotheses suggest that the western Canaries were formed by vigorous uplifting of marine strata. This mechanism in itself is very improbable as it would involve local vertical movements of up to 7 kilometres. In addition, it was disproved by the two NE-SW running faults through Tenerife, Gomera, Hierro and northwest of Gran Canaria, showing a downthrow on the southeastern side. But the present data are inadequate for verifying the possibility of compressional movements in the early stages of the formation of the Canaries.

The results of the present investigation are in accordance with hypotheses which suggest that the islands are independent volcanic edifices and that they are related to major fracture zones within the crust. It was shown that the crust around the four western islands of Hierro, La Palma, Gomera and Tenerife is essentially oceanic whereas Gran Canaria lies in the transitional zone between oceanic and continental crust. The origin of the five western Canaries is closely related to the formation of this fault pattern.

Although the crustal trends in the western area of the Canary Islands were established and a sufficiently good picture of the crustal structure had emerged, the latter is by no means complete. Further investigations are suggested to supplement the results already obtained with an aim at achieving a complete picture of the islands' structures:

i) extending the present marine gravity survey up to 200 km north and south of the Canaries ridge for an estimation of the regional isostatic compensation,

ii) conducting land gravity surveys over La Palma and Gomera to establish their local structures,

iii) verifying the depth of Tenerife's plug under the caldera by seismic methods,

iv) establishing the crustal structure under the Bouguer trough north of Gran Canaria in order to determine whether it is caused by subsidence of a crustal block or by cauldron subsidence, and

v) investigating the area around the eastern two islands by seismic refraction to establish the relationship between the islands and the African continent.

In conclusion, it may be stated that the present investigation has resolved the controversy concerning the origin of the Western Canary Islands.

ACKNOWLEDGEMENTS

The author wishes to thank Dr. B.P. Dash for his supervision. Thanks are also due to Messrs. K.O. Ahmed, J.L. Brander, P. Harwood, B. Hazelhoff-Roelfzema, P. Hubral, C.P. Summerhayes, Drs. W.N. Li and J.S. Tooms for help during the John Murray expedition. The author is grateful to the German scientists Professor H. Closs, Drs. K. Hinz and S. Plaumann, Messrs. K. Aric, H. Bungenstock, H.B. Hirschleber, H.A. Roeser and W. Weigel for their contributions to a successful data collection on board F.S. Meteor. The author is also indebted to Drs. G.D. Borley and W.I. Ridley for fruitful discussions. None of this work could have been done without the collaboration of the captains, officers and crews of F.S. Meteor, Tofinio and R.R.S. John Murray.

The author wishes to thank the Swiss National Foundation for granting a one-year scholarship and the Royal Dutch Shell for the award of a two-year scholarship.

BIBLIOGRAPHY

ABDEL-MONEM,A.,WATKINS,N.D. and GAST,P.W.,1967;Volcanic history of the Canary Islands.Trans.Am.Geoph.Un.,V48,pp226

ADAMS,W.M. and FURUMOTO,A.S.,1965;Refraction study of the Koolau volcanic plug.Pacif.Sci.,V19,pp296-305

BELOUSOV,V.V.,1967;Some problems concerning the oceanic earth's crust and upper mantle evolution.Geotectonics,V1,pp1-6

BIRCH,F.,1960;Velocity of compressional waves in rocks to 10 kilobars.Part 1:J.Geoph.Res.,V65,pp1083-1102

1961;Part 2:J.Geoph.Res.,V66,pp2199-2224

BLUNDELL,D.J. and PARKS,R.,1969;A study of the crustal structure beneath the Irish Sea.Geoph.J.R.astr.Soc.,V17, N1,pp45-62

BORLEY,G.D.,1969;pers.comm.

BRAVO,T.,1962;El circo de Las Canadas y sus dependencias. Bol.R.Soc.Esp.Hist.Nat.,V60,pp93-108

1964;Estudio geologico y petrographico de la isla de la Gomera.Estudios Geolog.,V20,pp1-56

CANN,J.R.,1968;Geological processes at mid-ocean ridge crests. Geoph.J.R.astr.Soc.,V15,pp331-341

DE SITTER,U.,1964;Structural geology.Int.Ser.i.Earth Sci.

DUBOURDIEU,G.,1959;La déformation récente de l'Afrique du Nord. Comp.rend.acad.sci.Paris,V249,pp2799-2802

1963;La lecon du séisme d'Agadir.Comp.rend.acad. sci.Paris,V256,pp723-726

EMILIANI,C.,1965;Science,V147,N3654,pp14

EWING,J. and EWING,M.,1959;Seismic refraction measurements on the Atlantic Ocean basins,in the Mediterranean Sea,on the Mid-Atlantic Ridge and in the Norwegian Sea.Bull.Geol.Soc. Am.,V70,pp291-318

EWING,M. and EWING,J.,1960;Geophysical measurements in the western Caribbean Sea and Gulf of Mexico.J.G.Res.,V65,4087

FURUMOTO,A.S. and WOOLLARD,G.P.,1965;Seismic refraction studies of the crustal structure of the Hawaiian Archipelago. Pacif.Sci.,V19,pp315-319

FURUMOTO,A.S.,THOMSON,N.J. and WOOLLARD,G.P.,1965;The structure of the Koolau Volcano from seismic refraction studies. Pacif.Sci.,V19,pp306-314

FUSTER,J.M.,1968a;Geology and volcanology of the Canary Islands. Gran Canaria.Inst.Lucas Mallada,Madrid

1968b;Tenerife

1968c;Fuerteventura

GASS,I.G.,1967;Geochronology of Tristan da Cunha group of islands.Geol.mag.,V104,N2,pp160-170

GLANGEAUD,L.,1954;Les éruptions tertiaires nord-africaines. Leur relation avec la tectonique méditerrannée. 19th Int.Geol.Cong.,Algiers,Sect.15,pp71-102

1962;Paléogéographie dynamique de la Méditerrannée et de ses bordures.In:Océan.Géol.Géoph.Médit. Occid.,ppl25-165,Centre Nat.Rech.Sci.,Paris.

GURNEY,G.B.,1964;A geophysical telemetry system.Lucas Eng.Rev., V1,N2,ppl6-23

HAMMER,S.,1939;Terrain corrections for gravimetric stations. Geophysics,V4,ppl84-194

HAUSEN,H.,1956;Fuerteventura.Some geological and geomorphological aspects of the oldland of the Canarian Archipelago. Acta geogr.,Soc.Geog.Fenn.,V15,N2

1958;On the geology of Fuerteventura(Canary Islands). Soc.Sci.Fenn.Comm.Phys.Math.,V22,N1,pp211

1961;Canarian calderas.A short review based on pers. impressions 1947-1957,Bull.Com.Geol.Finl.,V196, ppl79-213

1962;New contributions to the geology of Gran Canary. Soc.Sci.Fenn.Comm.Phys.Math.,V27,N1

1964;Rasgos geologicos generals de la isla de Hierro. Patron.Casa Colon,Madrid,V1o,p547

HEEZEN,B.C.,THARP,M. and EWING,M.,1959;The floor of the oceans. Part 1:The North Atlantic.Geol.Soc.Am.Spec.Pap.65

HERNANDEZ-PACHECO,E.,1910;Estudio geologico de Lanzarote y de las Isletas Canarias.Mem.R.Soc.Esp.Hist.Nat.,V6,N4,pp331

HESS,H.H.,1962;Petrologic studies.Geol.Soc.Am.,V73,pp599-620

1965;Drilling for scientific purposes.Geol.Sur.Canada Pap.66-13,pl49

HILL,M.N.,1957;Recent geophysical exploration of the ocean floor. Phys. and Chem. Earth,V2,ppl29-163

HINZ,K.,1967;pers.comm.

1968;Neuere geophysikalische Ergebnisse aus dem Bereich des äusseren Schelfs und Kontinentalabfalls, Erdöl + Kohle,V11,p677

HUGHES,D.S. and MAURETTE,C.H.,1957;Variations of velocity with temperature and pressure of some basic igneous rocks. Geophysics,V22,N1,pp23-31

JONES,J.G.,1966;Intraglacial volcanoes of southwest Iceland and their significance in the interpretation of the form of marine basaltic volcanoes.Nature,V212,N5062,pp586-588

KREJCI-GRAF,U.,1961;Vertikalbewegungen der Makaronesen.Geol. Rundschau,V51,pp73-122

LAUGHTON,A.S.,HILL,M.N. and ALLAN,T.D.,1960;Geophysical investigation of a seamount 150 miles north of Madeira. Deep Sea Res.,V7,ppll7-141

LE PICHON,X.,1968;Sea-floor spreading and continental drift. Jour.Geoph.Res.,V73,N12,pp3661-3697

LE PICHON,X.,HONTZ,R.E.,DRAKE,CH.L. and NAFE,J.E,1965;Crustal structure of mid-oceanic ridges.Seismic refr.measurements. J.Geoph.Res.,V70,pp319-339

LYELL,CH.,1855;Elements of Geology.London

MACFARLANE,D.J.,1968;The structure of some Atlantic islands as deduced from gravity and other geophysical data.Ph.D. thesis,University of London.

MACFARLANE,D.J. and RIDLEY,W.I.,1968;An interpretation of gravity data for Tenerife,Canary Islands.Earth+Plan.Sci.Lett., V4,N6,pp481-486

MALAHOFF,A. and WOOLLARD,G.P.,1966;Magnetic measurements over the Hawaiian Ridge and their volcanological implications. Bull.Volc.,V29,pp735-759

MANGHNANI,M.H. and WOOLLARD,G.P.,1965;Ultrasonic velocities and related elastic properties of Hawaiian basaltic rocks.Pacif.Sci.,V19,pp291-295

McBIRNEY,A.R.,1963;Factors governing the nature of submarine vulcanism.Bull.Volc.,V26,pp455-469

McBIRNEY,A.R. and GASS,I.G.,1967;Relation of oceanic volcanic rocks to mid-oceanic rises and heat flow.Earth+Plan.Sci. Lett.,V2,pp265

MIDDLEMOST,E.,1969;pers.comm.

MOORE,J.G.,1965;Petrology of deep-sea basalt near Hawaii. Am.J.Sci.,V263,pp40-52

NAFE,J.E. and DRAKE,CH.L.,1963;Physical properties of marine sediments.in:HILL,The Sea,V3,pp794-815

NAGY,D.,1966;The prism method for terrain corrections using digital computers.Pure and appl.Geoph.,V63,pp31-39

NAYUDU,Y.R.,1962;A new hypothesis for the origin of guyots and seamount terraces.The crust of the Pacific basin.Am.Geoph. Union,Geoph.Monograph N6

NETTLETON,L.L.,1939;Determination of density for reduction of gravimeter observations.Geophys.V4,pp176-83

1944;Geophysical prospecting for oil.McGraw-Hill Book Co.Ltd.,pp444

OFFICER,C.B.,EWING,M. and WUENSCHEL,P.C.,1952;Seismic refraction measurements in the Atlantic ocean.Part 4:Bermuda,Bermuda Rise and Nares Basin.Bull.Geol.Soc.Am.,V63,pp777-808

OFFICER,C.B. et al.,1959;Geophysical investigations in the eastern Caribbean:summary of 1955 and 1956 cruises.Phys. and Chem.Earth.,V3,pp110-198

PLAUMANN,S.,1967;pers.comm.

QUEROL,R.,1966;Regional geology of the Spanish Sahara.Sedim. basins of Afr.Coast.Part 1:Atlant.coast.Ass.Afr.Geol.Sur., Paris.

RAITT,R.W.,1954;Seismic refraction studies of Bikini and Kwajalein Atolls.US Geol.Sur.Prof.Pap.260-K,pp507-527

RAITT,R.W.,1957;Seismic refraction studies of Eniwetok Atoll. US Geol.Sur.Prof.Pap. 260-S

1963;The crustal rocks.in:Hill,M.N.,The Sea,V3, pp85-102,Int.Sci.Publ.

REYRE,D.,1966;Particularités géologiques des bassins côtiers de l'Ouest Africain.Sed.basins Afric.coast.Ass.Afr.Geol. Sur.,Paris,pp253

RIDLEY,W.I.,1968;Geology of Las Canadas area,Tenerife.Ph.D. thesis,University of London

ROSE,J.C. and BELSHÉ,J.C.,1965;Gravity and magnetic fields over the proposed Moho hole site north of Maui.Pacif.Sci., V19,pp374-380

ROTHE,P. and SCHMINCKE,H.U.,1968;Contrasting origins of the eastern and western islands of the Canarian archipelago. Nature,V218,pp1152

RYALL,A. and BENNETT,D.L.,1968;Crustal structure of southern Hawaii related to volcanic processes in the upper mantle. J.Geoph.Res.,V73,N14,pp4561-4582

RYBACH,L.,1962;Refraktionsseismische Untersuchungen im Raum Aare-,Limmat- und Surbtal.Beitr.z.Geol.Schweiz,Ser. Geophysik,N5

STEINHART,J.S. and MEYER,R.P.,1961;Explosion studies of continental structure.Carnegie Inst.Wash.Publ.622

STRANGE,W.E.,WOOLLARD,G.P. and ROSE,J.C.,1965;An analysis of the gravity field over the Hawaiian Islands in terms of crustal structure.Pacif.Sci.,V19,pp381-389

TALWANI,M.,WORZEL,J.L. and LANDISMAN,M.,1959;Rapid gravity computations for two-dimensional bodies with application to the Mendocino submarine fracture zone.J.Geoph.Res., V64,pp49-60

TALWANI,M. and EWING,M.,1960;Rapid computation of gravitational attraction of three-dimensional bodies of arbitrary shape.Geophysics,V25,pp203-225

TALWANI,M.,LE PICHON,X. and EWING,M.,1965;Crustal structure of mid-oceanic ridges.Part 2:Computed model from gravity and seismic refraction data.J.Geoph.Res.,V70,N2,pp341-352

VAN DER VOO,R.,1969;Paleomagnetic evidence for the rotation of the Iberian Peninsula.Tectonophys.,V7,N1, pp5-56

VENING MEINESZ,F.A.,1948;Gravity expeditions at sea,1923-1938. V4,Neth.Geodet.Comm.,Delft,pp233

VON BUCH,L.,1825;Physikalische Beschreibung der Kanarischen Inseln.Berlin.

WATKINS,N.D.,RICHARDSON,A. and MASON,R.G.,1966;Paleomagnetism of the Macaronesian Insular region:The Canary Islands. Earth+Plan.Sci.Lett.,V1,pp225-231

WATKINS,N.D. and RICHARDSON,A.,1968;Paleomagnetism of the Lisbon volcanics.Geophys.J.R.astr.Soc.,V15,pp287-304

WEIGEL,W.,1967;pers.comm.

WILSON,J.T.,1963;Hypothesis of the earth's behaviour.Nature, V198,N4984,pp925-929

WORZEL,J.L.,1959;Continuous gravity measurements on a surface ship with the Graf Sea Gravimeter.J.Geoph. Res.,V64,pp1299-1315

1965;Pendulum gravity measurements at sea 1936-1959.John Wiley and Sons,New York,Sidney, London.